

**OXYGENATED HYDROCARBON FUELS
FOR SOLID OXIDE FUEL CELLS**

by

JOHN CHRISTOPHER PREECE

A thesis submitted to
The University of Birmingham
for the degree of
DOCTOR OF PHILOSOPHY

School of Chemical Engineering
The University of Birmingham
December 2005

UNIVERSITY OF
BIRMINGHAM

University of Birmingham Research Archive

e-theses repository

This unpublished thesis/dissertation is copyright of the author and/or third parties. The intellectual property rights of the author or third parties in respect of this work are as defined by The Copyright Designs and Patents Act 1988 or as modified by any successor legislation.

Any use made of information contained in this thesis/dissertation must be in accordance with that legislation and must be properly acknowledged. Further distribution or reproduction in any format is prohibited without the permission of the copyright holder.

Abstract

In order to mitigate the effects of climate change and reduce dependence on fossil fuels, carbon-neutral methods of electricity generation are required. Solid oxide fuel cells (SOFCs) have the potential to operate at high efficiencies, while liquid hydrocarbon fuels require little or no new infrastructure and can be manufactured sustainably. Using hydrocarbons in SOFCs introduces the problem of carbon deposition, which can be reduced or eliminated by judicious choice of the SOFC materials, the operating conditions or the fuel itself. The aim of this project was to investigate the relationships between fuel composition and SOFC performance, and thus to formulate fuels which would perform well independent of catalyst or operating conditions.

Three principal hypotheses were studied. Any SOFC fuel has to be oxidised, and for hydrocarbons both carbon-oxygen and hydrogen-oxygen bonds have to be formed. Oxygenated fuels contain these bonds already (for example, alcohols and carboxylic acids), and so may react more easily. Higher hydrocarbons are known to deposit carbon readily, which may be due to a tendency to decompose through the breaking of a C-C bond. Removing C-C bonds from a molecule (for example, ethers and amides) may reduce this tendency. Fuels are typically diluted with water, which improves reforming but reduces the energy density. If an oxidising agent could also act as a fuel, then overall efficiency would improve.

Various fuels, with carbon content ranging from one to four atoms per molecule, were used in microtubular SOFCs. To investigate the effect of oxygenation level, alcohols and carboxylic acids were compared. The equivalent ethers, esters and amides were also tested to eliminate carbon-carbon bonding. Some fuels were then mixed with methanoic acid to improve energy density. Exhaust gases were analysed with mass spectrometry, electrical performance with a datalogging potentiostat and carbon deposition rates with temperature-programmed oxidation.

It was found that oxygenating a fuel improves reforming and reduces the rate of carbon deposition through a favourable route to CO/CO₂. Eliminating carbon-carbon bonds from a molecule also reduces carbon deposition. The principal advantage of blending with methanoic acid was the ability to formulate a single phase fuel with molecules previously immiscible with water.

Table of Contents

Chapter 1: Introduction.....	1
1.1: Project rationale.....	2
1.2: The global energy situation.....	4
1.2.1: Current fuel technologies.....	4
1.2.2: The global energy crisis.....	5
1.2.3: Climate change and the environment.....	6
1.2.4: The move to alternative and renewable fuels.....	7
1.3: Fuel cell technology.....	8
1.3.1: Background.....	8
1.3.2: Alkaline fuel cell (AFC).....	9
1.3.3: Proton exchange membrane fuel cell (PEMFC).....	10
1.3.4: Phosphoric acid fuel cell (PAFC).....	11
1.3.5: Molten carbonate fuel cell (MCFC).....	12
1.3.6: Solid oxide fuel cell (SOFC).....	12
1.4: SOFC technology.....	14
1.4.1: Cell design and fabrication.....	14
1.4.2: Electrolyte.....	16
1.4.3: Anode.....	18
1.4.4: Cathode.....	20
1.4.5: Interconnect.....	21
1.4.6: Stack design.....	22
1.4.7: Applications.....	23
1.5: Hydrocarbon fuels for SOFCs.....	24
1.5.1: Thermodynamics and kinetics.....	24
1.5.2: Fuel processing and reforming.....	27
1.5.3: Carbon deposition.....	28
1.5.4: Rationale of fuels studied.....	31
Chapter 2: Microtubular SOFCs.....	33
2.1: Summary and rationale.....	34
2.2: Cell manufacture - SOFC tubes.....	35
2.2.1: Electrolyte tube.....	35
2.2.2: Anode.....	36
2.2.3: Cathode.....	38
2.3: Cell manufacture - current collection.....	40

2.3.1: Anode: Ni mesh and pin, Ag plug.....	40
2.3.2: Cathode: Ag ink and wire.....	41
2.4: Experimental set-up.....	41
2.4.1: Cell manifolding.....	41
2.4.2: Furnace control and liquid fuel delivery.....	42
2.4.3: SOFC test rig.....	45
Chapter 3: Experimental methods and analysis.....	47
3.1: Experimental techniques.....	48
3.1.1: Reduction and cell loading.....	48
3.1.2: “Blank” electrolyte-only run.....	48
3.1.3: “Catalyst” catalyst-only run.....	50
3.1.4: “SOFC” SOFC run.....	51
3.2: Analytical techniques.....	53
3.2.1: Temperature-programmed oxidation.....	53
3.2.2: Quadrupolar mass spectrometry - MKS Mini-Lab.....	55
3.2.3: Quadrupolar mass spectrometry - calibration and rationale.....	57
3.2.4: Data processing and presentation.....	60
Chapter 4: Hydrogen and C-1 hydrocarbons.....	66
4.1: Hydrogen.....	67
4.1.1: Endurance tests.....	67
4.2: Methanol.....	69
4.2.1: Steam reforming.....	69
4.2.2: Electrical performance.....	71
4.2.3: Carbon deposition.....	73
4.3: Methanoic acid (formic acid).....	74
4.3.1: Steam reforming.....	74
4.3.2: Electrical performance.....	76
4.3.3: Carbon deposition.....	77
Chapter 5: C-2 hydrocarbons.....	80
5.1: Ethanol.....	81
5.1.1: Steam reforming.....	81
5.1.2: Electrical performance.....	84
5.1.3: Carbon deposition.....	84
5.2: Ethanoic acid (acetic acid).....	86
5.2.1: Steam reforming.....	87

5.2.2: Electrical performance.....	89
5.2.3: Carbon deposition.....	90
5.3: Ethane-1,2-diol (ethylene glycol).....	92
5.3.1: Steam reforming.....	93
5.3.2: Electrical performance.....	94
5.3.3: Carbon deposition.....	96
5.4: Methoxymethane (dimethyl ether).....	97
5.4.1: Steam reforming.....	98
5.4.2: Electrical performance.....	100
5.4.3: Carbon deposition.....	101
5.5: Methyl methanoate (methyl formate).....	102
5.5.1: Steam reforming.....	103
5.5.2: Electrical performance.....	105
5.5.3: Carbon deposition.....	106
5.6: N-methyl methanamide (N-methyl formamide).....	107
5.6.1: Steam reforming.....	108
5.6.2: Electrical performance.....	110
5.6.3: Carbon deposition.....	111
Chapter 6: C-3 and C-4 Hydrocarbons.....	115
6.1: Propane-1,2,3-triol (glycerol / glycerin).....	116
6.1.1: Steam reforming.....	116
6.1.2: Electrical performance.....	118
6.1.3: Carbon deposition.....	119
6.2: 2-Methoxyethanol.....	120
6.2.1: Steam reforming.....	120
6.2.2: Electrical performance.....	122
6.2.3: Carbon deposition.....	123
6.3: Dimethoxymethane (methylal / formaldehyde dimethyl acetal).....	124
6.3.1: Steam reforming.....	125
6.3.2: Electrical performance.....	126
6.3.3: Carbon deposition.....	127
6.4: Ethoxyethane (diethyl ether).....	129
6.4.1: Steam reforming.....	129
6.4.2: Electrical performance.....	130
6.4.3: Carbon deposition.....	131
6.5: Trimethoxymethane (trimethyl orthoformate).....	132

6.5.1: Steam reforming.....	133
6.5.2: Electrical performance.....	134
6.5.3: Carbon deposition.....	135
6.6: N,N-dimethyl methanamide (N,N-dimethyl formamide / DMF).....	137
6.6.1: Steam reforming.....	138
6.6.2: Electrical performance.....	138
6.6.3: Carbon deposition.....	139
Chapter 7: Blends with methanoic acid.....	142
7.1: Methanol / methanoic acid.....	143
7.1.1: Steam reforming.....	143
7.1.2: Electrical performance.....	144
7.1.3: Carbon deposition.....	145
7.2: Ethanol / methanoic acid.....	146
7.2.1: Steam reforming.....	146
7.2.2: Electrical performance.....	148
7.2.3: Carbon deposition.....	149
7.3: Methyl methanoate / methanoic acid.....	150
7.3.1: Steam reforming.....	151
7.3.2: Electrical performance.....	152
7.3.3: Carbon deposition.....	153
7.4: Dimethoxymethane / methanoic acid.....	154
7.4.1: Steam reforming.....	154
7.4.2: Electrical performance.....	156
7.4.3: Carbon deposition.....	157
7.5: Ethoxyethane / methanoic acid.....	158
7.5.1: Steam reforming.....	158
7.5.2: Electrical performance.....	160
7.5.3: Carbon deposition.....	160
Chapter 8: Discussion of results.....	162
8.1: Overview.....	163
8.2: Performance of fuels and blends.....	163
8.3: Mechanism(s) of carbon deposition.....	167
Chapter 9: Conclusions.....	171

Index of Figures

Figure 1: General operating principles of a fuel cell.....	9
Figure 2: General operating principles of a solid oxide fuel cell.....	14
Figure 3: Possible structure-transition state relationships for carbon deposition.....	30
Figure 4: Relational rationale for C-2 hydrocarbons studied.....	32
Figure 5: A typical microtubular solid oxide fuel cell.....	34
Figure 6: Firing profile for YSZ electrolyte.....	35
Figure 7: Anode compositional gradient.....	36
Figure 8: Firing profile for anode 1.....	38
Figure 9: Cathode compositional gradient.....	39
Figure 10: Co-firing profile for anode 2, cathode 1 and cathode 2.....	40
Figure 11: Schematic diagram of a manifolded microtubular SOFC.....	42
Figure 12: Stepper motor-driven syringes for liquid fuel delivery.....	42
Figure 14: Furnace with fuel evaporator and microtubular SOFC.....	45
Figure 13: Temperature-programmed oxidation rig with quartz tube.....	44
Figure 15: Schematic diagram of the SOFC and TPO test rig.....	46
Figure 16: "Blank" electrolyte-only tube.....	49
Figure 17: "Catalyst" catalyst-only tube.....	50
Figure 18: "SOFC" SOFC tube.....	51
Figure 19: Example idealised trends in electrical current output.....	53
Figure 20: Typical temperature-programmed oxidation example for N,N-dimethyl methanamide.....	54
Figure 21: Simplified schematic diagram of a quadrupolar mass spectrometer.....	56
Figure 22: Typical mass spectrometer scan example for an ethanol / water mixture.....	61
Figure 23: Typical composition against time trend example for an ethanol / water mixture....	62
Figure 24: Typical exhaust gas composition example for an ethanol / water mixture.....	64
Figure 25: Typical current and voltage against time trend examples for an ethanol / water mixture.....	65
Figure 26: Typical trends of current against time for SOFCs run on hydrogen.....	68
Figure 27: Methanol.....	69

Figure 28: Exhaust gas compositions of steam reformed methanol.....	70
Figure 29: Trends of relative current against time for steam reformed methanol.....	72
Figure 30: Carbon deposited as a percentage of carbon added for steam reformed methanol..	73
Figure 31: Methanoic acid.....	74
Figure 32: Exhaust gas compositions of steam reformed methanoic acid.....	76
Figure 33: Trends of relative current against time for steam reformed methanoic acid.....	77
Figure 34: Carbon deposited as a percentage of carbon added for steam reformed methanoic acid.....	79
Figure 35: Ethanol.....	81
Figure 36: Exhaust gas compositions of steam reformed ethanol.....	83
Figure 37: Trends of relative current against time for steam reformed ethanol.....	83
Figure 38: Carbon deposited as a percentage of carbon added for steam reformed ethanol....	86
Figure 39: Ethanoic acid.....	86
Figure 40: Exhaust gas compositions of steam reformed ethanoic acid.....	89
Figure 41: Trends of relative current against time for steam reformed ethanoic acid.....	90
Figure 42: Carbon deposited as a percentage of carbon added for steam reformed ethanoic acid.....	91
Figure 43: Ethane-1,2-diol.....	92
Figure 44: Exhaust gas compositions of steam reformed ethane-1,2-diol.....	92
Figure 45: Trends of relative current against time for steam reformed ethane-1,2-diol.....	95
Figure 46: Carbon deposited as a percentage of carbon added for steam reformed ethane-1,2-diol.....	97
Figure 47: Methoxymethane.....	98
Figure 48: Exhaust gas compositions of water saturated methoxymethane.....	99
Figure 49: Trends of relative current against time for water saturated methoxymethane.....	99
Figure 50: Carbon deposited as a percentage of carbon added for water saturated methoxymethane.....	102
Figure 51: Methyl methanoate.....	102
Figure 52: Exhaust gas compositions of steam reformed methyl methanoate.....	105
Figure 53: Trends of relative current against time for steam reformed methyl methanoate...	104

Figure 54: Carbon deposited as a percentage of carbon added for steam reformed methyl methanoate.....	106
Figure 55: N-methyl methanamide.....	107
Figure 56: Exhaust gas compositions of steam reformed N-methyl methanamide.....	110
Figure 57: Trends of relative current against time for steam reformed N-methyl methanamide..	111
Figure 58: Carbon deposited as a percentage of carbon added for steam reformed N-methyl methanamide.....	112
Figure 59: Propane-1,2,3-triol.....	116
Figure 60: Exhaust gas compositions of steam reformed propane-1,2,3-triol.....	117
Figure 61: Trends of relative current against time for steam reformed propane-1,2,3-triol...	118
Figure 62: Carbon deposited as a percentage of carbon added for steam reformed propane-1,2,3-triol.....	118
Figure 63: 2-Methoxyethanol.....	120
Figure 64: Exhaust gas compositions of steam reformed 2-methoxyethanol.....	122
Figure 65: Trends of relative current against time for steam reformed 2-methoxyethanol....	123
Figure 66: Carbon deposited as a percentage of carbon added for steam reformed 2-methoxyethanol.....	124
Figure 67: Dimethoxymethane.....	124
Figure 68: Exhaust gas compositions of steam reformed dimethoxymethane.....	126
Figure 69: Trends of relative current against time for steam reformed dimethoxymethane...	127
Figure 70: Carbon deposited as a percentage of carbon added for steam reformed dimethoxymethane.....	128
Figure 71: Ethoxyethane.....	129
Figure 72: Exhaust gas compositions of ethoxyethane.....	129
Figure 73: Trends of relative current against time for ethoxyethane.....	131
Figure 74: Carbon deposited as a percentage of carbon added for ethoxyethane.....	132
Figure 75: Trimethoxymethane.....	132
Figure 76: Exhaust gas compositions of steam reformed trimethoxymethane.....	134
Figure 77: Trends of relative current against time for steam reformed trimethoxymethane...	135
Figure 78: Carbon deposited as a percentage of carbon added for steam reformed trimethoxymethane.....	137

Figure 79: N,N-dimethyl methanamide.....	137
Figure 80: Exhaust gas compositions of steam reformed N,N-dimethyl methanamide.....	137
Figure 81: Trends of relative current against time for steam reformed N,N-dimethyl methanamide.....	139
Figure 82: Carbon deposited as a percentage of carbon added for steam reformed N,N-dimethyl methanamide.....	141
Figure 83: Exhaust gas compositions of steam reformed methanol / methanoic acid blends.	144
Figure 84: Trends of relative current against time for steam reformed methanol / methanoic acid blends.....	145
Figure 85: Carbon deposited as a percentage of carbon added for steam reformed methanol / methanoic acid blends.....	146
Figure 86: Exhaust gas compositions of steam reformed ethanol / methanoic acid blends....	148
Figure 87: Trends of relative current against time for steam reformed ethanol / methanoic acid blends.....	149
Figure 88: Carbon deposited as a percentage of carbon added for steam reformed ethanol / methanoic acid blends.....	150
Figure 89: Exhaust gas compositions of steam reformed methyl methanoate / methanoic acid blends.....	151
Figure 90: Trends of relative current against time for steam reformed methyl methanoate / methanoic acid blends.....	151
Figure 91: Carbon deposited as a percentage of carbon added for steam reformed methyl methanoate / methanoic acid blends.....	154
Figure 92: Exhaust gas compositions of steam reformed dimethoxymethane / methanoic acid blends.....	155
Figure 93: Trends of relative current against time for steam reformed dimethoxymethane / methanoic acid blends.....	156
Figure 94: Carbon deposited as a percentage of carbon added for steam reformed dimethoxymethane / methanoic acid blends.....	158
Figure 95: Exhaust gas compositions of steam reformed ethoxyethane / methanoic acid blends.....	159
Figure 96: Trends of relative current against time for steam reformed ethoxyethane / methanoic acid blends.....	160
Figure 97: Carbon deposited as a percentage of carbon added for steam reformed ethoxyethane / methanoic acid blends.....	161

Index of Tables

Table 1: Composition of YSZ electrolyte.....	35
Table 2: Compositions of graduated Ni/YSZ anodes.....	38
Table 3: Compositions of graduated LSM/YSZ cathodes.....	39
Table 4: Highest electrical performances of pure fuels.....	164
Table 5: Highest electrical performances of blended fuels.....	165
Table 6: Lowest carbon deposition rates for “SOFC” experiments of pure fuels.....	168
Table 7: Lowest carbon deposition rates for “SOFC” experiments of blended fuels.....	168

Chapter 1: Introduction

1.1: Project rationale

The solid oxide fuel cell (SOFC) has enjoyed a certain renaissance in recent research. Along with other types of fuel cell technology, it has been presented as part of several solutions to the growing global problems of climate change and security of energy supply. These solutions are not without their barriers to implementation, however, which is why such research is needed.

A sustainable future energy economy is likely to be based around a decentralised system of renewable electricity generation with the electron as the principal energy vector. While direct sources of energy (such as wind turbines) will provide primary power, fuel cells running on hydrogen or biologically-derived fuels will provide load balancing, remote applications and backup services. For fuel cell systems to be used effectively in this way, they require a fuel supply that can be sustainably generated, easily transported and easily stored. Most research into non-hydrogen-fuelled SOFCs has focused on natural gas (due to the existing infrastructure), but this is ultimately unsustainable. Liquid fuels meet all of the prior requirements, and have the additional advantage of high energy density. Biologically-derived fuels can be used directly or converted into a variety of different chemicals, although this will reduce the overall efficiency.

Fuels that are liquid at ambient temperatures tend to be hydrocarbons, making them unsuitable for mid- and low temperature fuel cells without external reforming (which also decreases the

overall efficiency). Both SOFCs and molten carbonate fuel cells (MCFCs) can theoretically utilise hydrocarbons directly, though the SOFC is a more promising technology due to ease of manufacture and potentially higher efficiencies when used for combined heat and power (CHP) or coupled with a gas turbine.

The direct use of hydrocarbon fuels, whilst attractive, has several problems. Any carbon-based fuel has an inherent tendency to deposit solid carbon on the anode of a SOFC, leading to a significant decline in performance over time and eventual failure. Oxidising or reforming agents (typically water) can mitigate this effect, but it has yet to be completely eliminated. “Heavy” hydrocarbons (containing many carbon atoms) tend to deposit carbon more readily than lighter ones, and so the fuel/oxidant ratio must be considered more carefully.

SOFCs have been shown to operate on reformed heavy hydrocarbons, but smaller hydrocarbons can theoretically be used with no external reforming, increasing efficiency and reducing stack costs. As any fuel has to be oxidised, oxygenated hydrocarbons may be more suited to SOFC operation than non-oxygenated ones. Thus, small oxygenated liquid hydrocarbons are a promising area of research and the topic of this thesis.

It can be speculated that the extent of carbon deposition is at least partially dependent upon the structure of the fuel. Larger molecules contain carbon-carbon bonds, and have a strong tendency to deposit carbon. This may be due to fragmentation through the cleavage of C-C bonds, lower stability or lower reactivity towards oxidation. A logical way to investigate this would be to test fuels with multiple, yet segregated, carbon atoms. Examples include

dimethoxymethane and methyl methanoate, the preliminary test results of which have been published.^[1-3]

Carbon deposition is not the only mechanism by which SOFC performance degrades, but is often dominant with hydrocarbon fuels. Effects such as nickel agglomeration (the gradual aggregation of Ni particles, reducing catalytic activity and the three-phase boundary area) can cause severe long-term problems, but are beyond the scope of this study.

There are several types of SOFC, but the microtubular design can be manufactured quickly and easily, and has very low start-up and shut-down times. This makes it especially suitable for testing different fuel formulations, as an acceptable throughput can be achieved. Although the electrical performance is lower, especially in single-cell tests, this is not as relevant to fuel reforming - the reaction products and relative changes in electrical output are more significant and so are studied here.

1.2: The global energy situation

1.2.1: Current fuel technologies

Since the Industrial Revolution and the advent of the modern age, accessible sources of energy have become increasingly important to human society. Logically, technologies to convert one type of energy into a more useful type (such as coal into electricity) have been developed and

refined over the same period. Current energy development can be loosely categorised into stationary and portable applications. Stationary applications tend to focus on electricity generation for national and local grid supplies, whereas portable applications consider both electricity and motive power.^[4]

Grid electricity generation in the developed world has evolved to suit large, centralised power stations distributing electricity along a network. Most operate on thermal principles, driving a generator via a steam or combustion turbine. Combined cycle plants (utilising both types of turbine) with co-generation (combined heat and power) typically run at an efficiency of around 55%, and there are additional losses incurred during transmission.

Portable power sources are dominated by batteries (for electrical power) and the internal combustion engine (for motive power). Batteries, whether primary or secondary cells, utilise chemical reactions to generate electrical current and research has focused on size, weight and capacity. Internal combustion engines (jet, rotary and piston) burn hydrocarbon fuels to provide motive power via the heat and pressure generated and research has focused on fuel efficiency and emissions.

1.2.2: The global energy crisis

Global energy needs are currently met predominantly by coal, oil and gas, with significant smaller contributions from nuclear and hydro. These energy sources, with the exception of hydro, are finite - the supply of fuel will eventually run out. There is much debate surrounding

the issue of just how long it will be economically and environmentally viable to continue extracting fossil fuels, but most analysts agree that the practice will decline and cease sometime in the mid-to-late-twenty-first century.^[5]

The oil crises of 1973 and 1979 threw the dependence of the developed world upon oil supply into sharp relief. Rapidly rising prices had a crippling effect upon industrial and domestic energy use, prompting measures such as fuel rationing. Security of oil supply has since become a more important issue, exemplified by recent wars in the Persian Gulf. The global demand for oil is set to rise rapidly in the coming decades, due to increased consumerism in the West and emerging markets in countries such as China and India.

Global energy uncertainty is not limited to oil. Ageing electricity grids, privatisation and decommissioning of old power stations have led to electricity crises in developed countries. Similar situations, though usually for different reasons, exist in the developing world. As with oil, electricity demand is predicted to rise sharply in the coming decades.

1.2.3: Climate change and the environment

In addition to concerns about the supply of fossil fuels, there is a global scientific consensus that emissions of greenhouse gases are causing the Earth's climate to change. Converting fossil fuels into a more useful form of energy (with the exception of nuclear) invariably involves burning them, which releases carbon dioxide into the atmosphere. Increased levels of

atmospheric CO₂ enhance the greenhouse effect, causing excessive global warming with subsequent effects on other climatic processes such as ocean currents.

There are environmental considerations surrounding most current fuel technologies. The extraction of oil and gas is damaging to wildlife in the area, and access to supplies often leads to military action. Coal and uranium mining also damage the local environment and can be hazardous to workers. Hydro power requires the flooding of large areas, displacing people and destroying the existing landscape. Even the growing of biofuels, supposedly carbon-neutral, is causing the destruction of tropical rainforests and taking up land that would otherwise have been used for food crops.

Although there has been little political movement on the issue, most governments agree that human emissions of CO₂ and other greenhouse gases (such as methane) must be drastically reduced. Ultimately, this will require wholesale changes in modern lifestyles and in the way electricity is generated and distributed.

1.2.4: The move to alternative and renewable fuels

The realisation that supplies of fossil fuels will eventually decline (increasing extraction costs), coupled (more recently) with the threat of various environmental catastrophes, has stimulated interest in “alternative” and renewable energy sources. These have little or no reliance on fossil fuels and produce little or no pollution. Examples include wind turbines, solar photovoltaic panels and geothermal stations.

There has also been interest in increasing the efficiency of current technology (reducing energy demand rather than increasing supply), with a parallel reduction in fuel use and pollution. Common examples include hybrid vehicles, domestic co-generation of heat and power and wall cavity insulation.

There is a general consensus that humans cannot consume at present levels without seriously endangering the entire planet, yet governments are unwilling to disrupt the status quo and risk corporate ire by investing resources in new technologies. A limited amount of funding has been made available, but it will take considerable political will to force a complete shift in energy policies.^[6]

1.3: Fuel cell technology

1.3.1: Background

Fuel cells are examples of “alternative” technologies that have enjoyed increased interest in recent years due to energy security and environmental considerations. Although the concept was demonstrated in the mid-nineteenth century, viable models were not developed until the 1960's.

All fuel cells work on similar principles; they are essentially batteries capable of operating with a continuous supply of fuel. Fuel and oxidant are separated and react at electrodes to give

ions and electrons. Ions travel through an ion-conducting membrane while electrons travel around an external circuit to do work (Figure 1).

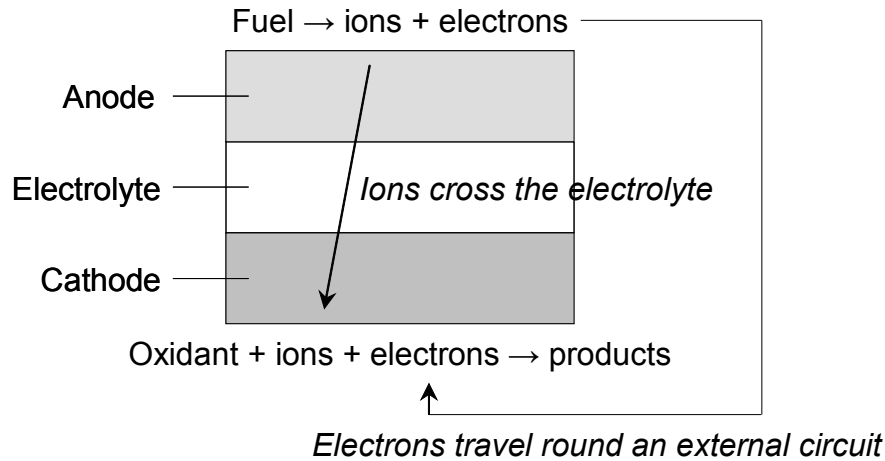
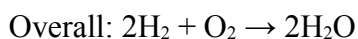


Figure 1: General operating principles of a fuel cell

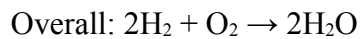
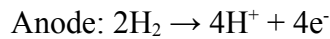
1.3.2: Alkaline fuel cell (AFC)

The alkaline fuel cell (AFC) uses an aqueous alkaline solution (e.g. KOH) as an electrolyte, with hydroxyl (OH^-) as the mobile ion. The electrolyte is easily poisoned, so pure oxygen or purified air and pure hydrogen are required. AFCs were used on NASA's Apollo missions and on the space shuttle, though are now being phased out in favour of PEMFCs.

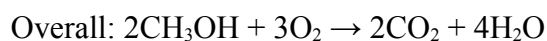


1.3.3: Proton exchange membrane fuel cell (PEMFC)

Proton exchange membrane fuel cells (also called polymer electrolyte membrane fuel cells) have similar operating requirements to the AFC - they require pure hydrogen and oxygen, and are poisoned by CO and CO₂. The principal difference is in the use of a solid, proton-conducting electrolyte such as Nafion[®], a sulfonated fluoroethene, and carbon-supported platinum catalysts in the electrodes. Due to these catalysts, PEMFCs are relatively expensive and, if used with hydrocarbon fuels, require reforming subsystems to produce a poison-free fuel stream.



The direct methanol fuel cell (DMFC) is a type of PEMFC that uses methanol directly at the anode rather than hydrogen. The rate of reaction is very slow, resulting in low efficiency, and fuel can be absorbed into the electrolyte membrane. However, the advantages of a liquid fuel mean that there is still much interest in perfecting this type of fuel cell:

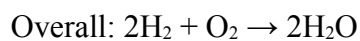
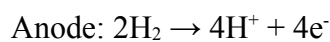


Although DMFCs produce CO₂ as an exhaust gas, methanol can be fermented from biological material in a similar manner to ethanol, making the overall fuel life cycle carbon-neutral.

PEMFCs are widely used in portable applications such as vehicles and mobile devices due to their low (<100 °C) operational temperatures and rapid start-up times. Most commercial research is focused on bringing this type of fuel cell to market.

1.3.4: Phosphoric acid fuel cell (PAFC)

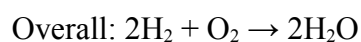
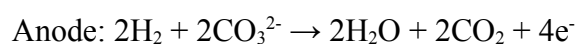
The phosphoric acid fuel cell (PAFC) is characterised by its use of phosphoric acid (H₃PO₄) as a proton-conducting electrolyte. It operates at a typical temperature of 220 °C (phosphoric acid freezes at 42 °C, so the temperature is usually maintained for the lifetime of the cell) and is tolerant to small concentrations of CO and CO₂. Hydrogen fuel is often reformed on-site from natural gas or another readily-available feedstock.



This type of fuel cell system is well-established, having been used for several decades in backup and CHP applications. Typical installations are in the 200 kW range, but multi-MW plants have been built for grid-quality power.

1.3.5: Molten carbonate fuel cell (MCFC)

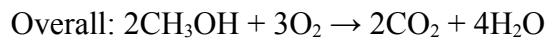
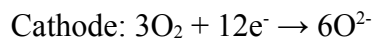
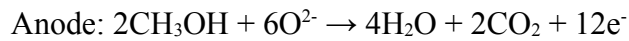
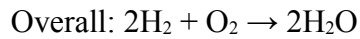
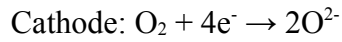
Molten carbonate fuel cells (MCFCs) operate at relatively high temperatures, typically 650 °C. The electrolyte is a carbonate-conducting mixture of sodium and potassium carbonates that becomes liquid at operating temperatures. This type of fuel cell is tolerant to CO and CO₂ (CO can even be oxidised as a fuel), allowing hydrocarbon fuels to be used.



CO₂ is required as an input in order to generate the CO₃²⁻ ions. Some of this can be supplied if air (rather than pure oxygen) is used as an oxidant, but it is commonly recycled from the anode exhaust gas. Captured CO₂ from hydrocarbon-based power generation could also be used, reducing greenhouse gas emission.

1.3.6: Solid oxide fuel cell (SOFC)

The solid oxide fuel cell (SOFC) operates at high temperatures (typically 600 °C - 1000 °C) and is characterised by the use of a solid-phase oxide ion-conducting electrolyte. Like the MCFC, this type of fuel cell is tolerant to CO and CO₂, and can oxidise hydrocarbons (methanol is used here as an example) directly on the anode - a process known as electrocatalytic oxidation.



One of the main differences of the high temperature fuel cells (i.e. MCFC and SOFC) from other types is the direction of ion conduction. Ions are generated by reduction of the oxidant at the cathode and travel through the electrolyte to oxidise the fuel, rather than fuel being oxidised at the anode and ions travelling through the electrolyte to reduce the oxidant. The flow of electrons is unchanged (Figure 2).

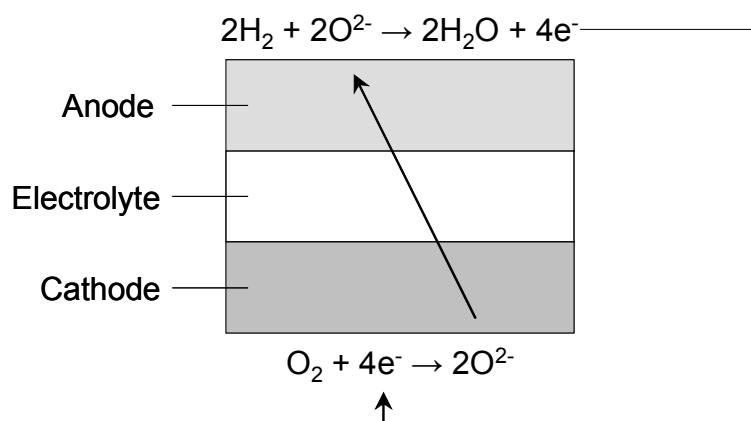


Figure 2: General operating principles of a solid oxide fuel cell

Oxidation and reduction reactions at the electrodes take place in a region known as the three-phase boundary, which exhibits mixed ionic and electronic conductivity. This allows fuel / oxidant, electrons and ions to enter and leave a reaction zone. The greater the area of the three-phase boundary, the more efficient the reduction and oxidation reactions will be.

Currently, the main development issues in typical SOFCs are those of operation on hydrocarbons (the fuels tend to deposit carbon on the anode), long-term performance (metal particles in the anode agglomerate over time, reducing the effectiveness) and stability to electrical and thermal cycling.^[7]

1.4: SOFC technology

1.4.1: Cell design and fabrication

Advances in SOFC design have been principally limited to refinements of the basic tubular and planar architectures, seeking to solve the various inherent problems. Key design and fabrication issues are the delivery (manifolding) and flow of fuel gases, the optimisation of electrical/electrochemical performance and the thermal/mechanical management of the cell itself.

Planar SOFCs are similar in appearance to the operating principles diagram (Figure 2), with flat components arranged in layers like rock strata. Gases are delivered to the flow assembly

either through an internal (integrated) or external manifold^[8] and various configurations have been used to enhance gas flow across electrodes,^[9] usually as part of the interconnect or electrode design. Uniform gas flow simplifies thermal and mechanical management, as the number of hot / cold zones is reduced. Tubular and microtubular SOFCs have an identical layering arrangement, but components are applied to an elongated tube like a concentric target design. These SOFCs due to their shape tend to have far simpler manifolding, flow and thermal requirements,^{[10], [11]} and a flattened tube design for shorter conduction pathways has recently been developed.^[12] There is also some interest in single chamber (SC) SOFCs, where the fuel and oxidant are mixed and exposed to a selective fuel cell rather than being separated.^{[13], [14]}

As outlined previously, a SOFC is made up of several layers, and generally the thinner these layers are the better a cell will perform (through reduced ionic or electronic resistance). However, mechanical support via a relatively thick (>100 μm) layer is required to prevent the cell breaking under even small amounts of mechanical stress. Support may come from the electrolyte, anode, cathode, interconnect or an inert porous substrate,^[8] each method with advantages and disadvantages. Current research tends towards the development of anode-supported cells in order to reduce the electrolyte thickness and thus the operating temperature (see the next section).^[15]

Cell fabrication is based on particulate methods, deposition methods or a combination of the two to make the mechanical support and other cell components. The particulate approach involves tape casting^{[16], [17]} or tape calendaring^[18] (for planar SOFCs), or extrusion^{[19] - [21]} (for

tubular), all of which are relatively simple and inexpensive. Deposition methods are considerably more complex, and are often used to lay down thin layers upon an existing support. They include screen printing,^[22] sputtering,^{[23], [24]} dip coating,^[25] spin coating,^[26] spray pyrolysis,^{[27], [28]} electrophoretic deposition,^[29] slip casting,^[30] electrochemical vapour deposition (EVD)^{[31], [32]} and plasma spraying.^[33]

1.4.2: Electrolyte

Since solid oxide fuel cells first emerged in the 1970's and 1980's, the focus of electrolyte development has been on improving oxide ion conductivity and reducing the operational temperature. Specific ion conductivity increases with temperature, and hence absolute ion conductivity can be increased by either increasing the temperature or reducing the electrolyte thickness. In all electrolytes, oxide ion conduction only becomes significant above ≈ 600 °C, which puts severe constraints on the types of materials that can be used and thus increases costs.

The best known oxide ion conductors have the fluorite, perovskite or pyrochlore structure, and of these the stabilised zirconias are most commonly used in SOFCs.^[34] Early compositions used CaO-stabilised ZrO₂ (CSZ), but this was quickly replaced with Y₂O₃-stabilised ZrO₂ (YSZ)^[35] due to higher ion conductivity and lower activation enthalpy.

YSZ forms the basis for the majority of modern SOFC electrolytes,^{[36], [37]} and has been extensively studied due to its high ionic conductivity, low electronic conductivity and stability

under both oxidising and reducing conditions.^{[38] - [40]} There is little current research into optimal doping levels or structural refinement, as these are well known, though there is some interest in fabrication method-property relationships (for example, nanocrystalline powders^{[41] - [43]}).

Within zirconia research, there is much interest in dopants other than Y_2O_3 that may give better performance as a SOFC electrolyte. Sc_2O_3 and Yb_2O_3 in particular have been studied due to improved ionic conductivities,^{[44], [45]} though cost and long-term performance issues currently limit their effectiveness.

As an alternative to doped ZrO_2 , doped CeO_2 is another fluorite that has been extensively studied due to very high ionic conductivities.^{[46], [47]} However, it exhibits electronic conductivity at high temperatures and tends to reduce if oxygen partial pressures are low, reducing its potential as an electrolyte material.^{[36], [37]} Research has focused on intermediate temperature (<700 °C^[48]) applications and suitable dopants to improve high temperature behaviour.^[49] Examples of typical dopants include CaO , Y_2O_3 , Gd_2O_3 , Sm_2O_3 and Bi_2O_3 .

Bi_2O_3 has also been studied as a potential intermediate temperature electrolyte material,^{[50], [51]} usually with doping to avoid reduction. The BIMEVOX class of electrolytes,^[52] $Bi_2V_{1-x}Me_xO_y$ where Me is a metal (such as $Bi_2V_{0.9}Cu_{0.1}O_{5.35}$), are based on $Bi_4V_2O_{11}$ and exhibit very high ionic conductivity, but tend to decompose at elevated temperatures.

Several electrolytes based on the perovskite (ABO_3) structure have been investigated with the aim of lowering the SOFC operating temperature.^{[53], [54]} Examples include $LaGaO_3$ doped with group 2 or transition elements,^{[55] - [57]} Ca-doped $LaAlO_3$ ^[58] and $LaScO_3$.^[59] Electrolytes with other structures such as $Ba_2In_2O_5$,^[60] $Sr_3In_2HfO_8$ ^[61] and $Nd_{10}Si_6O_{27}$ ^[62] have also been studied, but to a much lesser extent due to effective market domination by the fluorites and perovskites.

It is also possible for SOFCs to use proton-conducting electrolytes, though these are not as widely studied as the oxide-conducting ones. The ability to conduct protons was first demonstrated in doped $BaCeO_3$,^{[63], [64]} and since then in improved perovskites such as Y-doped $BaZrO_3$ ^[65]. These electrolytes are attractive when considering operation on hydrocarbons due to a reduction in coking and immediate water removal^[66].

1.4.3: Anode

A SOFC anode is responsible for oxidising the fuel, and so must be able to operate under a strongly reducing environment whilst retaining high electronic conductivity and high activity for fuel oxidation reactions (thus, high ionic conductivity). On a more practical level, it must have high porosity for gas transportation and similar thermal properties to the other cell components so that there is no deformation / delamination upon heating or cooling.^[15]

At the high operating temperatures required by the oxide ion-conducting electrolyte, only materials such as nickel, cobalt and the noble metals make suitable anode materials under the

conditions set out above.^{[37], [67]} Anodes made of pure metals such as Ni, Co, Pt and Ru have been used,^[68] but the mismatch in thermal expansion coefficients caused fracture and delamination upon heating to operational temperature, resulting in loss of activity.

In order to fabricate an acceptable anode, a metal-ceramic composite known as a cermet was developed where metal particles are dispersed with a ceramic material (usually the same as the electrolyte). The most common anode is the Ni/YSZ cermet, used due to the low cost and high activity of nickel and the relative ubiquity of the YSZ electrolyte, which has been extensively studied.^{[15], [69]} Adding YSZ to the Ni anode provides a better thermal expansion coefficient match,^[70] increases the three-phase boundary area^[71] and inhibits Ni particle sintering / agglomeration^[72] without preventing electronic conduction.^[73]

Activity and stability towards hydrocarbon fuels is an important issue when considering anodes, and much research is concentrated on this. Although the Ni/YSZ anode is highly active for H₂ oxidation, it is less convenient for hydrocarbon fuels due to carbon deposition, sulfur poisoning^[74] and metal dusting^[75] (a phenomenon where an anode corrodes into a fine dust of metal particles and carbon, also seen for Fe and Co-based anodes).

Metals other than Ni and ceramics other than YSZ have also been investigated for use in composite anodes. Co/YSZ^[76] and Ru/YSZ^[77] have received some attention, but high costs have limited their use. Ni-YSZ anodes have been outperformed by Ni/Gd- or Sm-CeO₂ (Ni/GDC or Ni/SDC) at lower temperatures,^{[78], [79]} and Ni/TiO₂-YSZ at higher temperatures.^[80]

Work has also been done on Cu-CeO₂-YSZ composites for lower temperature operation and lower carbon deposition when fuelled with hydrocarbons.^{[81] - [83]}

Mixed ionic and electronic conducting oxides also make suitable anode materials, and tend to have better thermal expansion coefficient matches with the electrolyte due to their ceramic nature. Both Gd- and Sm-doped CeO₂ have been studied as anodes as well as an electrolytes (the dopants aid with reforming, as the pure oxides perform well on H₂ but have low catalytic activity towards hydrocarbons),^{[49], [84]} and TiO_x-based anodes such as TiO_x-YSZ,^[85] Y_{0.2}Zr_{0.62}Ti_{0.18}O_{1.9},^[86] and La/Nb/Y-SrTiO₃,^{[87], [88]} have also been investigated. Lanthanum chromite (LaCrO₃)-based materials are currently used as interconnects in some SOFC stacks and have shown good potential as anode materials, especially when doped with Sr^[89] or other group 2 or transition elements.^[90]

1.4.4: Cathode

In a similar manner to the anode, the cathode must have good mixed ionic and electronic conductivity, stability under strongly oxidising conditions and a thermal expansion coefficient close to that of the electrolyte. Few materials meet these requirements, and the most abundant cathode materials at present are the doped lanthanum manganites (LaMnO₃), *p*-type perovskite oxides, which replaced more costly materials such as Sn-doped In₂O₃.^[91]

The most common cathode material is LaMnO₃ doped with Sr to give La_{1-x}Sr_xMnO_{3-x/2} (LSM),^{[92], [93]} and different properties can be obtained by substituting the various metals for other ones

(examples include Y, Ce, Nd, Ca, Co and Pr).^[36] Similarly, the LaCoO₃ cathode base^{[94], [95]} is often doped with Sr, Ce, Dy and Fe.^[96] Solid solutions of doped LaMnO₃ with LaCoO₃^[97] and LaCrO₃^[98] have also been studied.

Although doped LaMnO₃ and LaCoO₃ have an effective monopoly on current cathode composition, there is some research into other compounds such as Sm_{1-x}Sr_xCoO₃ (SSC),^[99] Pb₂Ru₂O_{6.5}^[100] and La_{1-x}Sr_xCuO_{2.5-δ}.^[101]

Far more research is conducted into anodes than cathodes for two principal reasons. Firstly, as mentioned above, few materials meet the strict operational requirements. Secondly, a shift towards electrode support and the use of hydrocarbon fuels places more emphasis on the anode as the (more complicated) reforming and oxidation reactions take place there. By comparison, the reduction of O₂ is well understood.

1.4.5: Interconnect

Interconnects are of more relevance when multiple cells are arranged in a stack, but are always required to transport electrons in and out of a system. They must be stable in both the oxidising and reducing environments of air and fuel, exhibit high electronic conductivity and low ionic conductivity, and have suitable thermal properties.^[8] The only known materials that meet these requirements are the rare earth chromites and some metallic compounds.

The most common ceramic interconnect material is group 2-doped LaCrO_3 (which is also being investigated as an anode),^{[102],[103]} but Ca-doped YCrO_3 has also received some attention^[104] due to greater stability. The principal disadvantage with these materials is that they are difficult to sinter to full density, primarily due to the vaporisation of Cr-O species,^[105] and viable methods of processing the rare earth chromites are still being investigated.

Interconnects based on metallic components would eliminate most of the problems associated with ceramic-based ones (principally the fabrication difficulties and cost),^[106] but inevitably require a drop in the SOFC operating temperature. Cr-based alloys (for example, Cr 5Fe $1\text{Y}_2\text{O}_3$ ^[107]) and high-Cr ferritic steels^[108] enjoy most research attention, but Ni-based alloys^[109],^[110] and FeCrAlY-Ag steels^[111] are also studied.

The main disadvantages of metallic interconnects are their tendencies to release cathode-poisoning Cr species^[112] (for example, H_2CrO_4) and to form insulating oxide layers.^[113] Both of these problems are under investigation via improved formulations and protective coatings (for example, LaCoO_3 with Sr- LaCrO_3 ^{[114],[115]}).

1.4.6: Stack design

Although single-cell tests provide useful information about fuel reactions and construction materials, for any SOFC to be used in a real-world application it must form part of a multi-cell stack. There are several ways of connecting individual cells together in series and/or parallel

so that they form a single unit,^{[8], [37]} most of which depend strongly on the type of cell (i.e. tubular or planar).

Planar cells by their general shape tend to be more easily incorporated into stacks. The flat-plate design in particular allows simple stacking with the shape of the interconnect providing fuel and oxidant flow channels. The monolithic design uses corrugated cell components, and due to the relative complexity of their manufacture these has not been developed as much as the pure flat-plate design. Both require high temperature sealing around the plate edges, which is a continuing unsolved problem.

Microtubular stacks are connected simply in series and parallel by connecting cathode wires between cells and anodes at the fuel manifold.^[116] Larger, more commercialised, systems (such as the Siemens-Westinghouse) adopt an advanced seal-less design where LaCrO_3 interconnects and Ni felt join adjacent anodes and cathodes, eliminating the need for high temperature gas-tight seals.

The segmented series configuration lays down planar-like cells on a tubular support, allowing improved efficiency through reduced resistance. A similar concept with planar supports, known as the integrated planar SOFC, has recently been developed at Rolls-Royce.^[117]

1.4.7: Applications

SOFC technology is currently too expensive and insufficiently advanced to have many applications outside of research and development. Cost reduction will come with further

refinement of materials and designs, as will the required improvements in long-term performance and stability.

Several potential applications exist, however, from mW levels up to GW. As even intermediate temperature SOFCs run relatively hot, residential and commercial CHP is a major niche that SOFCs are well suited to. Increased efficiency, reduced emissions and the growing trend for distributed energy systems make stationary generation an important research area. For larger (100 MW +) installations, SOFCs combined with gas turbines offer similar advantages for centralised generation.

The high operating temperatures, while an advantage for stationary applications, can be a significant drawback for portable uses due to the relatively high volumes required for insulation and peripheral systems. They may find use on larger vehicles such as trains and ships as auxiliary power or backup units.

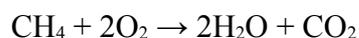
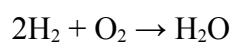
1.5: Hydrocarbon fuels for SOFCs

1.5.1: Thermodynamics and kinetics

Thermodynamically, the work of a SOFC can be defined in terms of the Gibbs free enthalpy of reaction, $\Delta^r G$. It can be shown that the electrical current is proportional to the amount of used fuel and that the reversible work is proportional to the reversible voltage.^[10]

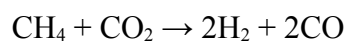
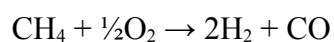
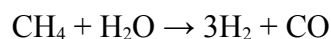
Thermodynamic studies of suitable SOFC fuels tend to focus on equilibrium reaction products and optimal fuel compositions / operating conditions, while kinetic studies, for the same reasons, focus on the myriad competing reactions.

The “basic” fuel cell reactions are the oxidation of hydrogen to water, the oxidation of carbon monoxide to carbon dioxide and the direct oxidation of hydrocarbons (methane is used here as an example). All are exothermic and have Gibbs free energy changes (at 900 °C) of -249 kJ mol^{-1} , -282 kJ mol^{-1} and -796 kJ mol^{-1} respectively:

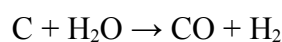
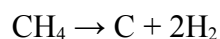
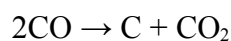
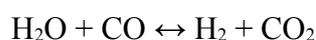


Instead of direct oxidation, fuels can be reacted with an oxidising agent (a process known as reforming); the most common methods being steam reforming, partial oxidation and dry reforming. Steam and dry reforming are endothermic, while partial oxidation is exothermic.

The objective is not to oxidise the fuel to CO_2 , but to produce gases (typically H_2 and CO) that are more suitable for use in a fuel cell:



During fuel cell operation, there are other competing reactions between the various gases. The most common are the water gas shift reaction (exothermic, so SOFC temperatures favour CO production) and the Boudouard reaction (endothermic) to form carbon on the anode. Carbon can also be formed through hydrocarbon pyrolysis, and removed through steam gasification (both endothermic):



The details of methane reactions have received surprisingly little attention considering that it is the principal component of natural gas. Of the various reforming methods, exhaust gas recycling (CO_2 / dry reforming) was shown to be the most efficient,^[118] and the $\text{CH}_4/\text{H}_2\text{O}$ ratio had no effect upon the rate of reaction (though it did affect the equilibrium).^[119] A more recent study showed the reaction kinetics to be more complex and dependent on the partial pressures of both H_2 and H_2O .^[120]

As with methane, methanol is a strong candidate fuel for future SOFC applications, and yet has not been the subject of extensive thermodynamic studies. Since an initial investigation,^[121] the reforming mechanisms have been derived^[122] and the conditions for H_2 production optimised.^{[123], [124]}

Ethanol is easy to produce and handle but difficult to use in fuel cells (due to its tendency to deposit carbon), making it a subject of some interest. Since initial reviews for MCFC applications,^{[125], [126]} studies have focused on steam reforming,^{[127], [128]} CO₂ reforming and partial oxidation^[129] at various steam ratios, temperatures and pressures to generate H₂-rich fuel feeds for low temperature fuel cells.^[130]

Apart from two recent studies,^{[131], [132]} the thermodynamics and kinetics of other light oxygenated SOFC fuels have not received much attention, although their potential has been noted.^[133]

1.5.2: Fuel processing and reforming

As described earlier, two of the principal advantages of SOFCs are tolerance to CO/CO₂ and the ability to use hydrocarbon fuels without the need for an external reformer. Any reforming required can take place either directly on the anode (direct internal reforming)^{[134], [135]} or with an integrated reformer in the fuel cell stack itself (indirect internal reforming).^[136]

Catalysed steam reforming reactions only require nickel particles, but electrocatalytic oxidation can only occur at the three-phase boundary. The graduated Ni/YSZ cermet provides both a fixed catalyst and an extended area where fuel molecules can combine with oxide ions to lose electrons. The most common reforming mechanisms are the water gas shift reaction,^[137] partial oxidation^{[138], [139]} and CO₂ oxidation (dry reforming),^{[140], [141]} all of which are susceptible (to varying degrees) to carbon deposition and catalyst re-oxidation. They have

been studied extensively over several decades,^{[8], [142]} leading to a good understanding of the reactions involved, the activities of various catalysts and the optimal levels of fuel and oxidant. In addition to these well-known methods, hydrocarbons containing more oxygen than carbon (such as methanoic acid, CH_2O_2) can be considered as oxidising agents as well as fuels. This would increase the overall efficiency by either increasing the fuel's energy density (through lower fractions of water) or reducing the need for gaseous oxidant addition.

SOFCs can also, in theory, operate directly on hydrocarbons via electrocatalytic oxidation,^[143] but this often leads to increased carbon deposition. For deposited carbon to be removed from the anode, it has to be oxidised (by H_2O or O^{2-}), resulting in the formation of new carbon-oxygen bonds. If these bonds already exist in the molecule (for example, as in CH_3OH rather than CH_4), they may either reduce the likelihood of the carbon being deposited in the first place or remain when the C-Ni bond is formed (as in $\text{Ni}(\text{CO})_6$), making subsequent desorption more favourable. The carbon atom is effectively pre-oxidised, which should reduce the need for external oxidising agents and thus increase efficiency.

Several sulfur-containing compounds (such as H_2S , HSC_2H_5 and $\text{C}_4\text{H}_8\text{S}$) are found in naturally-occurring hydrocarbons or are added as odourants. SOFC anodes and reforming catalysts are slightly tolerant to sulfur, but are irreversibly poisoned by high levels or prolonged exposure.^{[74], [134]} The removal of sulfur-containing compounds is an additional step in the fuel processing, reducing overall efficiency.

1.5.3: Carbon deposition

Although the high operating temperature and metallic anode of the SOFC make it suitable for the direct reforming of hydrocarbons, the principal drawback is that of carbon deposition. This is a well-known effect,^{[144], [145]} and occurs to some extent with virtually all hydrocarbon fuels. The more carbon atoms a molecule contains, the more carbon deposition is likely to occur (through fragmentation and higher “carbon density”).^{[146], [147]} This deposition leads to the deactivation of catalyst sites and, in extreme cases, physical blockage or fracture of the cell. It is avoided by judicious choice of reaction conditions (e.g. temperatures too low for carbon to form) or by the addition of an oxidant (typically water) to oxidise deposited carbon to CO₂. A C:O ratio of at least 1 is usually required to avoid carbon build-up, and carbon-free conditions may necessitate a ratio of up to 8.

Different carbon species are known to exist, and are deposited at varying rates depending upon the reaction conditions. Carbide species (C bonded to Ni) are formed below ≈ 350 °C, and so are not usually observed in SOFCs. Adsorbed (amorphous) carbon is formed above ≈ 350 °C, and graphitic layers above ≈ 450 °C;^[148] both can be deposited in hydrocarbon-fuelled SOFCs.

Metal-carbonyl, metal-alkyl and metal-alkene complexes (through σ -bonding and π -backbonding) are well known in liquid-phase organometallic chemistry. Various mechanisms for the formation of metal-carbon bonds have been described, but none have been applied to gas-phase heterogeneous catalysis. Interactions between metals and larger alkyls often proceed

via a three- or four-membered transition state. If a fuel molecule contains carbon-carbon bonds, then there is an additional carbon atom in close proximity when a C-Ni bond is formed, increasing the probability of further carbon deposition. If the close atom is (for example) an oxygen, then a single C-Ni bond and a good leaving group (CO) are formed instead (Figure 3). This theory of carbon atom separation is tested in several of the fuels used.

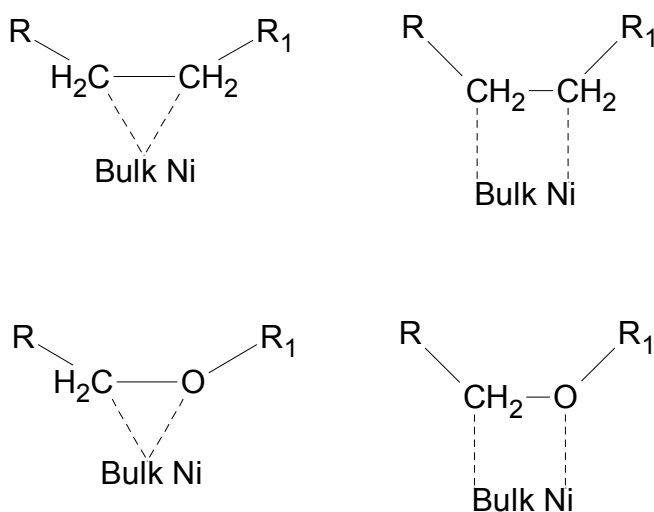


Figure 3: Possible structure-transition state relationships for carbon deposition

Small levels of carbon deposition have been shown to be beneficial to cell performance.^[149]

Following reduction, Ni particles are dispersed on the anode surface and separated for maximum surface area (and hence maximum catalytic activity). Depending on the method of manufacture and the reduction conditions, Ni particle size may vary from nanometres to micrometres. Deposited carbon can link these particles, improving electrical conductivity and thus increasing current output. If the rate of carbon deposition is sufficiently low so as not to hinder catalytic activity, overall cell performance is improved.

Much research has been undertaken into alternative anode compositions (for example, doping with Mo, Cu, Ru or Au)^{[148], [150], [151]} and operating conditions^[152] which reduce the amount of coking. The more oxidant (e.g. steam) required to inhibit carbon deposition, the lower the efficiency of the cell will be - hence the drive to find other ways of preventing performance loss. The approach of modifying the fuel itself, other than through reforming reactions, has not been extensively studied and is thus the principal objective of this investigation.

1.5.4: Rationale of fuels studied

Hydrogen and C-1 hydrocarbons were studied to provide baseline data against which other, not so well-understood, fuels could be compared. The key elements of the theories to be tested were the effects of carbon pre-oxidation, the separation of carbon atoms and the use of another fuel as an oxidising agent. A typical progression between different fuels for the first two cases is shown in Figure 4, illustrating the process for C-2 hydrocarbons.

As the main theoretical argument of this thesis concerns structure-performance relationships, the fuels studied were selected principally for their molecular architecture. Considerations such as the practicality of applications and sustainable sources were noted, but of less concern than those of academic interest. Specific reasons for the use of particular fuels are noted in the accompanying text, but all illustrate aspects of the theories to be tested.

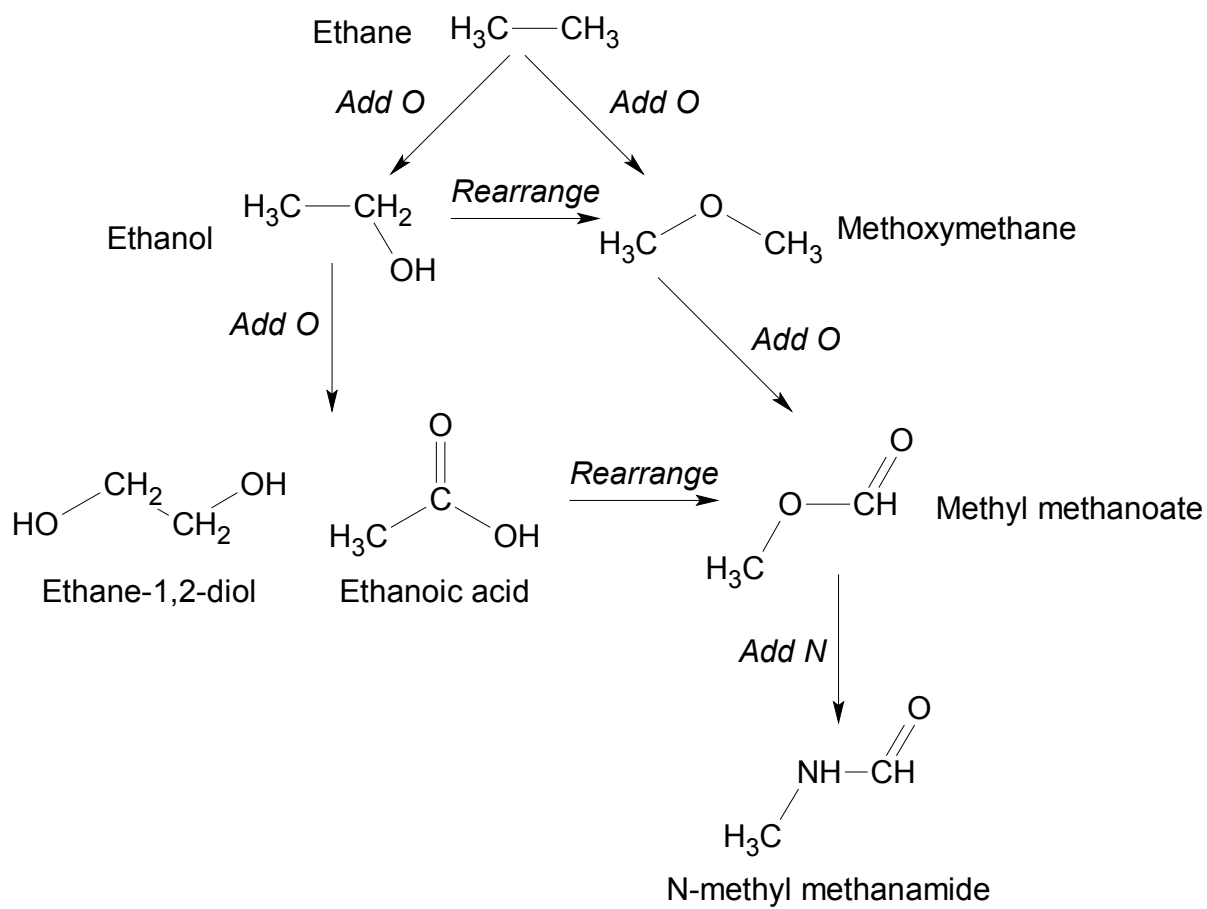


Figure 4: Relational rationale for C-2 hydrocarbons studied

Chapter 2: Microtubular SOFCs

2.1: Summary and rationale

Experiments were conducted on 3 mm diameter electrolyte-supported microtubular SOFCs, with an electrolyte thickness of approximately 220 μm and an active electrode length of approximately 40 mm. As the focus of this study was fuel composition and reactions, this design was chosen for its ease of manufacture, lack of complex manifolding requirements and rapid start-up / shut-down times. Various fuels were delivered to the SOFC; electrical performance was measured with a potentiostat and exhaust gases were analysed with an on-line MKS Mini-Lab quadrupolar mass spectrometer.

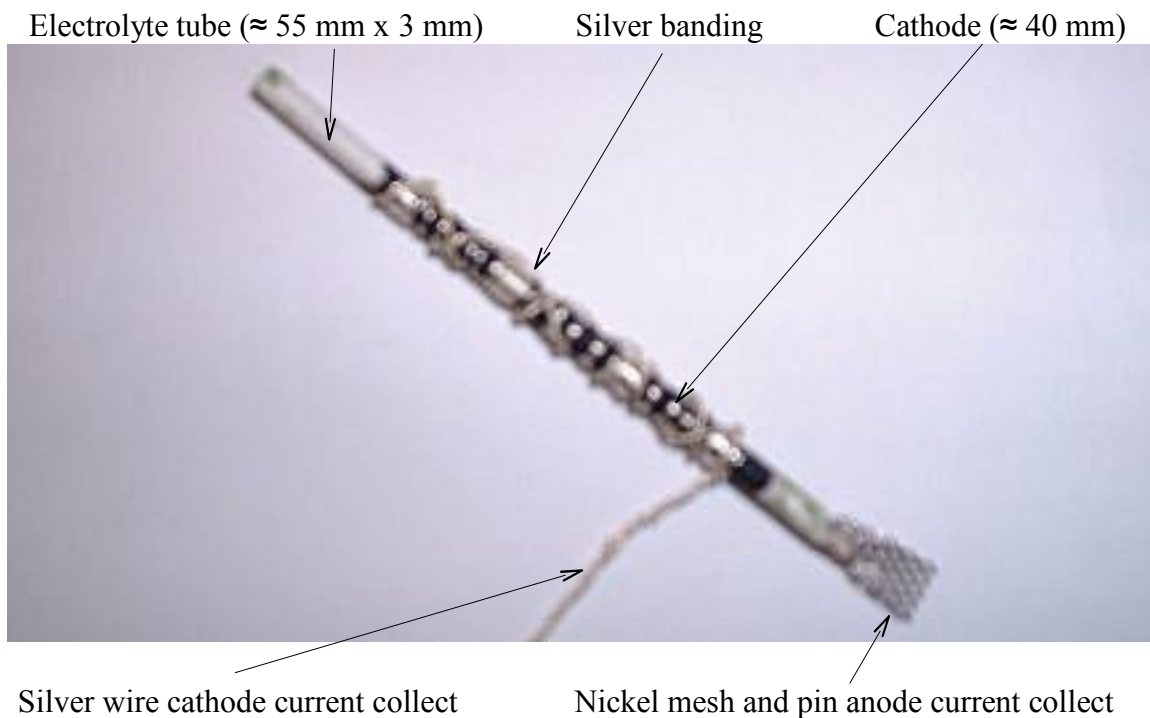


Figure 5: A typical microtubular solid oxide fuel cell

2.2: Cell manufacture - SOFC tubes

2.2.1: Electrolyte tube

Electrolyte tubes were composed principally of oxide ion-conducting yttrium oxide-stabilised zirconium dioxide (yttria-stabilised zirconia; referred to here as YSZ). YSZ (MELOX 8Y; 8 mol% yttria) and cellulose (Culminal MHEC 25000 PF) were mixed thoroughly in a Winkworth 1Z SS mixer, and distilled water added over several hours to give a stiff plastic colloid (Table 1).

Component	Amount / g
MELOX 8Y	500.0
MHFC 25000 PF	19.3
Water	109.5

Table 1: Composition of YSZ electrolyte

The electrolyte paste was ram extruded through a brass die using a Testometric M500-100 AX. Wet tubes were placed in wooden supports and allowed to dry overnight, resulting in long, brittle tubes. These were inserted into pre-fired zirconia tubes to prevent deformation, fired (Figure 6) and cut to give 60 mm tubes of 3 mm external diameter and 220 μm wall thickness.

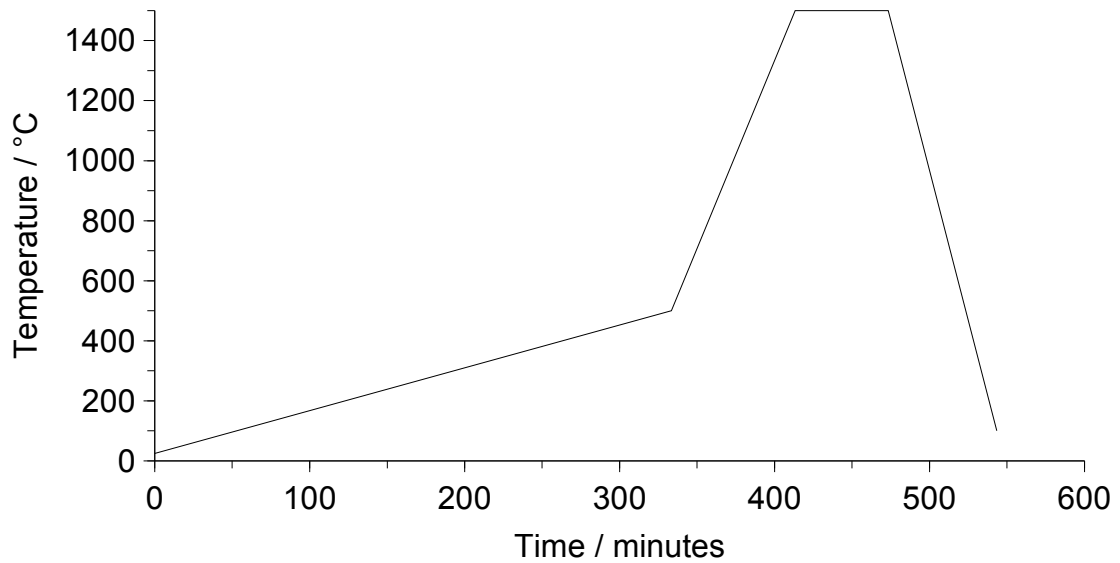


Figure 6: Firing profile for YSZ electrolyte

2.2.2: Anode

A short compositional gradient was used to improve anode efficiency. The layer in contact with the electrolyte had a 50/50 Ni/YSZ ratio to match thermal expansion coefficients whilst retaining oxide ion and electrical conductivity; a 85/15 Ni/YSZ ratio was applied on top of this to improve fuel reforming and maximise electronic conductivity (Figure 7).^[153] The CeO₂ in the anode layer in contact with the fuel aided reforming by acting as an oxygen source ($2\text{CeO}_2 \rightarrow \text{Ce}_2\text{O}_3 + \frac{1}{2}\text{O}_2$).

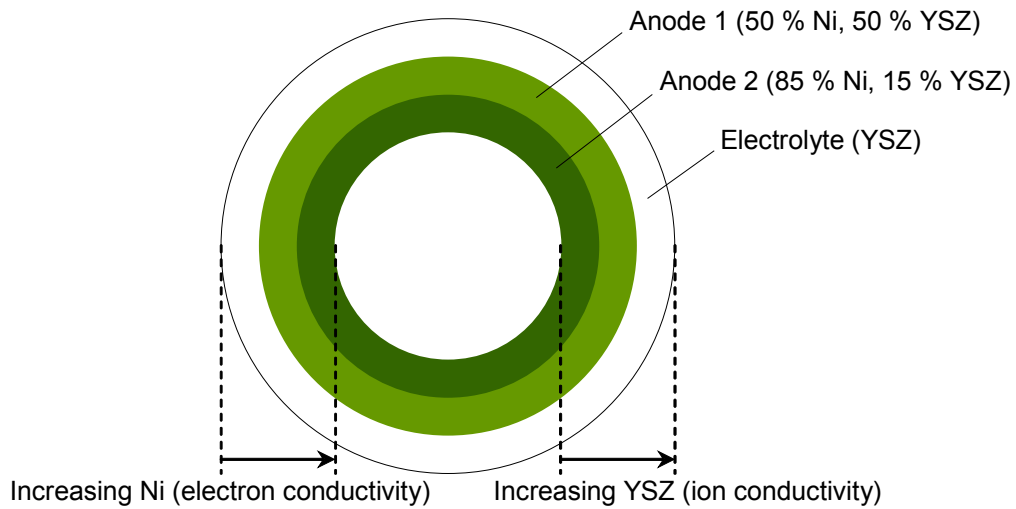


Figure 7: Anode compositional gradient

Anodes were prepared by adding components to a plastic milling pot and vibro-milling for several hours to give a mobile slurry (Table 2), which was then applied directly to the electrolyte. The tube was attached to a fixed-delivery pipette and the anode slurry sucked up to a point determined by the set delivery volume. Excess slurry was expelled with a short throughput of compressed air, and the tube was allowed to dry before being fired (Figure 8). As the length and diameter of the cells were consistent, the amount of anode slurry applied was consistent between cells. The pressure and volume of air used to expel the excess slurry was also regulated, giving low variability in the amount of anode material per cell. Anode 2 required a different firing profile to anode 1, and was co-fired with the cathodes (Figure 10) to avoid unnecessary energy waste.

Component	Anode 1 amount (50/50)	Anode 2 amount (85/15)
NiO (Aldrich)	23.5 g	21.4 g
YSZ (Tosoh TZ8Y)	6.0 g	2.0 g
KD2	0.6 g	0.5 g
Polyvinyl butyral (Wacker)	1.0 g	1.2 g
CeO ₂ (MEL)	-	1.0 g
YSZ (MEL 9.5Y)	6.0 g	-
Acetone (RdH)	22.0 ml	14.0 ml

Table 2: Compositions of graduated Ni/YSZ anodes

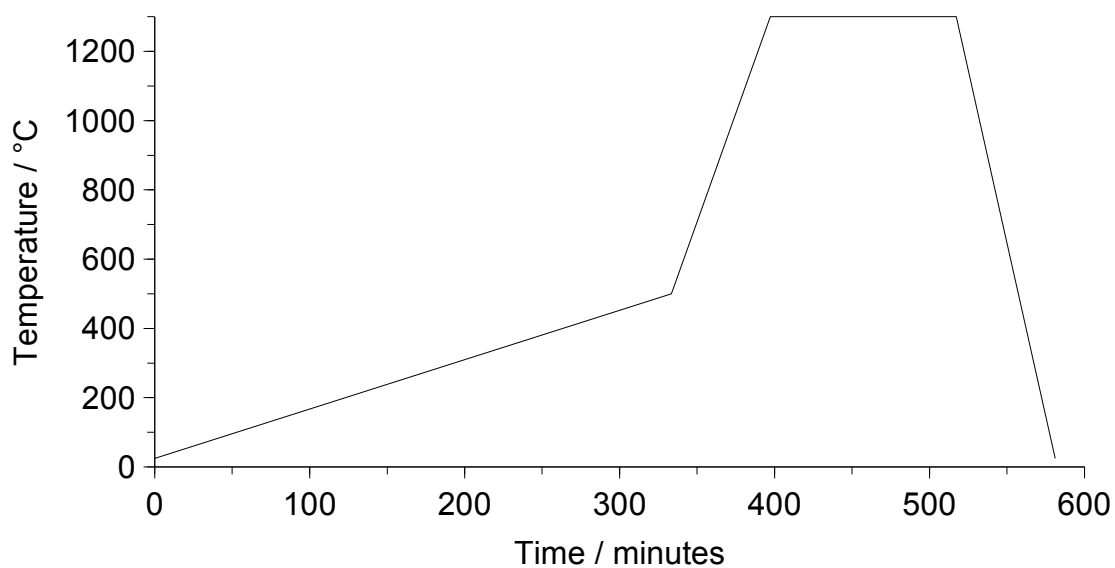


Figure 8: Firing profile for anode 1

2.2.3: Cathode

As with the anode, a compositional gradient was used for the cathode: a 50/50 LSM/YSZ ratio next to the electrolyte and a 85/15 LSM/YSZ ratio on top of this (Figure 9). Cathodes slurries were prepared in a similar manner to the anode ones (Table 3).

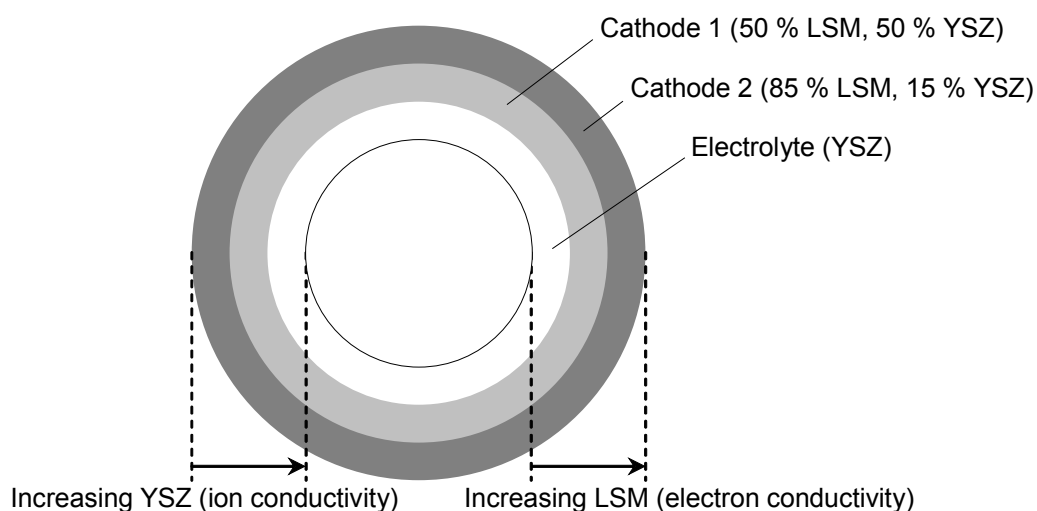


Figure 9: Cathode compositional gradient

Component	Cathode 1 amount (50/50)	Cathode 2 amount (85/15)
$\text{La}_{0.5}\text{Sr}_{0.5}\text{Mn}$ oxide (Praxair)	6.5 g	10.0 g
YSZ (Tosoh TZ8Y)	5.8 g	1.6 g
KD2	0.25 g	0.4 g
Glycerol trioleate (Aldrich)	0.2 g	-
Terpineol (Aldrich)	-	3.0 g
Acetone (RdH)	16.0 ml	14.0 ml

Table 3: Compositions of graduated LSM/YSZ cathodes

Cathode 1 was applied to the exterior of the electrolyte tube with a paintbrush and allowed to dry overnight. Cathode 2 was then applied directly over this and allowed to dry. Both cathodes and anode 2 were co-fired (Figure 10) to give the final microtubular SOFC.

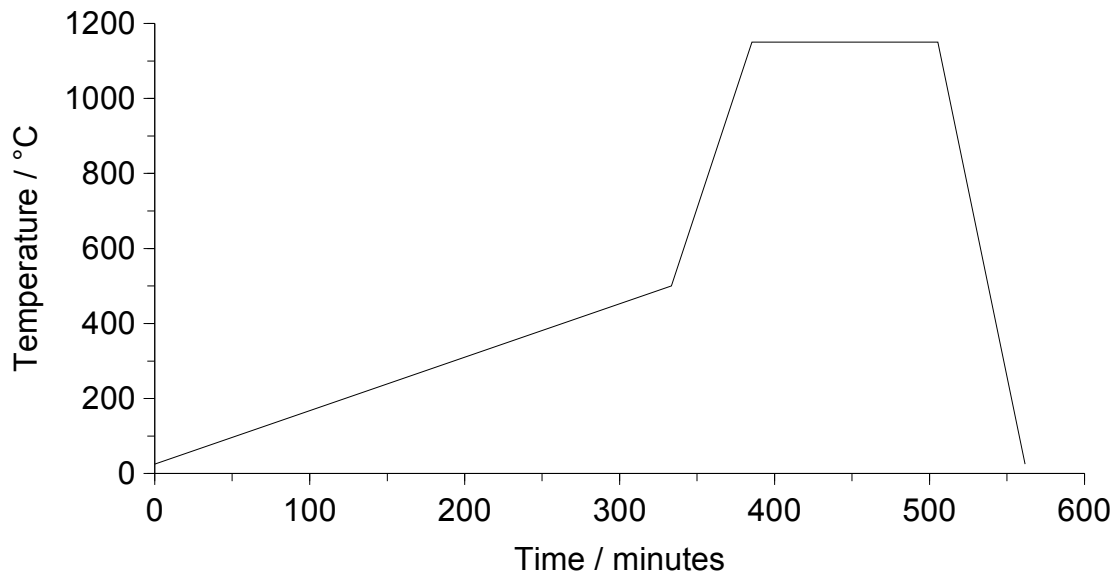


Figure 10: Co-firing profile for anode 2, cathode 1 and cathode 2

2.3: Cell manufacture - current collection

2.3.1: Anode: Ni mesh and pin, Ag plug

As nickel metal has a much higher specific electrical conductivity than the Ni/YSZ anode, a nickel mesh (DexMet MicroGrid) was inserted into the fuel cell to act as a current collector which would still allow fuel to come into contact with the anode. This mesh was held in place with a sized nickel pin (Micro Metallic), which also provided an additional conduction

pathway. When the cell was manifolded (see later), a silver plug was used to carry the current out of the cell assembly.

2.3.2: Cathode: Ag ink and wire

To improve the electrical conductivity of the cathode, silver ink (Alfa Aesar) was applied in four ≈ 3 mm bands along the cell. Silver wire (Advent 99.9 %; 0.25 mm diameter) was wound firmly around the cell (≈ 56 turns; 28×2) to carry the current out.

2.4: Experimental set-up

2.4.1: Cell manifolding

Assembled SOFCs were inserted into a drilled Macor block / zirconia tube and fixed in place with FortaFix AL/CS adhesive. A silver plug (made from melted and shaped silver wire) and silver ink were used to seal the anode current collect for complete SOFCs; catalyst tube and blank tube (see later) blocks did not have the additional current collection hole drilled (Figure 11).

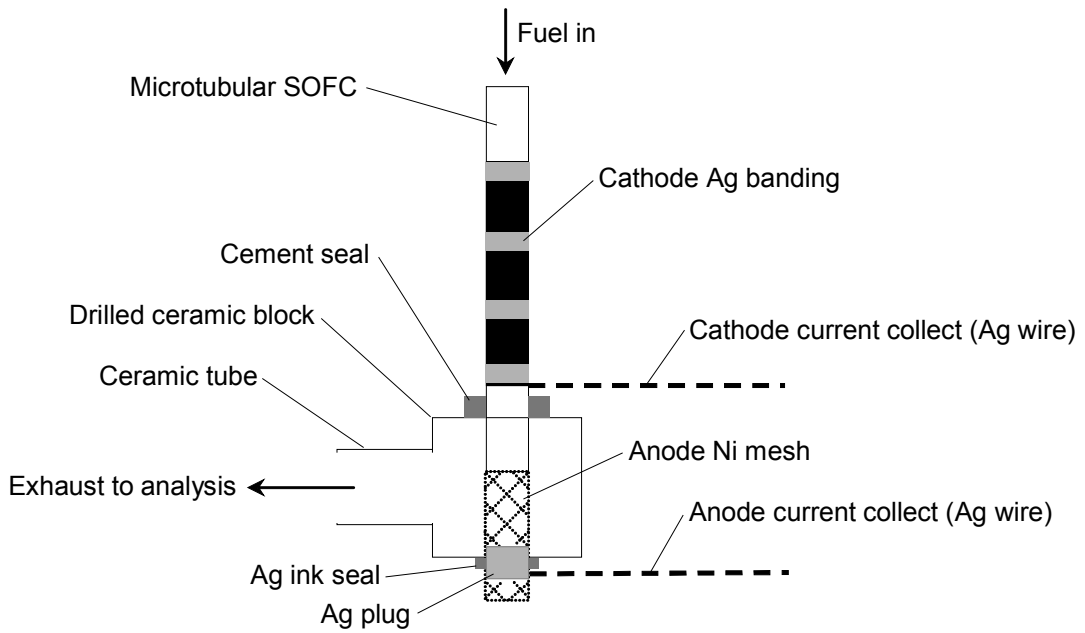


Figure 11: Schematic diagram of a manifolded microtubular SOFC

2.4.2: Furnace control and liquid fuel delivery

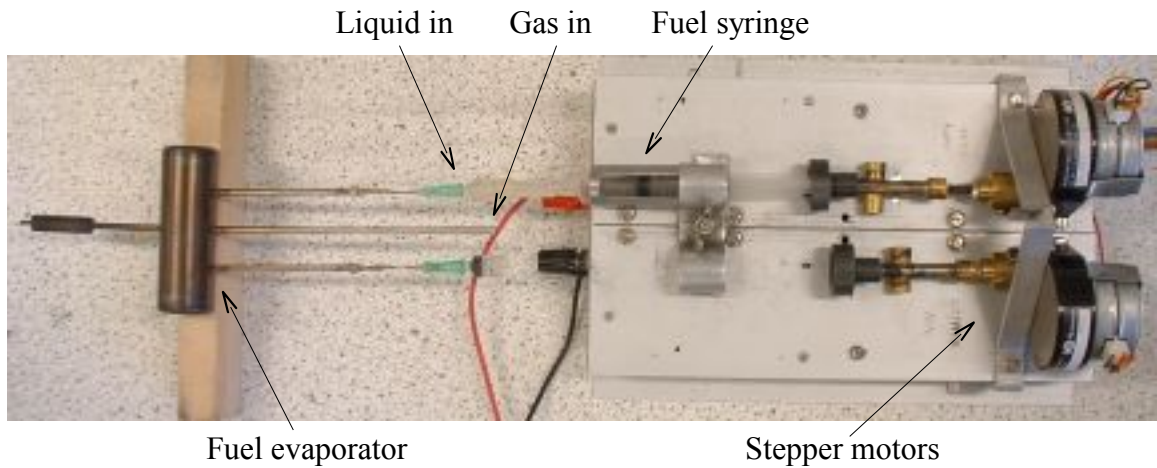


Figure 12: Stepper motor-driven syringes for liquid fuel delivery

Both liquid and gaseous fuels could be delivered to a manifolded cell via a heated evaporation chamber. This consisted of a short sealed section of stainless steel tubing with entry tubes for

fuels and a sized exit tube to feed directly into the SOFC (Figure 12). Delivery of liquid fuels in this way allowed precise control over the fuel composition, as the proportion of fuel components entering the SOFC would be the same as that in the fuel syringe. With a heated saturator arrangement,^[154] different components would have different vapour pressures and might not be volatile at all.

The cell was sealed into the manifold using cement, which provided a reasonable seal to prevent gases escaping. However, the nature of the liquid delivery rig did not allow sealing at the entry end. Experiments in cementing this end resulted in cell fracture under thermal expansion and difficulty in removing used cells from the injector. Packing the space around the cell / injector with insulating wool had little or no effect, and occasionally caused problems when small pieces of wool entered the cell or burned. Manufacturing cells in such a way that the entry end was not in the hot zone (allowing the use of cold seals) was also attempted, but both liquid fuels and water tended to condense in the cold zone. Early experiments showed that the leak rate was only significant in the event of a loss of pressure in the evaporator, caused by a lack of fuel, or if the injector was inserted into the cell insufficiently far. It was therefore decided to run experiments in “leaky” mode, and to consider any air entering the cell as an additional reforming agent.

Liquid fuels and oxidants were delivered via 5 ml syringes attached to syringe ports welded into the evaporation chamber. These syringes were driven via LabVIEW-controlled stepper motors to ensure an even fuel flow. Gaseous fuels were delivered through an additional section of stainless steel tubing - in all experiments, there was a constant flow of inert gas to

carry fuel vapours to the SOFC and act as an internal reference standard for any exhaust analysis.

The twin-chamber furnace was purpose-built using Thermal Ceramics insulating fire bricks and nichrome ribbon (Advent Ni80/Cr20 1.5 mm x 0.13 mm) elements, and could accommodate the fuel evaporator and a manifolded fuel cell (Figure 13). A smaller furnace was constructed using the same materials for temperature-programmed oxidation experiments (Figure 14). All furnaces and chambers were controlled independently of each other from a single power supply via K-type thermocouple feedback.

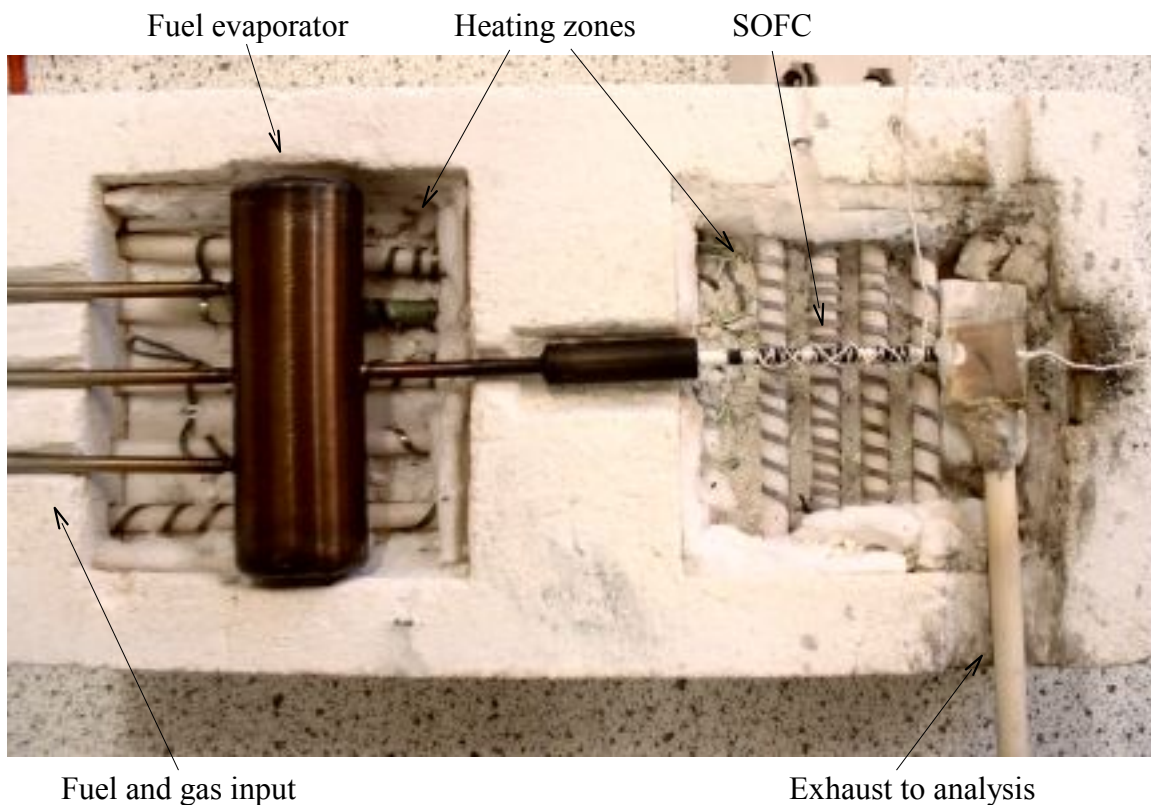


Figure 13: Furnace with fuel evaporator and microtubular SOFC

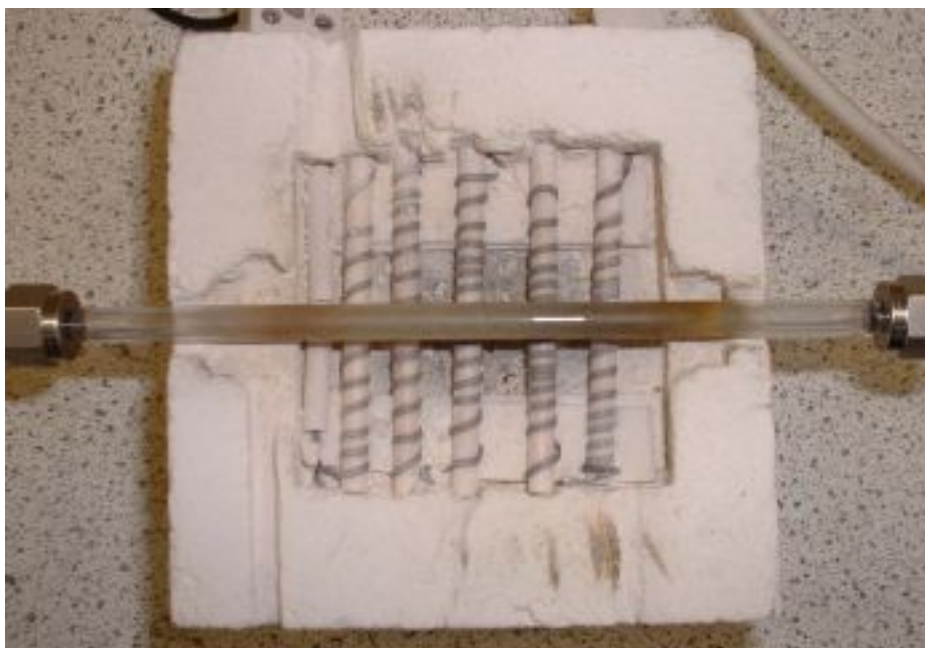


Figure 14: Temperature-programmed oxidation rig with quartz tube

2.4.3: SOFC test rig

The SOFC furnace was one part of a larger SOFC test rig, constructed principally from Swagelok 1/8" stainless steel tubing, connections and valves (Figure 15).

All gases were delivered via Unit Instruments 7300 mass flow controllers to the SOFC furnace; an additional helium supply to the mass spectrometer was controlled with a needle valve (this was used to maintain a flow of inert gas when an experiment was not running). Gases were not preheated due to the presence of the heated evaporation chamber.

Exhaust gases could be sent to the mass spectrometer for analysis, or vented if analysis was not required or a sample was to be taken. Both the exhaust manifold and mass spectrometer capillary were heated with nichrome elements to prevent any condensation.

SOFC electrical performance was monitored with a purpose-built potentiostat capable of varying electrical load as required. Current and voltage values were varied and logged using the same LabVIEW program as for syringe control.

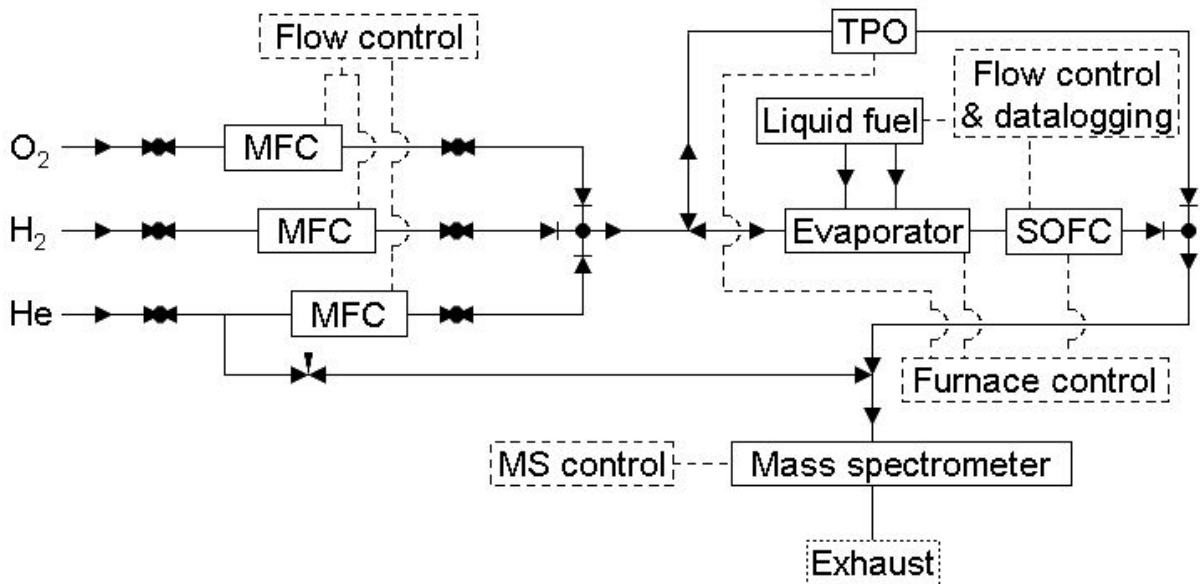


Figure 15: Schematic diagram of the SOFC and TPO test rig

Chapter 3: Experimental methods and analysis

3.1: Experimental techniques

3.1.1: Reduction and cell loading

Cells were heated to 850 °C under a constant flow (25 ml min⁻¹) of helium; hydrogen (20 ml min⁻¹) was then introduced to reduce the anode NiO to Ni. After approximately 20 minutes, the reduction process was complete (open circuit voltage was stable) and the cells were placed under electrical loading to maintain 0.5 V. This voltage was maintained for 15 minutes before any fuel was introduced.

Due to nickel sintering upon re-oxidation^[155], it was important that the anode was not exposed to air after reduction. Hence the hydrogen flow was maintained until fuel reaction products were shown on the mass spectrometer trace, indicating that there was sufficient fuel to prevent air displacing the lost hydrogen. This process is illustrated further in Figure 23. At the end of a run, the cell was cooled under a flow of inert gas to prevent any deposited carbon being oxidised. Only “blank” cells were re-used, as “catalyst” and “SOFC” cells were required for post-experimental analysis and the Ni mesh would not withstand thermal cycling.

3.1.2: “Blank” electrolyte-only run

Analysing the exhaust gas composition of a fuel cell gives information about the catalysed reforming reaction products, but not about the gases entering the cell or any reactions that



Figure 16: "Blank" electrolyte-only tube

would occur anyway (in the absence of a catalyst). If a fuel is mixed with water, heated to 300 °C and then heated to 850 °C (all of which takes place before a fuel enters the SOFC), it would be presumptuous to assume that it would remain unchanged.

To investigate this, a "blank" experiment was devised. An uninked (i.e. blank) electrolyte tube with the same dimensions as a SOFC was manifolded into the fuel rig and fuel run as normal (Figure 16). Thus, the exhaust gases would be the products of thermal cracking, uncatalysed (autothermal) reforming and any

catalytic ability of the YSZ electrolyte itself. These would be the same as those entering the SOFC. The results, when compared to those from other experiments, would indicate the tendency of a fuel to decompose and the reforming ability of the anode.

As there was no anode to reduce with this type of experiment, the standard procedure given above was deviated from. No H₂ was added, and fuel was injected directly as soon as the cell was at 850 °C.

In all results, this type of experiment is labelled as "blank" and appears first (on the left) in exhaust charts (Figure 24). TPO results are not given, as few fuels deposited carbon in the absence of a nickel anode and the tubes were therefore re-used.

3.1.3: “Catalyst” catalyst-only run



Figure 17: "Catalyst"
catalyst-only tube

The reforming ability of a SOFC is partly due to the physical presence of the Ni/YSZ catalyst and partly due to the oxygen ions coming through the electrolyte membrane. To determine how much each effect contributes to the overall reforming, a “catalyst” experiment was devised.

The gas composition entering the cell was already known (from a previous “blank” experiment), and so to determine the pure catalytic action an inked but unwired SOFC was used (i.e. a SOFC with anode and cathode but no Ag ink or current

collection, Figure 17). The exhaust gases would therefore be the

products of the fixed catalyst's passive action, and could be compared to “blank” experiments to show how well the Ni/YSZ performed alone.

The amount of carbon on the anode would also provide an indication of how well the fuel composition alone could prevent carbon deposition. SOFCs have the added advantage of oxygen diffusing through the electrolyte, which can oxidise deposited carbon and thus make a fuel appear less likely to deposit carbon than it actually is.

As this type of cell had no current collect wires, the standard procedure given above was deviated from. The anode was reduced under H_2 for 20 minutes as normal, but there was no

period of loading. Instead, fuel was injected once the anode was reduced and the hydrogen switched off once fuel was observed on the mass spectrometer (≈ 10 minutes).

In all results, this type of experiment is labelled as “catalyst” and appears second (in the centre) in exhaust charts (Figure 24), and first (on the left) in temperature-programmed oxidation charts (Figure 30).

3.1.4: “SOFC” SOFC run



Both the exhaust gas composition and electrical performance of the SOFC were measured in this experiment. In any real-world application, a fuel cell would be used to generate electricity and heat, and possibly to reform a hydrocarbon gas stream. Although SOFCs are extremely unlikely to be used singly, their performance with various fuels is not significantly altered under single-cell conditions (Figure 18).

Figure 18: "SOFC" SOFC tube

In all results, this type of experiment is labelled as “SOFC” and appears third (on the right) in exhaust charts (Figure 24), second (on the right) in temperature-programmed oxidation charts (Figure 30) and is the only component of electrical performance charts (Figure 29).

Based on the standard experimental procedure, a standard trend of electrical performance can be expected, at least initially (Figure 19). While the cell is being heated, there will be no electrical output. Once hydrogen is introduced, the anode will be reduced at open circuit voltage and no current will be drawn for 20 minutes (1). After reduction, the cell will produce current at close to the peak value for 15 minutes as it is loaded under hydrogen (2). Fuel will then be injected, increasing the amount of H₂ and CO and therefore increasing electrical output to the peak value (3). The reducing hydrogen will then be switched off and the current output will drop to a variable level depending upon the suitability of the fuel (4). At this point, several routes can be taken. If the SOFC can run well on the fuel, performance will be steady (5a). If the fuel is unsuitable or there is extensive carbon deposition, performance will drop (5b). If there is a small amount of carbon deposition, output will increase as C links Ni particles and then decline due to catalyst site blocking and nickel particle agglomeration (5c). Under experimental conditions, these effects often compete and so the current output is usually somewhere in-between these idealised routes.

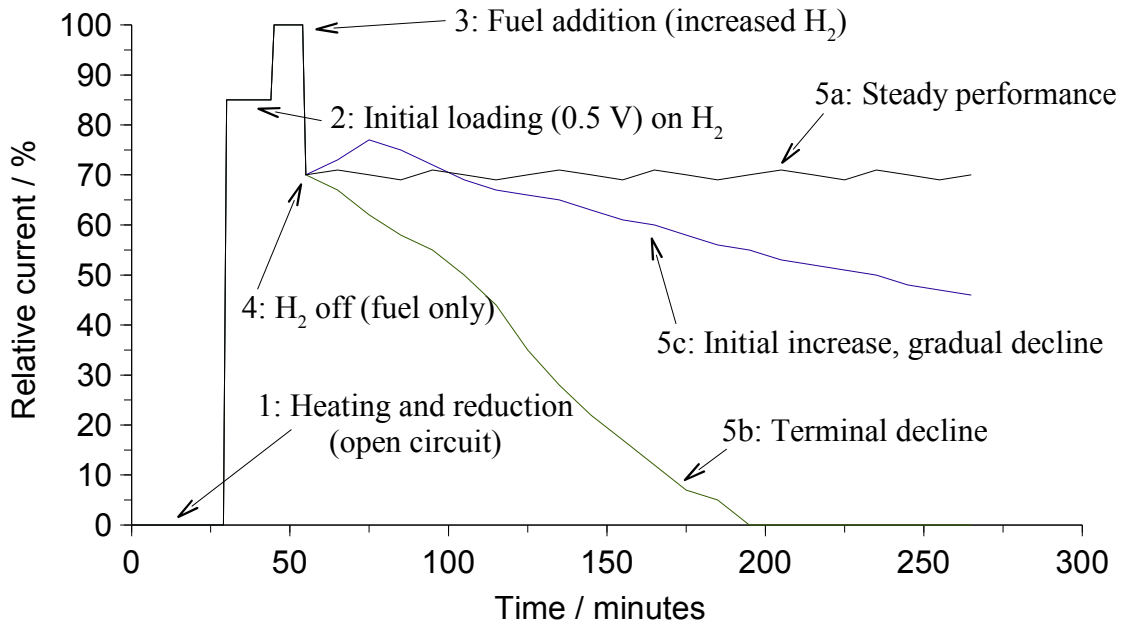


Figure 19: Example idealised trends in electrical current output

If there is sufficient fuel present in the SOFC to prevent the anode re-oxidising or agglomerating, then there may be no initial performance drop. This leads to the concept of a minimum fuel concentration (in the carrier gas) required for the SOFC to operate at maximum efficiency - the highest output for the lowest fuel throughput.

3.2: Analytical techniques

3.2.1: Temperature-programmed oxidation

The amount of carbon deposited on the SOFC anode could be determined by exposing the anode to an oxygen atmosphere and then monitoring the evolution of CO and CO₂ as the

carbon was oxidised. Used cells were broken up and packed into a quartz glass tube, which was placed in a furnace in the experimental rig described above (Figure 14). A constant flow of helium (20 ml min^{-1}) and oxygen (2 ml min^{-1}) was supplied, and the furnace was heated to $800 \text{ }^\circ\text{C}$ at a rate of $10 \text{ }^\circ\text{C min}^{-1}$.

At room temperature, carbon is stable in an oxidising atmosphere. As the temperature is increased, however, different types of carbon will evolve into CO or CO₂ at different times. Amorphous (adsorbed) carbon tends to oxidise around $300 \text{ }^\circ\text{C}$, whereas graphitic oxidises around $600 \text{ }^\circ\text{C}$. CO and CO₂ levels are monitored by an on-line mass spectrometer and plotted against temperature, and thus time (Figure 20).

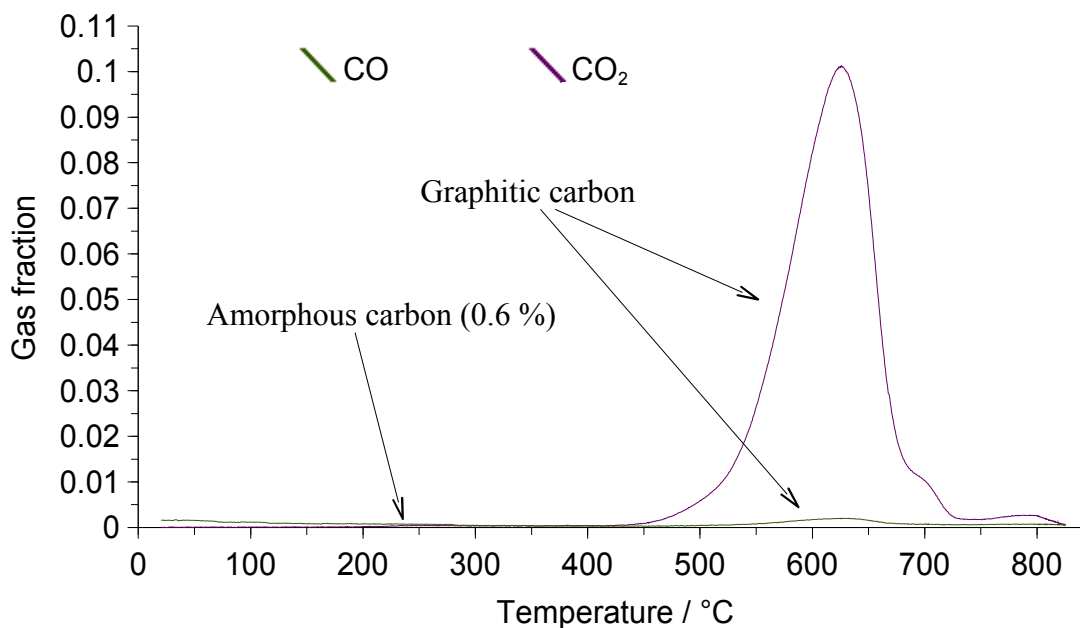


Figure 20: Typical temperature-programmed oxidation example for *N,N*-dimethyl methanamide

The temperature-programmed oxidation technique was calibrated against known amounts of carbon to give a relationship between the area under the CO and CO₂ peaks and the amount of carbon oxidised. While the calibration experiments produced similar amounts of CO and CO₂ (though with different trends against amount), most fuel cell experiments gave far more CO₂ than CO. This is due to the partial pressure of oxygen and the way that carbon is laid down on nickel anodes. When CO is formed, further oxidation to CO₂ is rapid unless another nearby carbon atom can be oxidised instead. With a SOFC anode, there is effectively a C-Ni chemical bond, which can be oxidised to give a Ni-C-O structure (which is further oxidised to Ni and CO₂). Clearly this is not present in pure carbon or carbon that is bonded to other C atoms instead of Ni -hence significant amounts of CO are only seen when there is extensive carbon deposition.

Quoting the absolute mass of carbon deposited on the anode can be slightly misleading, as different fuel compositions have different carbon contents. The amount of carbon entering the cell was calculated from the physical properties of the fuel mix and the time and rate of addition. This allowed the quantification of an amount of carbon relative to the amount added, giving an indication of the tendency to deposit.

3.2.2: Quadrupolar mass spectrometry - MKS Mini-Lab

Online exhaust gas analysis was carried out using a MKS Mini-Lab mass spectrometer. This utilises an electron ion source, quadrupole mass filter and Faraday cup detector (Figure 21).

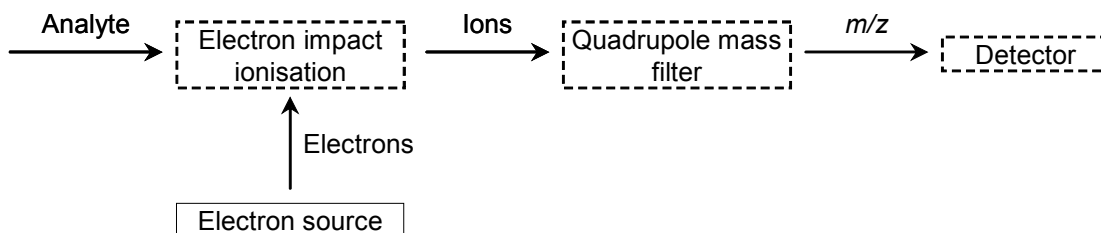


Figure 21: Simplified schematic diagram of a quadrupole mass spectrometer

In electron ionisation (EI), electrons are produced by electrically heating a wire filament.

These electrons are then accelerated towards an anode (energy is typically 70 eV) and interact with incoming analyte molecules on the way, causing ionisation and fragmentation.

Ionised and fragmented analyte molecules pass through the ionisation chamber and enter the mass quadrupole mass filter. This consists of four parallel rods with a DC potential applied in such a way that diagonally opposite rods have the same potential. A radio frequency AC potential is also applied to the rod pairs, and incoming ions travel down the centre of the quadrupole between the rods. For a given DC and AC voltage, only ions of a specific mass-to-charge ratio will pass through the quadrupole; others will have unstable oscillations and collide with a rod. A mass spectrum can be obtained by varying the voltages to detect ions across a range of mass-to-charge ratios.

Ions that pass through the mass filter are detected using a Faraday cup. This is a metal cup that becomes charged when ions collide with it, and is then discharged to give a small current equivalent to the charge on the captured ions.

3.2.3: Quadrupolar mass spectrometry - calibration and rationale

Mass spectrometer results are outputted as partial pressures, so (for example) if the amount of one gas increases the others will decrease accordingly even though there has been no change in their absolute amounts. Additionally, different gases interact differently with the ionisation source, mass filter and detector and so the relative peak height is not necessarily a reliable indication of the amount present.

In order to determine the actual gas composition, it is necessary to perform a series of calibration experiments for the relevant gases. These gases are mixed with a known, constant flow of an inert gas (such as helium or argon) so that measurements can be made relative to this reference. Then partial pressure measurements can be converted into actual fractions or normalised against the reference gas to give absolute amounts.

An unknown gas component k exists in a mixture of gases as a fraction G_k and will give a mass spectrometer signal m_k . In order to obtain a mass spectrometer signal corrected for relative ionisation sensitivity $m_k[c]$, a correction factor v_k is required, hence:

$$m_k[c] = v_k m_k$$

Where

$$v_k = \frac{G_k}{[m_k]^{cal}}$$

Where $[m_k]^{cal}$ is the mass spectrometer signal for a known gas fraction of component k (calibration).

If the component k exists with other components, the corrected fraction $G_k[c]$ is given by:

$$G_k[c] = \frac{m_k[c]}{\sum_i m_i[c]} = \frac{m_k \cdot v_k}{\sum_i m_i \cdot v_i}$$

Defining one gas component m_r to be absolute, which all other signals are measured relative to, gives:

$$G_k[c] = \frac{m_k \cdot v_k}{\sum_{i \neq r} m_i \cdot v_i + m_r \cdot v_r}$$

Factoring the bottom denominator by v_r gives:

$$G_k[c] = \frac{v_k}{v_r} \frac{m_k}{m_r + \sum_{i \neq r} m_i \cdot \frac{v_i}{v_r}}$$

And hence the calibration factor can be defined:

$$\kappa_i^r = \frac{v_i}{v_r} = \frac{G_i}{[m_i]^{cal}} \cdot \frac{[m_r]^{cal}}{G_r}$$

Hence:

$$G_k[c] = \frac{m_k \cdot \kappa_k^r}{m_r + \sum_{i \neq r} m_i \cdot \kappa_i^r}$$

For example, in a gas mixture containing He, H₂, CH₄, CO and CO₂ the corrected gas fraction of CH₄ using He as the reference standard would be given by:

$$G_{CH_4}[c] = \frac{m_{CH_4} \cdot \kappa_{CH_4}^{He}}{m_{He} + m_{H_2} \cdot \kappa_{H_2}^{He} + m_{CH_4} \cdot \kappa_{CH_4}^{He} + m_{CO} \cdot \kappa_{CO}^{He} + m_{CO_2} \cdot \kappa_{CO_2}^{He}}$$

If a gas mixture not containing the original reference gas is used, it is possible to use another gas *s* as the reference standard without determining new calibration factors. The factors are related thus:

$$\kappa_i^s = \frac{\kappa_i^r}{\kappa_s^r} = \frac{v_i}{v_r} \cdot \frac{v_r}{v_s}$$

In the following results, corrected gas fractions ($G_k[c]$; values from 0 to 1) are quoted. For reforming experiments, gas compositions did not vary largely with time and so it was not necessary to normalise against the reference gas to observe time-dependent effects. For temperature-programmed oxidation experiments, there were substantial compositional changes with time - however the area under the gas fraction peak was integrated and compared against a calibration graph, so normalisation was again largely unnecessary.

The rate of leakage from the cell was an unknown quantity. Although it is reasonable to assume that the rate of leakage is constant over a given experiment (around 5 %), gases will not leak at the same rate (hydrogen is especially prone to escape) and this rate may differ according to the concentration of the gas. Additionally, the rate of leakage is unlikely to remain constant between experiments due to unavoidable inconsistencies in cell manufacture and manifolding. The main effect on results was a decrease in sensitivity and an increase in experimental error. Leaks were compensated for (as much as possible) by measuring relative to a known reference standard, but otherwise ignored.

3.2.4: Data processing and presentation

The mass spectrometer scans the exhaust gas composition approximately every 3.5 seconds, outputting a chart of signal intensity values versus mass-to-charge ratio for the particular scan number (Figure 22). In post-experiment processing, the signal intensity values were adjusted for relative intensity and other gases, converted into gas fractions relative to the carrier gas and plotted to give a scatter graph showing the trend against time (Figure 23). For example, to

obtain the adjusted value for CO ($m/z = 28$) the values for atmospheric N₂ (deduced from the argon signal at $m/z = 40$) and CO₂ (deduced from the molecular ion at $m/z = 44$) were deducted from the raw signal prior to conversion into a gas fraction.

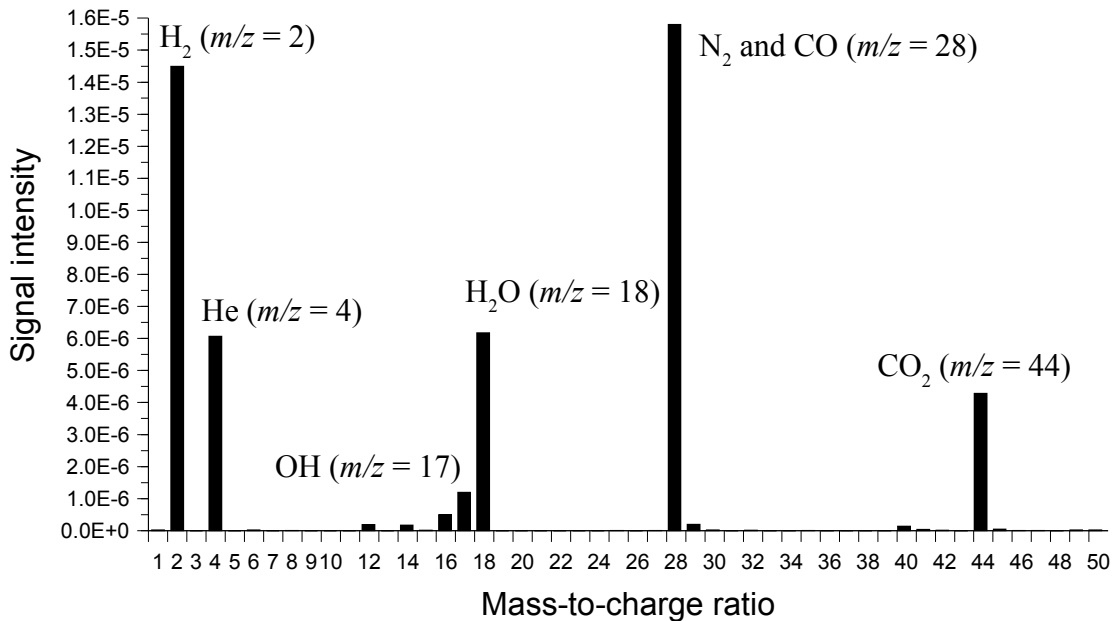


Figure 22: Typical mass spectrometer scan example for an ethanol / water mixture

The mass spectrometer cannot distinguish ions with identical mass-to-charge ratios (pertinent examples include N₂ and CO, and O and CH₄). As there was inevitably a small amount of air in the system, it was essential to remove it from the processed signal intensity values, otherwise certain m/z values would be overstated. The correction for air was done with a simple deduction of a known air spectrum relative to $m/z = 40$ (argon), effectively eliminating the background noise.

As outlined previously, fuel experiments follow a set procedure to add reproducibility. Figure 23 shows a typical exhaust gas composition trend against time (1 scan \approx 3.5 seconds) with the signal intensity values converted into gas fractions (i.e. after post-experimental processing).

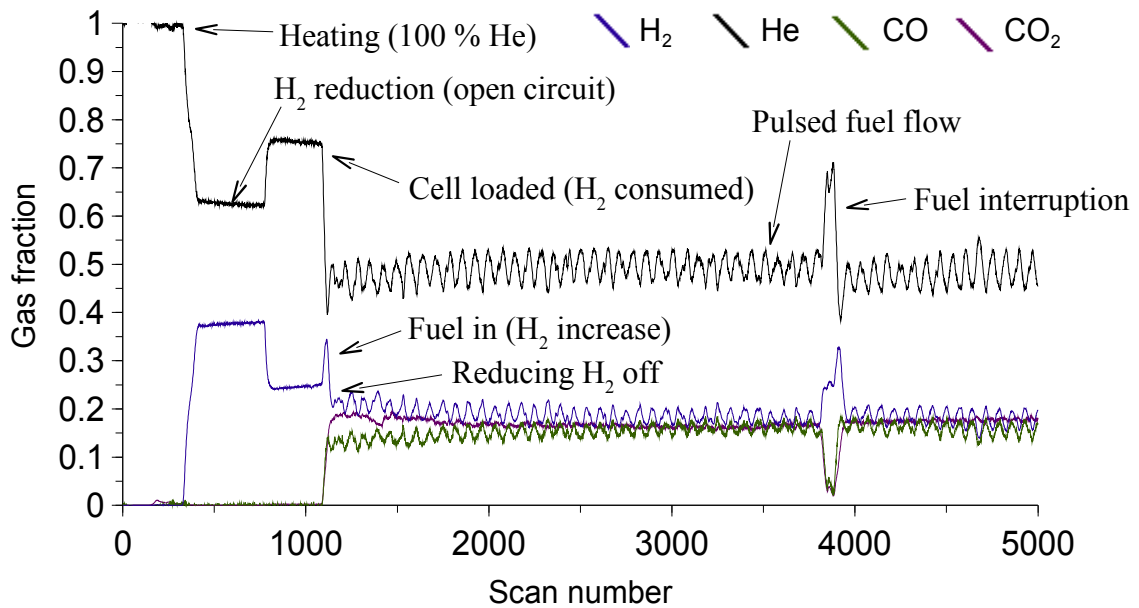


Figure 23: Typical composition against time trend example for an ethanol / water mixture

All experiments begin with the cell under in inert atmosphere (He), which is maintained until the temperature reaches 850 °C. After the cell has been reduced, the fuel consumption can be seen when current is drawn and H₂ is used up. The slight upward trend of H₂ during reduction is due to the process being gradual - maximum H₂ is consumed when there is maximum NiO. As the amount of NiO decreases, the amount of H₂ reaching the mass spectrometer increases. Once the fuel syringes are switched on, a variable amount of time will elapse before any fuel enters the SOFC. This is due to the (variable) time required for the stepper motors to make full contact with the syringe plungers and for the fuel vapours to displace the He and H₂

already in the evaporation chamber. Once the fuel enters the SOFC, an increase in H₂ is seen due to the fuel reformat. When the reducing H₂ is switched off, levels drop to those supplied only by the fuel.

By the nature of delivery, the flow of fuel reformat is pulsed. The stepper motors push against the syringe plungers incrementally, releasing droplets of fuel in volumes that vary with the viscosity and surface tension. Occasionally, a bubble of air becomes trapped in the syringe - due to the proximity to the furnace, fuel sometimes evaporates before reaching the evaporation chamber. This results in a temporary dip in reformat and concomitant spike in carrier gas. In the example given, the H₂ fraction also spikes - this was due to the hydrogen supply being temporarily switched on to avoid the air getting into the cell. Ordinarily the H₂ fraction would also dip.

To present meaningful exhaust gas composition results, the gas fraction values for the relevant gases (H₂, CH₄, CO, CH₃OH and CO₂) were averaged over the course of the experiment after the reducing H₂ was switched off (this was to avoid distorting results with artificially introduced gases). The average values could then be presented as a stacked bar chart and easily compared across the range of experiment types (i.e. blank, catalyst and SOFC) and carbon-to-oxygen ratios (i.e. added oxygen through water) for a given fuel (Figure 24).

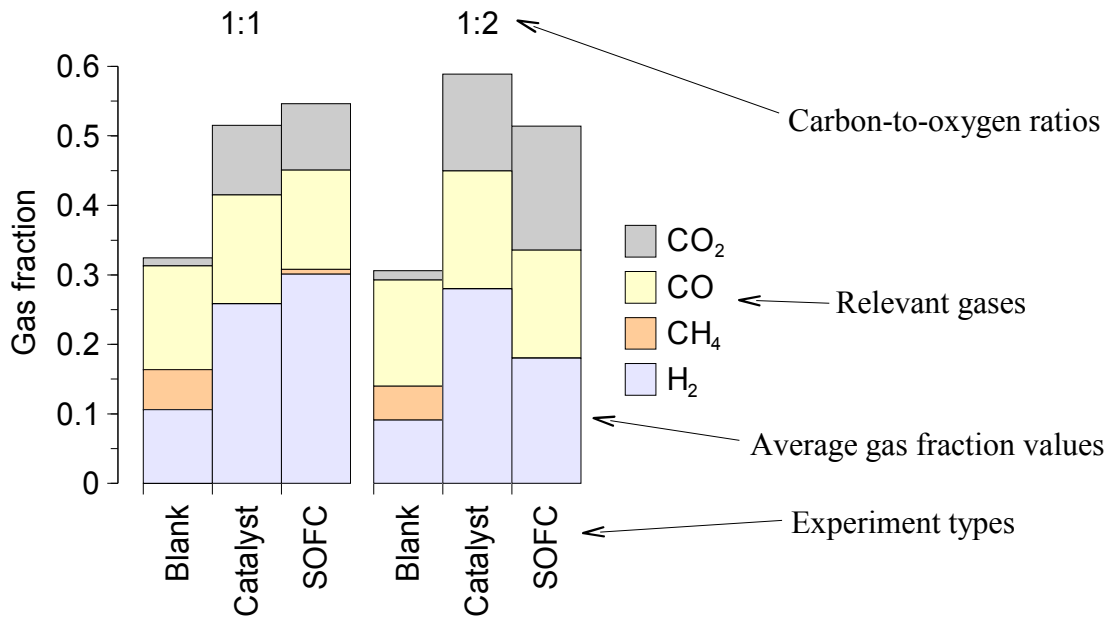


Figure 24: Typical exhaust gas composition example for an ethanol / water mixture

The value of the C:O ratio was actually the molar ratio of water molecules to carbon atoms, and was presented in this way to aid comparison between fuels. Quoting the molar ratio of steam to fuel could potentially be misleading, as the carbon content of the fuel varied from one atom to four atoms, all potentially able to be oxidised to CO₂.

When considering electrical performance, current output was measured at a fixed voltage (0.5 V) and presented as a trend against time (Figure 25). As a consequence of the variability between cells discussed earlier, current values were given relative to the highest recorded value to make comparisons possible.

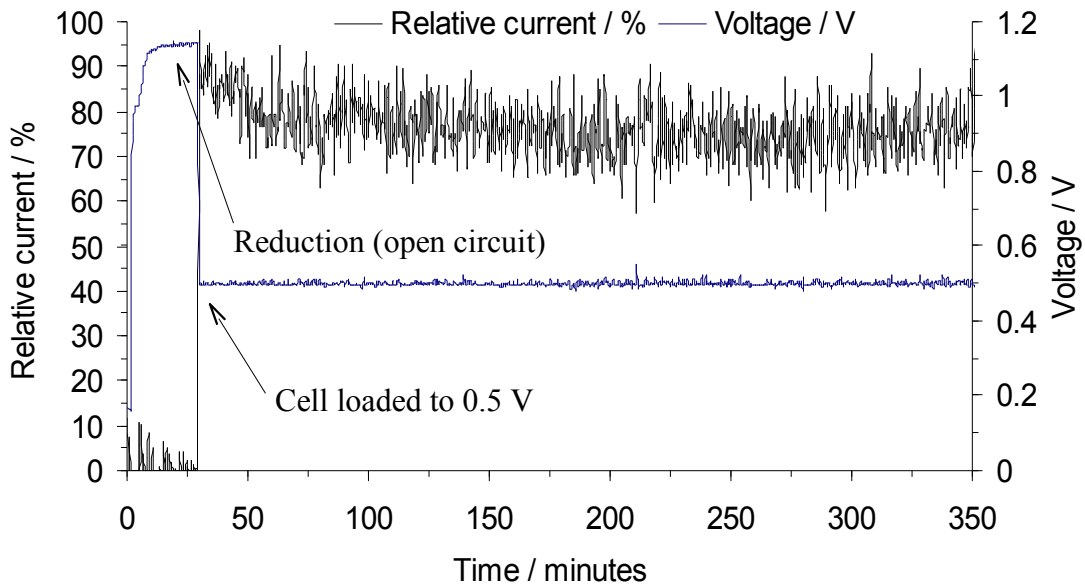


Figure 25: Typical current and voltage against time trend examples for an ethanol / water mixture

The signal-to-noise ratio for current values was quite low, with a variation of up to $\pm 20\%$. Fluctuations in current output were principally due to varying contact between the anode and nickel mesh and partly due to the pulsed nature of the fuel (fuel utilisation, and hence current, increased as the fractions of H_2 and CO increased). Relative current was therefore presented as a moving average over a period of several minutes to makes trends easier to see.

Temperature-programmed oxidation results (Figure 20) gave a simple percentage value for the amount of carbon deposited (relative to the carbon content of the fuel) and so were presented as bar charts for the range of experiment types (i.e. catalyst and SOFC) and carbon-to-oxygen ratios for a given fuel.

Chapter 4: Hydrogen and C-1 hydrocarbons

4.1: Hydrogen

Hydrogen and C-1 hydrocarbons such as methane and methanol have been the focus of much previous work, and so are useful as baseline comparisons for other fuels. Hydrogen in particular is almost always used to evaluate performance, and provides a good indication of the capabilities of a fuel cell.

Although it is the most abundant element in the known universe, hydrogen (H₂) does not occur in an extractable form on Earth. On industrial scales, it is currently produced via steam reforming of natural gas or electrolysis of water (though this is relatively energy intensive). Biological methods involving algae and biomass are the subject of several research studies.

4.1.1: Endurance tests

The performance of cells over relatively long periods of time is significant, as their intended use will be to generate electricity for as long as is required. SOFCs were run on a mixture of hydrogen and helium to establish how well cells perform under carbon-free conditions, and their current output plotted against time (Figure 26).

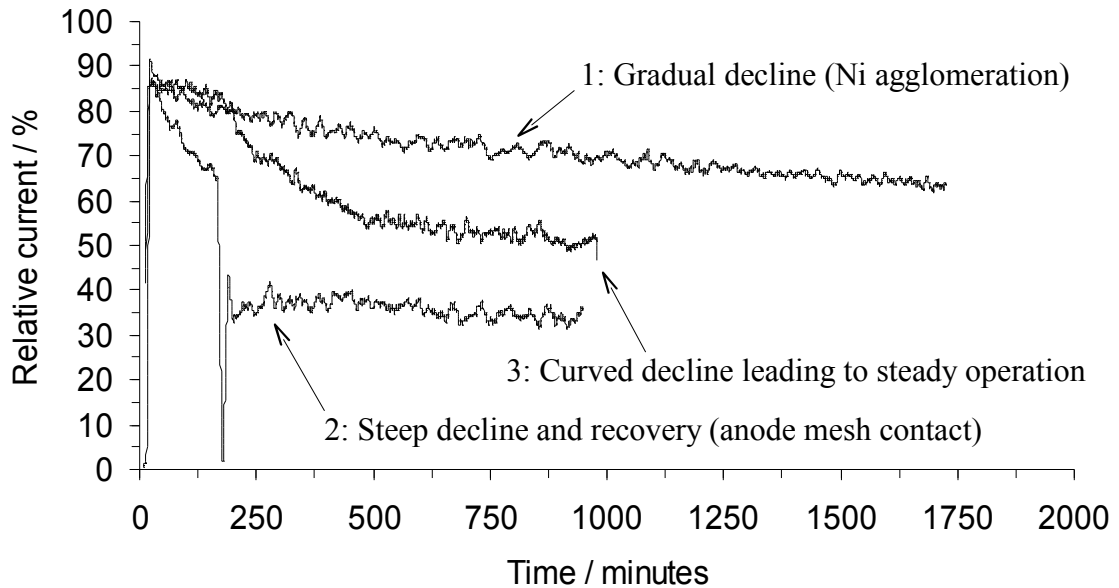


Figure 26: Typical trends of current against time for SOFCs run on hydrogen

A number of effects were observed, which will apply to hydrocarbon-fuelled SOFCs in addition to any caused by carbon deposition (Figure 19). The agglomeration of nickel particles in the anode (anode sintering) causes a gradual decline in current output, which will eventually level off (1). Poor physical contact between the anode current collect mesh and the anode can cause fluctuations in the current output, but this will often cease over time as an optimal position is reached (2). In many cells, both of these effects were seen and a typical current output curve had a steep initial decline as the anode mesh settled in place followed by a gradual levelling off as nickel agglomeration slowed (3).

Typical hydrocarbon fuel experiments were run for periods not exceeding 400 minutes, including the time required to reduce the anode and establish cell output on hydrogen. Based

on these hydrogen studies, a drop to between 40 % and 80 % of peak output may be expected with either a gradual decline (due to nickel agglomeration and/or carbon deposition) or stabilisation.

4.2: Methanol

$\text{H}_3\text{C—OH}$ Methanol is a logical liquid fuel to study for baseline performance. It is

*Figure 27:
Methanol*

volatile, contains only one carbon atom, is miscible with water and has been extensively studied for fuel cell applications. It is currently made from natural gas or coal via syngas, but carbon-neutral biological methods are also viable.

Existing work^[156] suggested that methanol would perform well, giving good yields of hydrogen / CO and depositing little carbon. The pre-oxidation of the carbon atom should also remove the need for extensive steam reforming - it is effectively a methane molecule that has partly progressed to full oxidation to CO₂.

4.2.1: Steam reforming

Methanol reformed readily even with no added water, but there was a significant increase in CO₂ levels as soon as a molar equivalent was introduced (Figure 28). This was entirely expected, as methanol was then being reformed as well as directly oxidised:

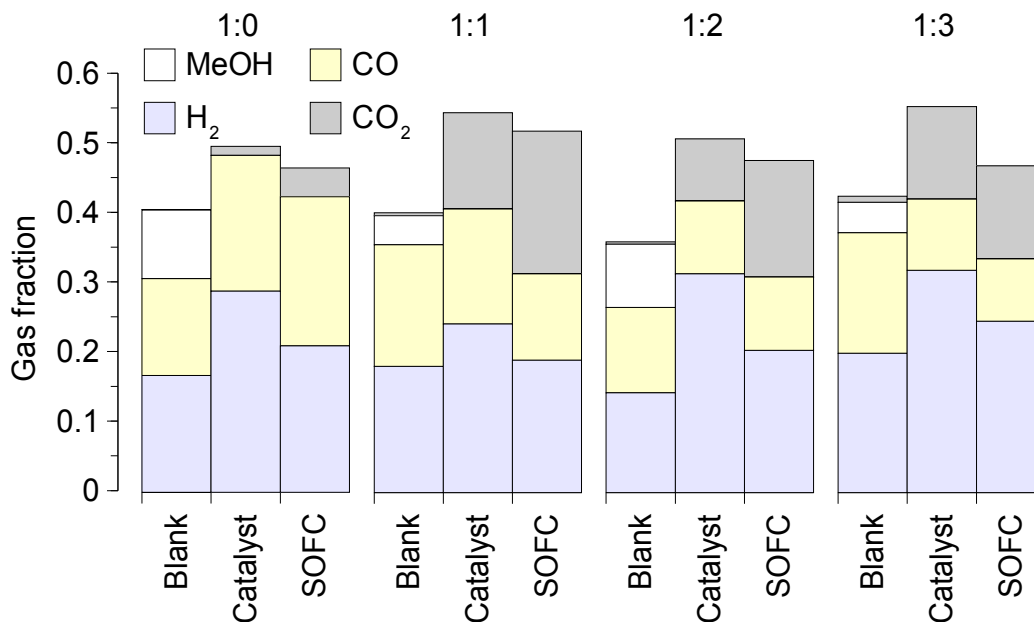
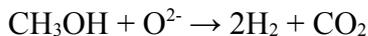
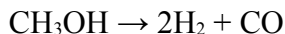


Figure 28: Exhaust gas compositions of steam reformed methanol

There was an equivalent drop in the MeOH (CH₃OH) level, supporting this conclusion. At the 1:2 and 1:3 ratios, there were slight increases in the H₂ levels but drops in the CO and CO₂ levels. Methanol oxidises directly to CO₂, so the trace at $m/z = 28$ was the sum of the CH₃OH cracking pattern and any CO from the fragmentation or oxidation of deposited carbon. As more methanol was reformed (with the increasing H₂O levels), less was present in the exhaust and therefore the $m/z = 28$ trace reduced. The apparent drop in CO₂ levels was due to the equilibrium of the water-gas shift reaction ($\text{CO} + \text{H}_2\text{O} \leftrightarrow \text{CO}_2 + \text{H}_2$) - as more methanol was

reformed to CO₂ and H₂, the equilibrium was pushed towards CO and H₂O. This equilibrium, and those between the other reactions, eventually give optimal compositions, hence the similarity between the “catalyst” and “SOFC” experiments.

Of all the fuels tested, only methanol remained stable after passing through the cell furnace (visible as $m/z = 31$; H₃CO⁺). It is likely that methanoic acid will also remain relatively intact, but ionisation will give a CO₂ fragment, indistinguishable from any CO₂ produced by reforming.

4.2.2: Electrical performance

A similar trend was seen for all carbon-to-oxygen ratios (Figure 29), suggesting that the decline in electrical output was not due to a lack of effective reforming (see earlier) or carbon deposition (see later). The gradual decline was consistent with the anode sintering seen for hydrogen (Figure 26), but was not reproducible when similar mixtures of gases were run. This suggests that the methanol itself is significant. Exhaust gas analysis (Figure 28) shows that methanol molecules enter the fuel cell intact, which is the principal difference between these experiments and those conducted on gas mixtures. Anode slurries are prepared in acetone, but the components are equally soluble in methanol - hence the vapours may corrode the Ni-YSZ cermet and disrupt the three-phase boundary area. The exhaust gas composition remained constant over the course of the experiment, so catalytic reforming was not inhibited but fuel cell operation was.

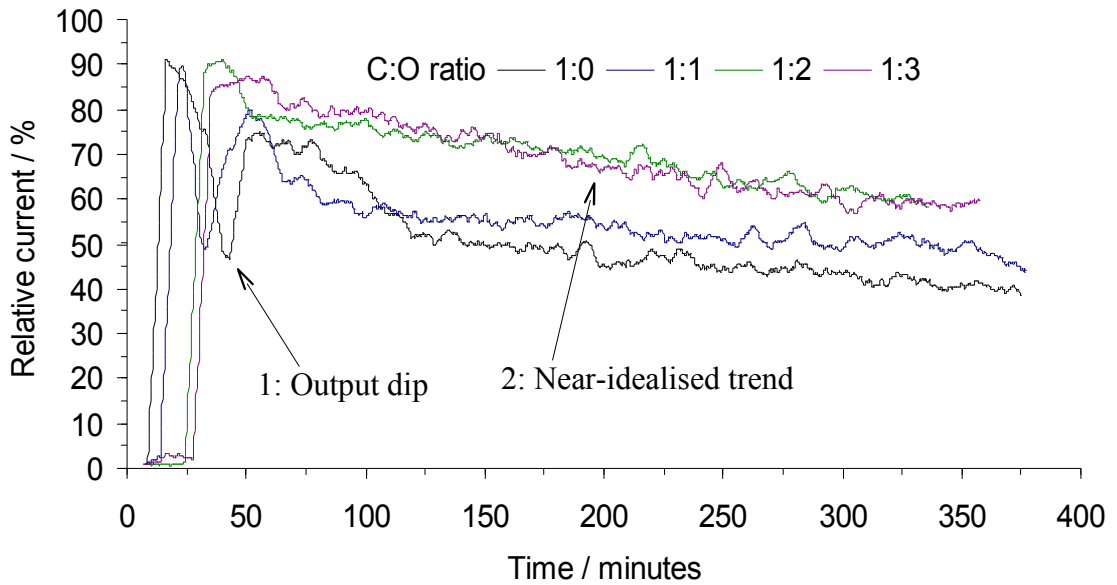


Figure 29: Trends of relative current against time for steam reformed methanol

The 1:0 and 1:1 ratios showed sharp dips in current output before normal operation resumed (1). These were most likely due to the anode current collection mesh settling into place during hydrogen reduction and loading, as both were temporary and the eventual current output was notably lower than the 1:2 and 1:3 ratios despite higher fuel concentration (the dilution effect).

The 1:3 ratio showed a near-idealised trend against time, as outlined previously (Figure 19). The periods of reduction, initial loading, output increase due to fuel addition, loss of reducing H_2 and final trend were all visible. The improved performance of the 1:2 and 1:3 ratios relative to the 1:0 and 1:1 suggests that carbon deposition is the main cause.

4.2.3: Carbon deposition

Methanol is known to deposit little carbon, and even with no added water only 0.05 % of the fuel's carbon content was left on the anode (Figure 30). For all carbon-to-oxygen ratios, a similar amount of carbon was deposited for both “catalyst” and “SOFC” experiments. This meant that oxygen ions coming through the electrolyte did not encounter any carbon to oxidise beyond that which could be oxidised by the added water, a result of the generally low carbon levels.

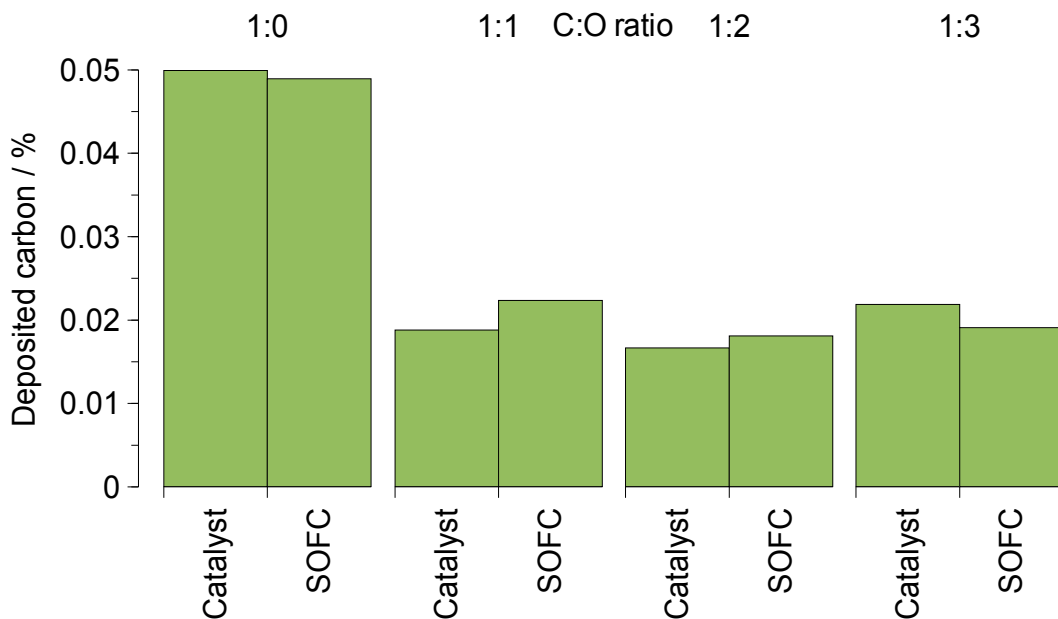


Figure 30: Carbon deposited as a percentage of carbon added for steam reformed methanol

The 1:1, 1:2 and 1:3 ratios all gave similar rates of carbon deposition, indicating that the deposition mechanism is oxidant-independent or that the carbon is not removable by steam or oxide ions. This was unexpected, as at the 1:2 and 1:3 ratios the excess steam should have

been sufficient to remove all carbon regardless of the rate of deposition. It is worth noting that the amounts involved are extremely small (0.02 %) and so carbon deposition is probably not the primary cause of the performance degradation.

4.3: Methanoic acid (formic acid)

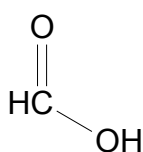


Figure 31:
Methanoic
acid

Methanoic acid is similar to methanol, with the pre-oxidation level of the carbon atom raised from an alcohol to a carboxylic acid. This allows the effects of increased pre-oxidation to be studied - the methane molecule is now almost fully oxidised to CO₂ and has only to lose the additional hydrogen atoms.

Methanoic acid is produced as a by-product during the manufacture of ethanoic acid and other chemicals, but can also be derived from methanol (though the method is quite energy intensive). Like methanol, it has been the subject of some interest due to its small size and thus inherent tendency not to deposit carbon.^[156]

4.3.1: Steam reforming

Methanoic acid was (expectedly) characterised by low levels of H₂ and high levels of CO₂ (Figure 32), as the molecule was by its structure effectively pre-reformed (two hydrogen atoms being replaced by one oxygen). The highest fractions were seen for the “blank” experiments due to the molecule reaching the mass spectrometer intact and giving a standard

cracking pattern. H₂ levels were lower for catalysed reforming due to the formation of H₂O, which due to its stability contributes little to the $m/z = 2$ peak. H₂ and CO levels were lower for “SOFC” experiments than “catalyst” due to their consumption as fuel, indicated in part by slightly higher CO₂ levels.

The overall decline in exhaust gas levels as carbon-to-oxygen ratios increased was principally due to the increasing fuel dilution (with water). As no further oxidation of the carbon atom can take place, additional oxidant has little effect:

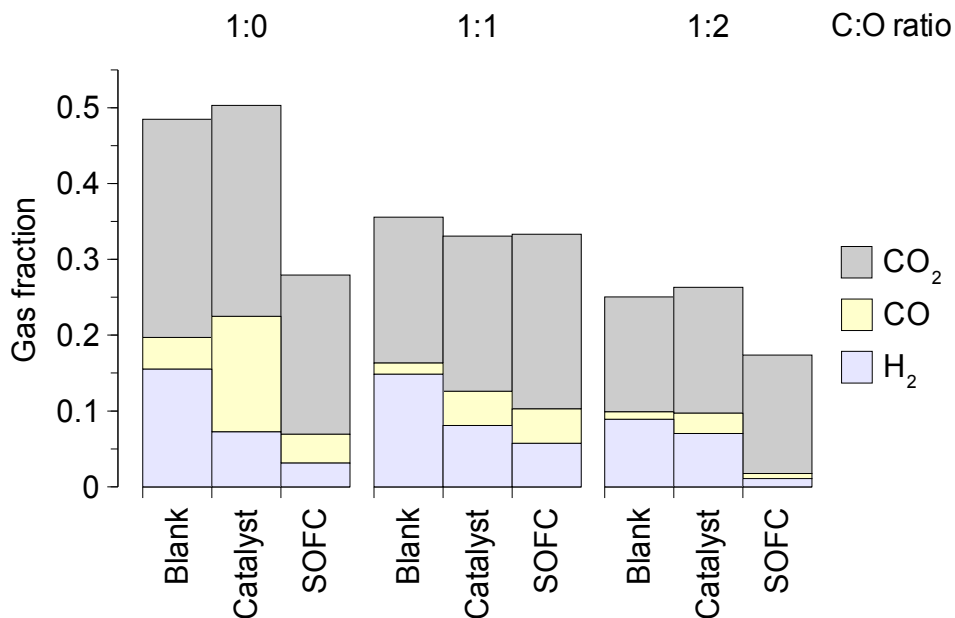
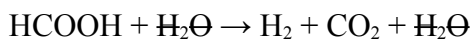
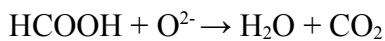


Figure 32: Exhaust gas compositions of steam reformed methanoic acid

4.3.2: Electrical performance

As with methanol (Figure 29), a similar trend was seen for all carbon-to-oxygen ratios. Unlike methanol, however, there was no apparent decline in current and the output was stable at 30 % - 50 % of peak output after a steep initial decline (Figure 33). This large decline is typical of a fuel which reforms to low H_2 and CO levels - there is little immediate fuel to replace the reducing H_2 and so, while fuel utilisation is high, electrical output is low.

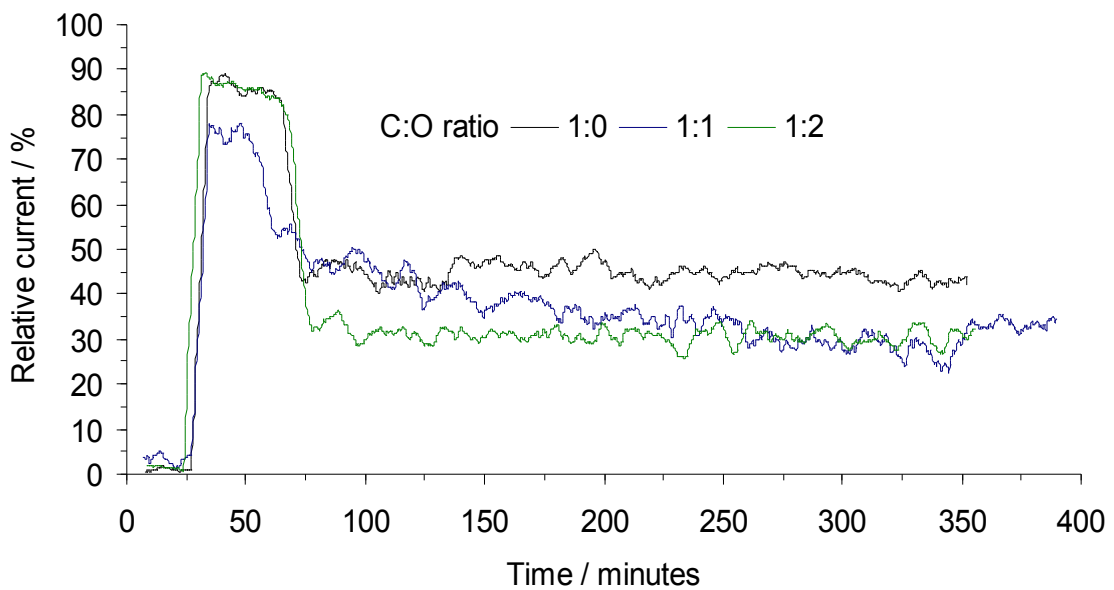


Figure 33: Trends of relative current against time for steam reformed methanoic acid

Electrocatalytic oxidation of methanoic acid is theoretically possible, and it (apparently) made a significant contribution to the overall current output given the low levels of H_2 and CO. In stark contrast to methanol, the presence of unreformed methanoic acid did not seem to be

detrimental to the anode at all. Although the current output was less than half of what it would have been on hydrogen, performance was steady.

Based on the reforming and electrical data, increasing the pre-oxidation level of a carbon atom aids long-term performance but reduces the production of potentially useful gas (i.e. H₂ - two hydrogen atoms are effectively replaced by an oxygen). Increasing the fuel flowrate may improve the current output, at the risk of increased carbon deposition.

4.3.3: Carbon deposition

With the exception of the 1:1 ratio “catalyst” experiment, methanoic acid generally deposited less carbon than methanol (Figure 29), as would be expected from the higher pre-oxidation level of the carbon atom. Any carbon must come from direct electrocatalytic oxidation of CO (via reverse water-gas shift from H₂ and CO₂) through the Boudouard reaction (Figure 34).

The amount of carbon deposited in the “SOFC” experiments increased with increasing steam levels; behaviour counterintuitive to accepted mechanisms. The equilibrium for steam reforming of methanoic acid is independent of steam concentration, as has already been demonstrated, but the electrocatalytic reaction equilibrium is not. Increasing H₂O pushed the equilibrium towards HCOOH, and thus the electrochemical reaction to give H₂ and CO₂ (and therefore C and CO). Although increased water and O²⁻ levels should remove additional carbon, this is not always the case (as seen with methanol).

The “catalyst” experiments also showed an unexpected trend, with far more carbon being deposited at the 1:1 ratio than any other. The 1:0 and 1:2 ratios showed typical levels; the 1:0 ratio being similar to methanol (0.05 %) and the 1:2 ratio being below the detection limit. This trend supports the argument above that carbon is formed through electrocatalytic oxidation, as none can take place in the “catalyst” experiments. Therefore, additional steam only affects HCOOH levels through dilution effects and is free to oxidise any carbon. The anomalously high figure for the 1:1 ratio was also reflected in the electrical performance (Figure 33), which showed a curved decline and eventual stabilisation instead of an immediate drop to steady operation. The most obvious explanation is a more susceptible anode due to the variability in cells, but the experiment would need to be repeated to verify this.

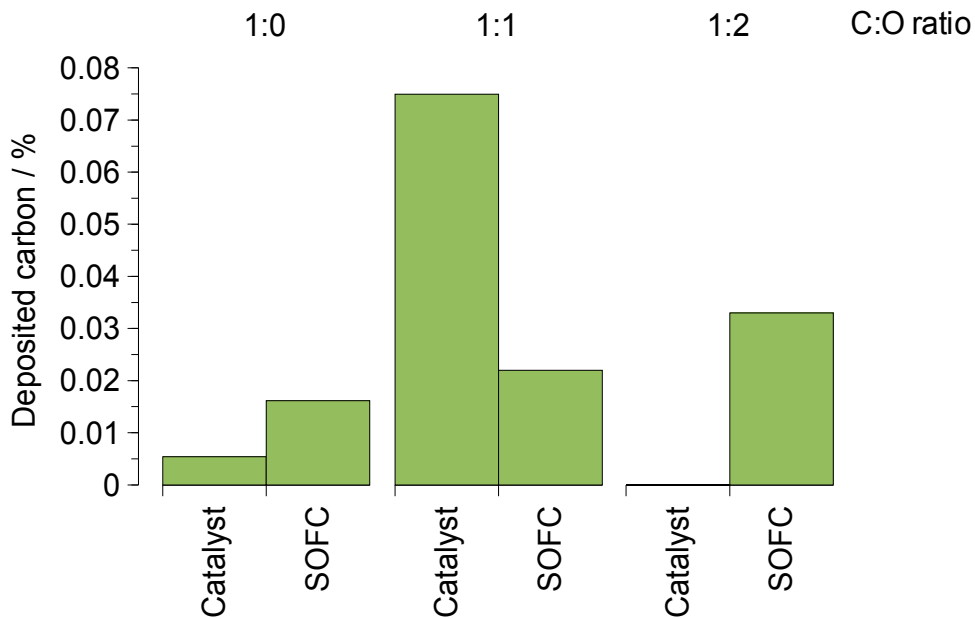


Figure 34: Carbon deposited as a percentage of carbon added for steam reformed methanoic acid

Chapter 5: C-2 hydrocarbons

5.1: Ethanol

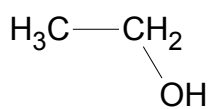


Figure 35:
Ethanol

Ethanol was the logical first choice of C-2 hydrocarbons to study. It differs from methanol only by the presence of a -CH₃ functional group, and has very similar physical properties. When considering catalytic reforming, the presence of an easily broken C-C bond increases the number of potential reactions and capacity for carbon deposition considerably. It has been widely studied as a potential fuel for both fuel cells and internal combustion engines, and thus its behaviour is well understood.

Ethanol is of particular interest because it is easily produced by fermentation from biological matter, a method that is currently employed on a large scale for both domestic consumption and motor fuel. It is non-toxic, easily stored, has a reasonably high energy density and can be transported using existing infrastructures. For SOFC applications, it is completely miscible with water, thus allowing a single phase fuel to be used.

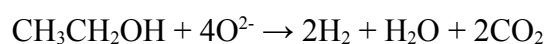
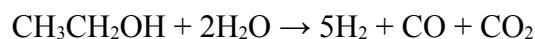
5.1.1: Steam reforming

When ethanol was used directly with no added water, there was an immediate build-up of carbon at the fuel inlet, causing the cell to block and fracture within thirty minutes. A carbon-to-water ratio of at least one was required in order to run meaningful experiments. This problem could have been avoided by reducing the fuel flowrate, but to make valid comparisons between cells (and hence fuels) the rate of fuel delivery was kept constant.

Thermodynamic studies of ethanol steam reforming^{[157] - [160]} suggested that the reaction products would principally consist of hydrogen, methane, carbon monoxide and carbon dioxide, with little or no ethanol, ethene or ethanal. Production of H₂ and CO₂ was found to be favoured as the carbon-to-oxygen ratio increased, a typical composition at around 850 °C having 4 moles of H₂ to 2 of CO and 0.5 of CO₂.

No ethanol ($m/z = 45$, CH₃CH₂O⁺) was observed in the exhaust, indicating complete decomposition or reforming even without any catalyst. The “blank” exhaust composition was similar for all carbon-to-oxygen ratios, demonstrating that any autothermal reforming was independent of oxidant level (Figure 36).

At the 1:1 ratio, two moles of water (i.e. one molecule of water per carbon atom) were added. This was sufficient to oxidise both carbon atoms, but not completely to CO₂. The “SOFC” experiment showed higher levels of H₂ than the “catalyst” - as the SOFC would consume some H₂, electrocatalytic oxidation must have been taking place as well as steam reforming:



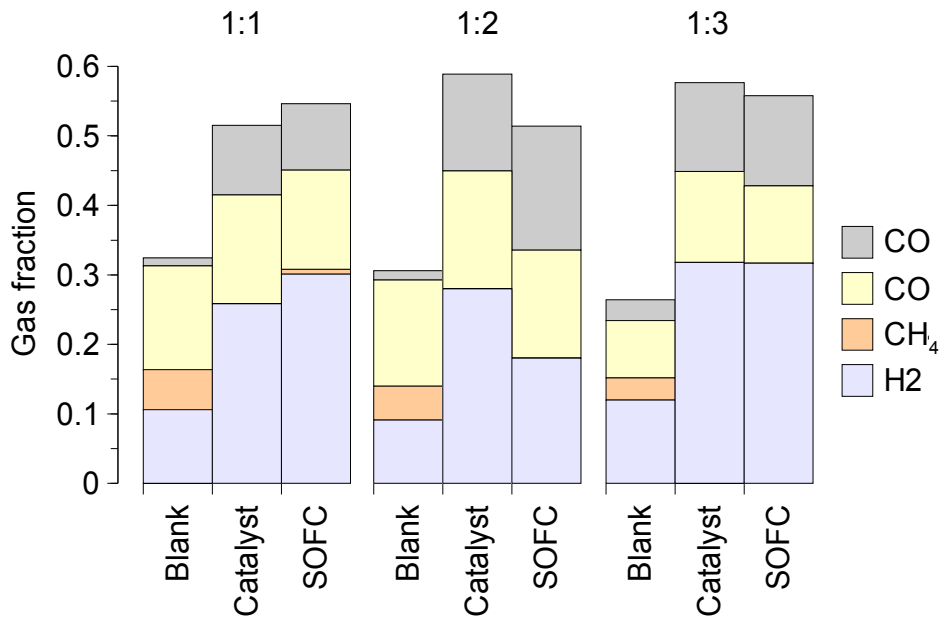


Figure 36: Exhaust gas compositions of steam reformed ethanol

At the 1:2 ratio, the “SOFC” experiment consumed a significant amount of H₂ and produced more CO₂ than the “catalyst”, which was reflected in higher electrical performance (Figure 37). The exhaust composition at the 1:3 ratio was similar for the “catalyst” and “SOFC” experiments, indicating that some electrocatalytic oxidation was taking place in a similar way to the 1:1 ratio. More H₂ was observed for this ratio than the 1:2 ratio due to the 1:2 ratio's high electrical output (converting H₂ to H₂O), but CO levels were slightly lower and CO₂ levels were typical. The additional steam drove the water-gas shift reaction in the H₂ and CO₂ direction, reducing CO and altering the steam reforming equilibrium.

5.1.2: Electrical performance

Compared to the constant decline seen for methanol (Figure 29), ethanol gave good electrical output. The anode damage, and thus, gradual decline, was not evident - the trends were similar to those seen for hydrogen (Figure 26), which could be expected as the principal component of the reformat was H₂. A gradual initial decline was seen, followed by steady output (Figure 37; Figure 19 type 5a).

The lack of anode damage may be due to an increased tendency to form reactive species through the cleavage of the C-C bond (-CH₃ and -CH₂OH) - the formation of the same species from methanol would require a stronger C-H or C-O bond to be broken. Ethanol has also been shown to decompose more readily at elevated temperatures, so fewer potentially solvating vapours will reach the anode in the first place.

The constant high current output at the 1:2 ratio is in contrast to the usual trend of increasing dilution leading to decreasing energy density. As seen in the previous section, there was an optimal amount of H₂O and the fuel consumption was higher than usual. Although the 1:3 ratio yielded higher levels of H₂ (partially due to lower fuel utilisation), dilution of the fuel and blocking of catalyst sites by H₂O (leading to a reduction in the three-phase boundary area) meant that overall performance was reduced.

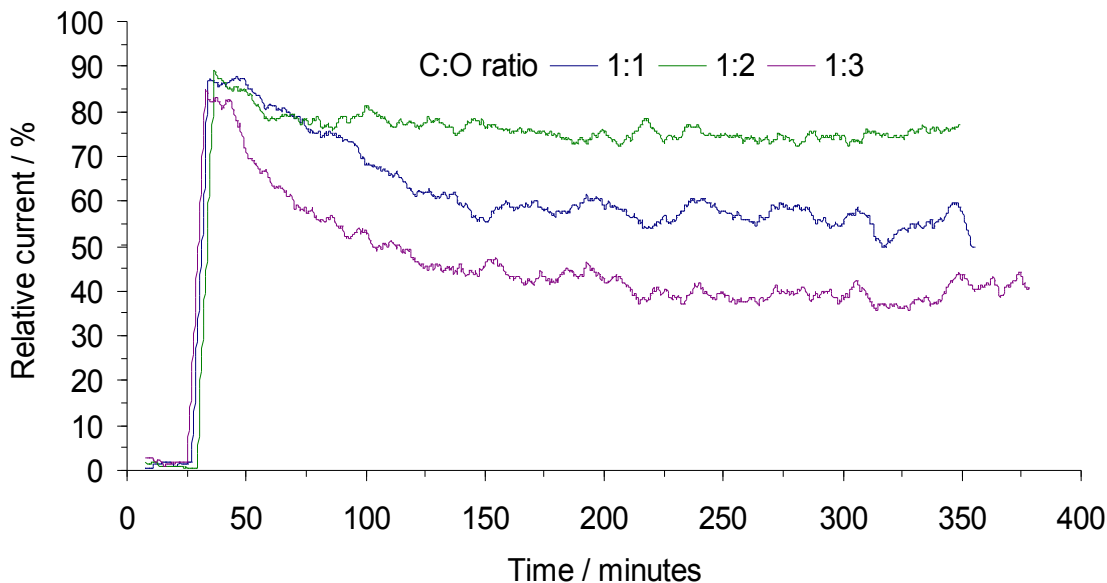


Figure 37: Trends of relative current against time for steam reformed ethanol

5.1.3: Carbon deposition

In a similar manner to the “SOFC” experiments for methanoic acid (Figure 34), the “catalyst” experiments showed a paradoxical trend of carbon deposition rates increasing with increasing steam levels (Figure 38). The “SOFC” experiments, however, behaved as expected with the 1:3 ratio having significantly lower carbon levels than the 1:1 and 1:2. The 1:1 and 1:2 ratios were similar due to similar levels of “free” H₂O, as explained in the previous section on steam reforming.

No electrocatalytic oxidation takes place during “catalyst” experiments, so no reforming with water as a product takes place and therefore additional levels will not push equilibria towards the fuel side. The exhaust gas compositions (Figure 36) were similar for all three carbon-to-

oxygen ratios - the additional water, therefore, had little effect on the steam reforming equilibria. Excessive steam levels are known to block catalyst sites, resulting in Ni particles that are dissociated from YSZ. These may be more susceptible to carbon deposition, although the optimum balance between the various reactions has been shown to lie at even higher steam levels.^[160]

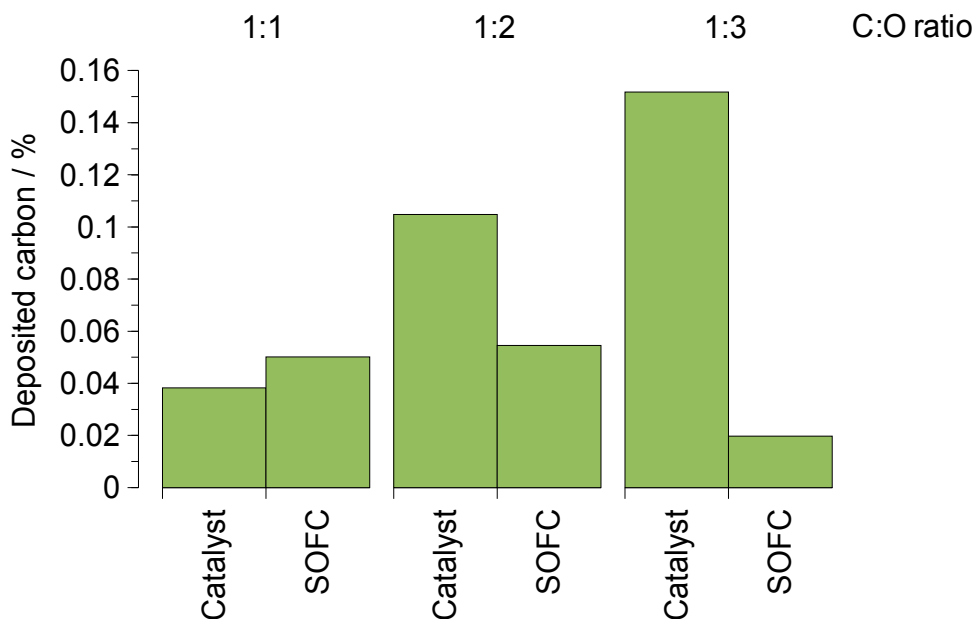


Figure 38: Carbon deposited as a percentage of carbon added for steam reformed ethanol

The deposition rate at the 1:2 “SOFC” experiment ($\approx 0.06\%$) was clearly not detrimental to the cell performance. How much carbon needs to be deposited on the anode before a performance drop becomes significant remains to be determined, and is not always apparent as SOFCs can produce current by oxidising deposited carbon to CO_2 .^[161]

5.2: Ethanoic acid (acetic acid)

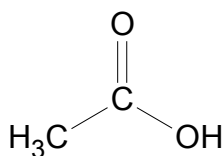


Figure 39:
Ethanoic acid

By raising the pre-oxidation level of ethanol's alcohol carbon further, ethanoic acid is obtained (a similar situation to that of methanol and methanoic acid). Although not widely used as a fuel, this molecule was chosen for academic reasons to study the effects of the C=O group by comparison to ethanol (i.e. the merits of -CH₂OH versus -COOH).

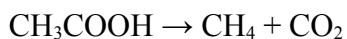
Ethanoic acid is very similar to ethanol, with the terminal alcohol group oxidised further to a carboxylic acid. It has been produced in low concentrations by fermentation for centuries, but modern industrial methods use methanol, butane or acetaldehyde as feedstocks. Of these, methanol can be produced from renewable sources.

For reasons such as relative difficulty of production when compared to extractable fuels such as methane, the potential of ethanoic acid as a SOFC fuel has received very little attention. Studies^{[162]-[164]} have tended to focus on precious metal-catalysed reforming at high carbon-to-oxygen ratios, and it has been noted that the formation of oligomers (via ethenone) can block catalyst sites.

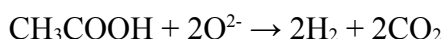
Ethanoic acid should show a higher tendency to produce CO₂ due to the full oxidation of one of the carbon atoms. The stability of the CO₂ molecule, however, may encourage cleavage of the C-C bond and thus increase carbon deposition.

5.2.1: Steam reforming

As with ethanol, ethanoic acid proved impossible to use without at least equimolar water due to extensive carbon deposition and rapid cell failure. With no catalyst present (the “blank” experiments), few products were seen (Figure 40). Ethanoic acid is known to decompose into methane or ethenone above 440 °C, but neither of these molecules were observed:



When exposed to the Ni/YSZ catalyst (the “catalyst” and “SOFC” experiments), ethanoic acid gave lower levels of H₂ and higher levels of CO₂ than ethanol (Figure 36). This was to be expected given the similar results for methanol / methanoic acid and the steam reforming / electrocatalytic oxidation reactions which give the same amount of CO₂ as ethanol but less H₂:



At the 1:1 ratio, the SOFC principally consumed H₂ as a fuel, with only small amounts of CO being oxidised to CO₂. At the 1:2 ratio, however, the SOFC still consumed H₂ but produced more CO and less CO₂ than the “catalyst” experiment. This is not possible in a steady-state system, as the amount of carbon must balance. If the SOFC was oxidising H₂ preferentially then CO would have risen (as less was being used as a fuel) and CO₂ would have dropped (for

the same reason), but this behaviour would be unusual. The relatively high levels of carbon deposition may have reduced the catalytic activity towards CO oxidation, but CO and CO₂ would also have been expected from the steam oxidation of this carbon.

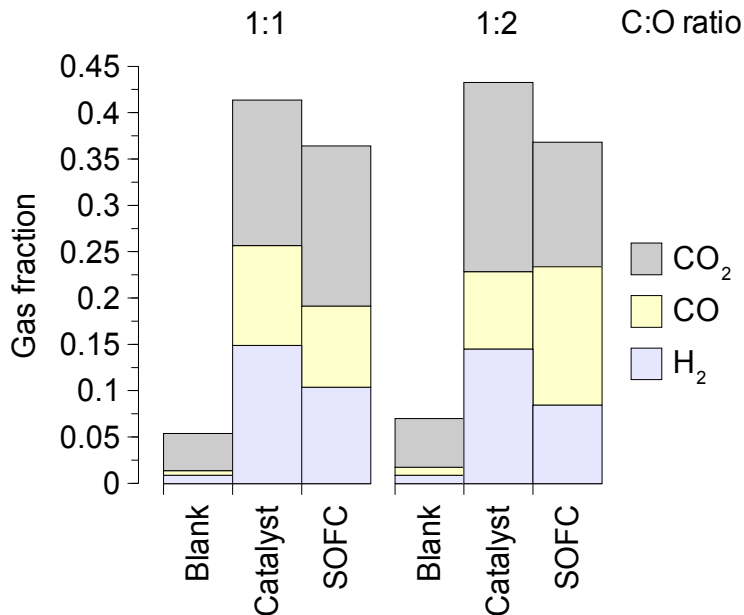


Figure 40: Exhaust gas compositions of steam reformed ethanoic acid

5.2.2: Electrical performance

At the 1:1 ratio, there was a constant steep decline (Figure 19 type 5b). As the exhaust output had typical H₂ and CO levels, this was most likely due to carbon deposition on the anode. The 1:2 ratio showed a steep initial decline followed by stabilisation at 50 % of peak output (Figure 41). As the gas composition entering the SOFC was similar to that at the 1:1 ratio, the amount of carbon deposited was the principal factor in performance loss.

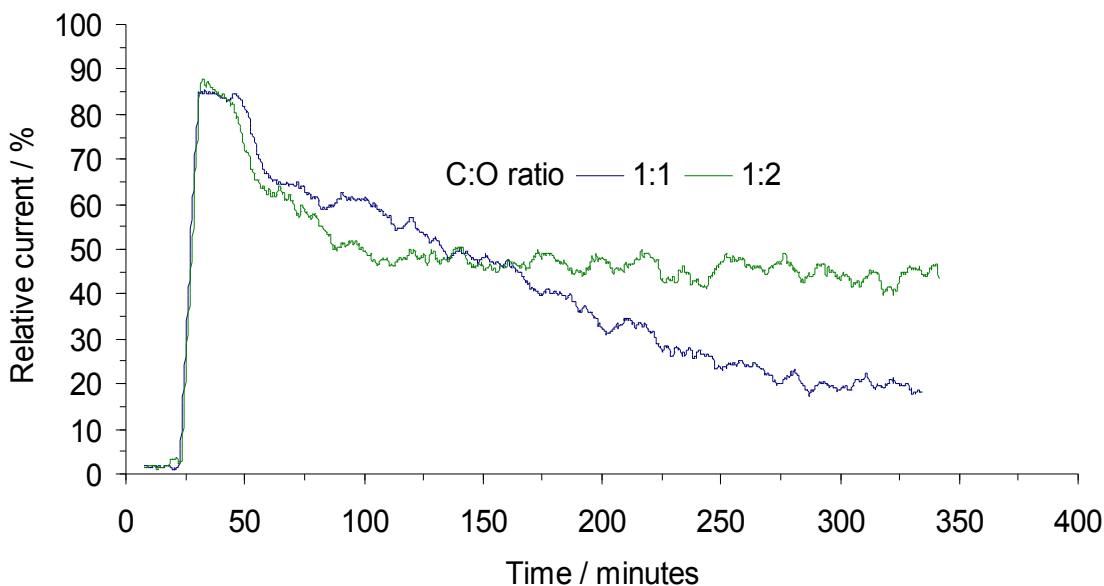


Figure 41: Trends of relative current against time for steam reformed ethanoic acid

The initial reductions in performance after the reducing H_2 was switched off were much greater than those observed for ethanol ($\approx 25\%$ as opposed to $<10\%$). This was simply due to the lower levels of H_2 in the reformed fuel stream and the greater stability (and therefore greater chance of reaching the anode intact, forcing electrocatalytic oxidation) of ethanoic acid.

5.2.3: Carbon deposition

Although the exhaust gas compositions and electrical performances were comparable (if poorer) to those obtained for ethanol, carbon deposition was higher by a factor of twenty (Figure 42). This is the reverse of the general trend for methanol / methanoic acid, and is due entirely to the additional carbon atom. During catalytic and electrocatalytic oxidation, CO_2 is

an excellent leaving group and will usually remain intact. For methanoic acid, it is effectively already formed. This is also true for ethanoic acid, but there is an additional -CH₃ group left over, which is likely to bond to Ni. This effect is not seen as much for ethanol as the pre-oxidised carbon is less stable and thus not so likely to leave, giving more time for both carbon atoms to be oxidised by H₂O or O²⁻.

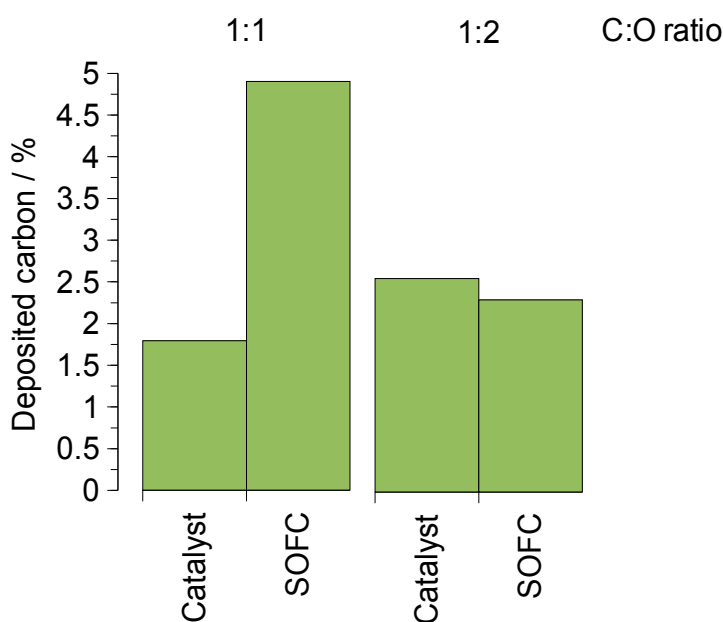


Figure 42: Carbon deposited as a percentage of carbon added for steam reformed ethanoic acid

For the “catalyst” experiments, the same rising trend obtained for ethanol was seen. This was less likely to be due to catalyst site blocking from the increased “free” H₂O, as the C:O ratio was lower. The difference was close to experimental error, however, and the “SOFC” experiments gave a more typical decreasing trend. At the 1:1 ratio, carbon was deposited at an apparently greater rate in the “SOFC” experiment than in the “catalyst” due to the deposition

Very little previous work on its use in SOFCs exists, due (like ethanoic acid) to the relative difficulty of production when compared to fuels such as methane; studies have tended to focus on the suitability of metal catalysts to produce hydrogen^{[165], [166]}. Like ethanol, though, it has good physical properties and is completely miscible with water.

Due to the structural similarity with ethanol, ethane-1,2-diol was expected to behave in a very similar manner. The extra -OH group would decrease the amount of hydrogen easily available, but aid reforming to CO or CO₂. If the molecule decomposed immediately at the C-C bond, however, then it could behave more like methanol due to the formation of two identical -CH₂OH species.

5.3.1: Steam reforming

Like previous C-2 hydrocarbons, ethane-1,2-diol proved impossible to use without at least one mole of water as an oxidising agent and diluent. Not only did the neat fuel deposit carbon readily, but the high viscosity led to a tar-like substance forming in the fuel evaporator. The addition of water increased fuel mobility sufficiently to avoid this problem.

At both carbon-to-oxygen ratios, there was sufficient water for the reforming reaction to go to completion. Without catalysis, CH₄ was observed in the exhaust stream, indicating that some methane was formed from a decomposition reaction which also explained the high CO levels:



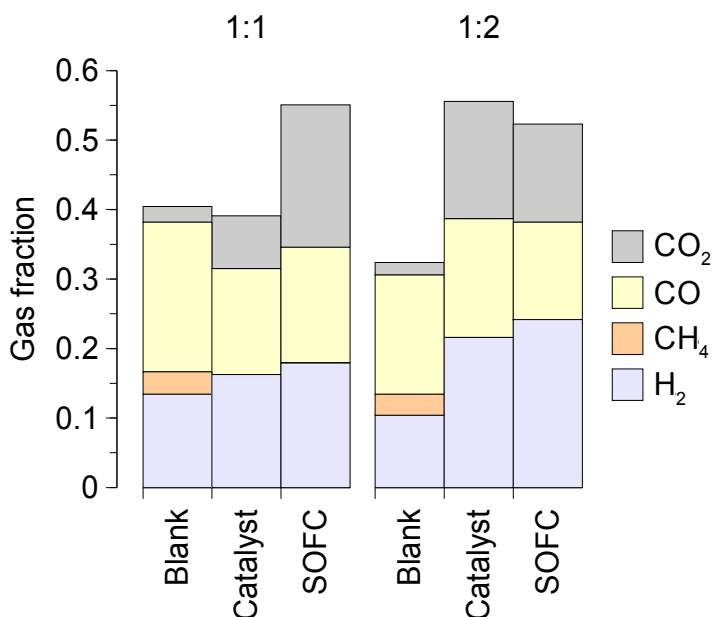
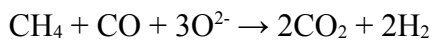
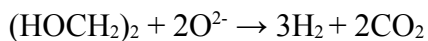


Figure 44: Exhaust gas compositions of steam reformed ethane-1,2-diol

At the 1:1 ratio, the “SOFC” experiment gave slightly higher H₂ and CO levels than the “catalyst”, but significantly higher CO₂ levels (Figure 44). In addition to steam reforming, electrocatalytic oxidation was taking place and the CH₄ and CO produced through decomposition (above) were also oxidised to CO₂:



At the 1:2 ratio, both CO and CO₂ levels were lower in the “SOFC” experiment than in the “catalyst”, though the H₂ levels were higher. This was similar to the result for ethanoic acid,

but the preferential consumption of H₂ clearly cannot apply. The differences in gas fraction were within experimental error, however, and could be better defined by repeating the runs.

The 1:2 ratio showed higher H₂ levels than the 1:1, though overall CO and CO₂ levels were similar. The presence of more water favoured irreversible fuel reforming to H₂ and CO₂, which drove the reversible water-gas shift reaction to CO and H₂O.

5.3.2: Electrical performance

The electrical output of an ethane-1,2-diol-fuelled SOFC gave no performance increase when the fuel entered the cell, and was characterised by a very long decline leading to stable operation (Figure 45). The output levels of 20 % (1:1) and 50 % (1:0) were significantly lower than those for ethanol (Figure 37) despite the higher pre-oxidation level. The lower H₂ levels from reforming contributed to this, but there is also a steric argument as ethane-1,2-diol is much larger than ethanol and may not be able to approach the fixed catalyst as easily.

Despite higher H₂ levels at the 1:2 ratio, electrical performance was much lower than at the 1:1 ratio. This dilution effect has been observed before, and was a consequence of the lower fuel concentration resulting in reduced electrocatalytic oxidation. In this case, increased steam levels actually seemed to be detrimental overall - the higher H₂ levels were offset by poorer current output and higher carbon deposition.

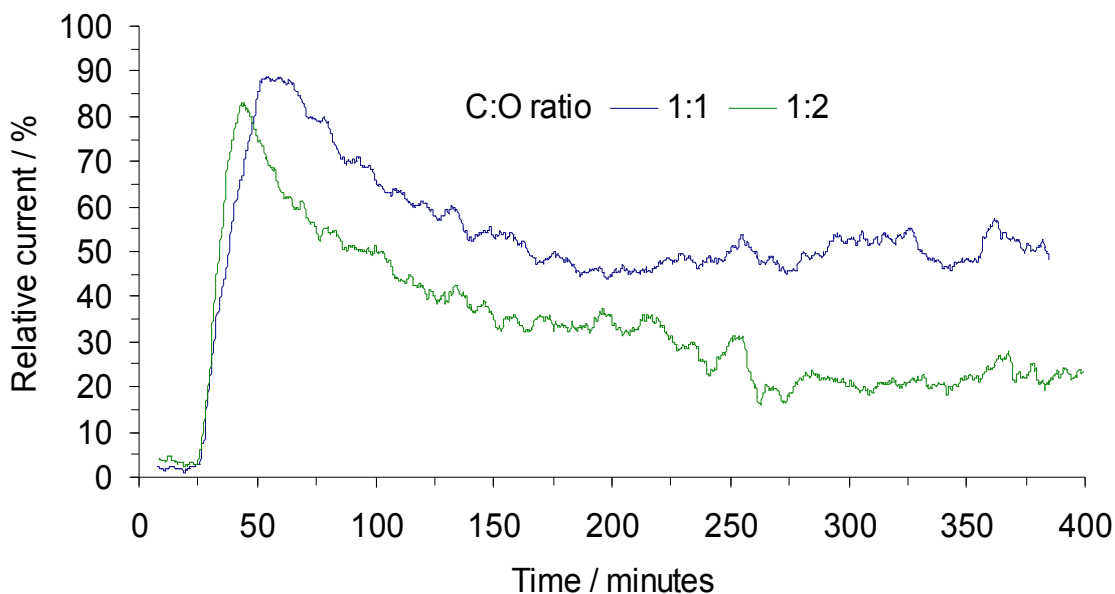


Figure 45: Trends of relative current against time for steam reformed ethane-1,2-diol

5.3.3: Carbon deposition

Although ethane-1,2-diol ($C_2H_6O_2$) is empirically similar to ethanol (C_2H_6O) and ethanoic acid ($C_2H_4O_2$), carbon levels were comparable to those of methanol (Figure 30). This was strong evidence that the molecular structure has a significant effect on carbon deposition rates.

The reverse trend to that of ethanoic acid was obtained - carbon levels decreased with increasing water for “catalyst” experiments and increased for “SOFC” experiments (Figure 46). As with ethanol, the deposition rate was not detrimental to SOFC performance, although it was lower by a factor of three (0.02 % as opposed to 0.06 %). The reduced carbon deposition for the 1:1 “SOFC” experiment may be due to the higher electrical performance, and hence higher rate of electrocatalytic oxidation.

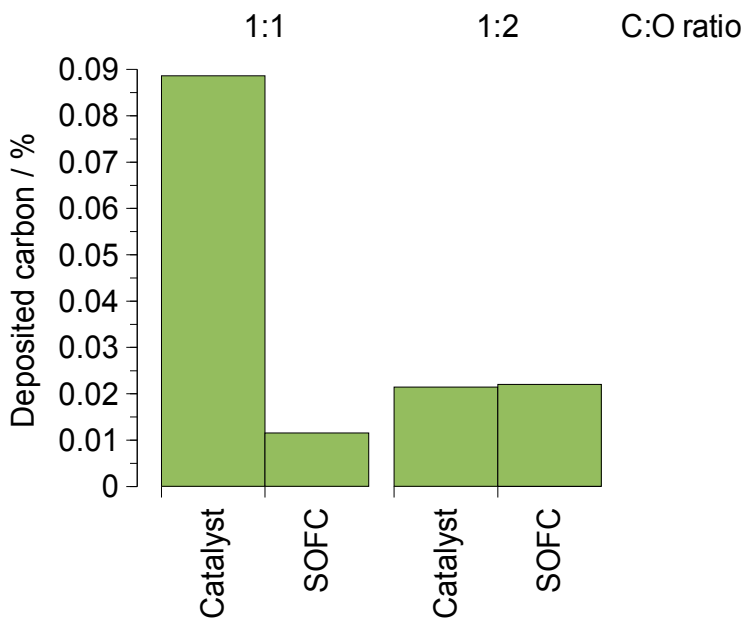


Figure 46: Carbon deposited as a percentage of carbon added for steam reformed ethane-1,2-diol

5.4: Methoxymethane (dimethyl ether)

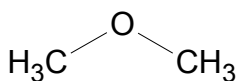


Figure 47:
Methoxymethane

To investigate the effect of the carbon-carbon bond on fuel performance, the ethanol isomer methoxymethane was used. This gas has the same empirical formula as ethanol (C₂H₆O), but the separation of the carbon atoms by an oxygen leads to vastly different physical properties. It is water-soluble, which may aid with reforming and storage, and is highly flammable. From the theories outlined in the introduction, the lack of carbon-carbon bonds should reduce the rate of carbon deposition - although the levels for ethanol were not excessive to begin with.

Methoxymethane is made from natural gas, biogas or methanol, which allows carbon-neutral production if biological feedstocks and renewable energy are used. It is widely used as an aerosol propellant (after the discontinuation of CFCs) and in the automotive industry as a relatively clean-burning fuel or fuel additive. Relatively few studies have been carried out on it, and work has focused on catalytic oxidation^{[167] - [169]}

5.4.1: Steam reforming

As methoxymethane is a gas, it was not possible to use the standard syringe arrangement as had been done for other fuels. A constant flow of gas ($\approx 10 \text{ ml min}^{-1}$) was mixed with the inert carrier gas and bubbled through a water saturator at room temperature. As methoxymethane is water-soluble and helium is not, a steady flow of helium and the equilibrium fraction (from the water and headspace) of methoxymethane was delivered to the fuel cell, resulting in a carbon-to-oxygen ratio of about 6:1. This made comparison with other fuels more difficult, but was the most practical way of delivering the fuel. Mixing the fuel with the carrier gas and adding the water via a (fuel) syringe resulted in immediate carbon build-up and blockage at the cell inlet.

The rate of fuel delivery to the cell was much higher than that used for liquid fuel delivery, resulting in increased fractions of hydrocarbon products (Figure 48). Methoxymethane decomposed readily to H_2 and CO and even without nickel catalysis (the CH_3 was due to the fragmentation pattern), but the low C:O ratio meant that the fuel cracking pattern coincided with any reforming products:

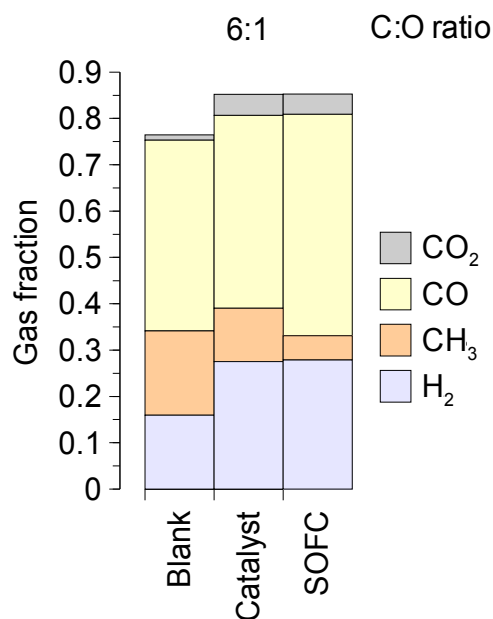
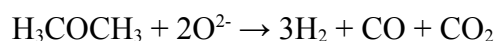
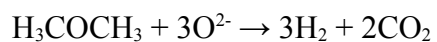
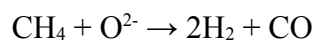


Figure 48: Exhaust gas compositions of water saturated methoxymethane

With the high carbon-to-oxygen ratio (limited by the vapour pressure of water), only small amounts of steam reforming could take place and rapid decomposition limited electrocatalytic oxidation:



The “catalyst” and “SOFC” experiments yielded almost identical amounts of H₂ and CO₂, but the SOFC consumed CH₄ and produced CO. This is typical of a methane-fuelled SOFC; the lack of increased CO₂ levels was due to the absence of steam:



5.4.2: Electrical performance

The trend of a methoxymethane-fuelled SOFC was initially typical of a cell with moderate amounts of carbon deposition (Figure 19 type 5c), but maintained steady output instead of showing a decline (Figure 49). The initial rise (1) was due to the formation of conducting carbon particles between nickel particles, which eventually damaged the anode and cause an output drop (2). Instead of the decline becoming terminal, however, in this case the deposited carbon was oxidised to CO and output was steady (3).

The consistent high output (in contrast to most liquid-delivered fuels) was a result of the higher fuel concentration. It was found that increasing the liquid fuel delivery rate caused pressure build-ups in the evaporator from the high liquid-to-gas expansion ratio, and so a lower standard flowrate was used. The minimum flowrate for methoxymethane, however, was effectively fixed by the type of cylinder used and so the results above are not necessarily indicative of improved performance relative to the other fuels studied.

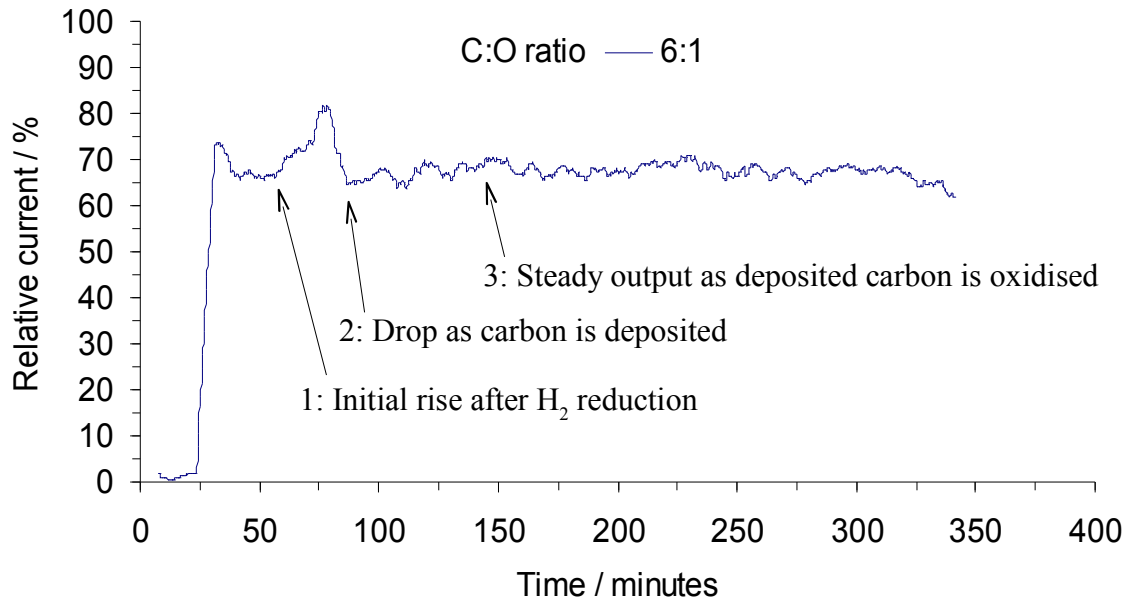


Figure 49: Trends of relative current against time for water saturated methoxymethane

5.4.3: Carbon deposition

The high dissociation (to CH_4 and CO) and electrocatalytic oxidation rates, coupled with the relatively low H_2O levels, meant that carbon deposition rates were high (Figure 50). The increased fuel concentration also caused more carbon-containing molecules to contact the anode. The large disparity between the “catalyst” and “SOFC” experiments, despite similar exhaust gas compositions (Figure 48), demonstrated the ability of the SOFC to use deposited carbon as a fuel.

A 0.5 % deposition rate is not excessive, and indeed ethanoic acid was observed to operate with a rate of 2 % (Figure 42). However, given the extremely high deposition rate for the

“catalyst” experiment, it is likely that the cell would eventually fail, especially if any amount of time was spent at open circuit voltage.

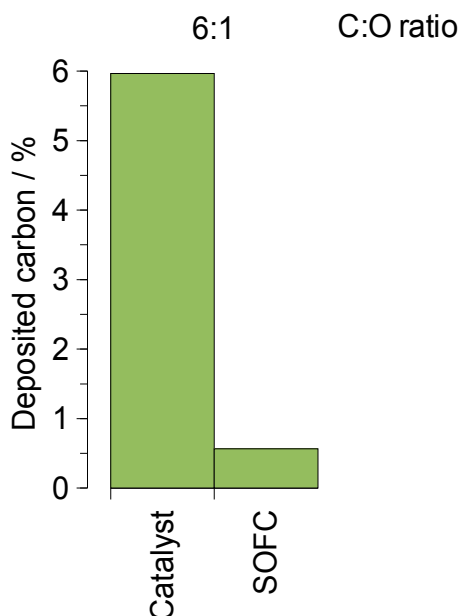


Figure 50: Carbon deposited as a percentage of carbon added for water saturated methoxymethane

5.5: Methyl methanoate (methyl formate)

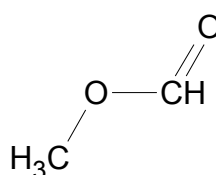


Figure 51: Methyl methanoate

Remaining with the carbon atom separation argument, the pre-oxidation level of a methoxymethane carbon atom was raised to an aldehyde to give methyl methanoate. This is in slight contrast to the previous experiments (where alcohols were raised to carboxylic acids), but consistent as it can

also be viewed as the modification of methanoic acid to replace the alcoholic hydrogen with a -CH₃ group.

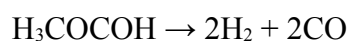
Structurally, methyl methanoate is similar to methoxymethane in that it contains two carbon atoms linked by an oxygen (eliminating a potential C-C bond). Physically, it is a low-boiling point liquid that is slightly miscible with water. It can be produced easily from methanol and methanoic acid, or methanol and carbon monoxide; all of which can be generated renewably.

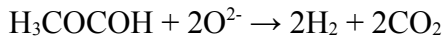
The fact that methyl methanoate is a liquid allows more accurate control over the amount of water in the fuel mix, and removes some of the potential problems with storage and transportation. It should behave like methoxymethane, with a greater tendency to form CO₂ (and possibly carbon) due to the increased oxidation of one carbon atom, much like ethanoic acid compared to ethanol.

The potential of methyl methanoate as a SOFC fuel has never been the subject of a published study, and its mention in reforming has been solely as an intermediate in the decomposition of methanol.^[170]

5.5.1: Steam reforming

At the 1:0 ratio, the “blank” experiment showed the expected mass spectrum of methyl methanoate fragmentation products; either from thermal decomposition or fragmentation in the spectrometer (Figure 52). With catalysis, reforming to H₂ and CO took place, and the SOFC both consumed these products and oxidised the fuel directly:





The use of a substoichiometric amount of water (the 2:1 ratio) favoured the production of equal amounts of CO and CO₂, but this was only observed in the “SOFC” experiment (due to electrocatalytic oxidation and consumption of CO). As methyl methanoate already has a carbon-to-oxygen ratio of 1, it should reform to CO very easily. If the amount of water required for stable operation can be reduced, then the energy density and efficiency can be improved.

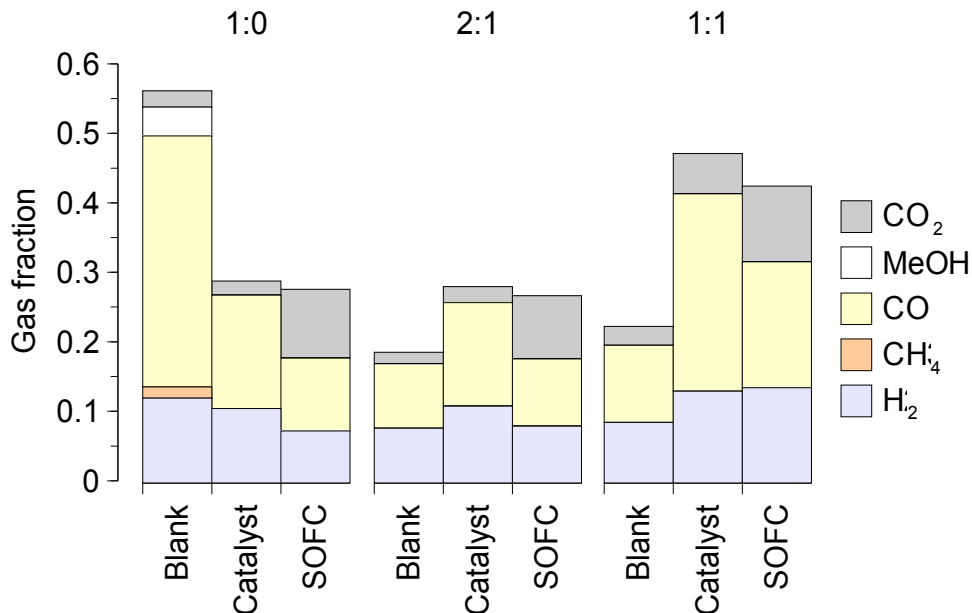
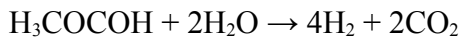
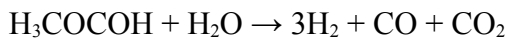


Figure 52: Exhaust gas compositions of steam reformed methyl methanoate

The 1:1 ratio showed higher H₂, CO and CO₂ levels from the stoichiometric amounts of water, which allowed complete reforming. H₂ levels were similar for “catalyst” and “SOFC” experiments, suggesting that the amount of additional H₂ formed from electrocatalytic oxidation was greater than the amount that could be readily consumed by the SOFC.

5.5.2: Electrical performance

All carbon-to-oxygen ratios showed a steep initial decline, with the 1:0 and 2:1 ratios not recovering and the 1:1 ratio stabilising at ≈20 % of peak output (Figure 53). The terminal declines were steeper but not dissimilar to those seen for methanol (Figure 29), which may be expected due to the rapid fragmentation to the methanol-like -OCH₃ and -COH described earlier.

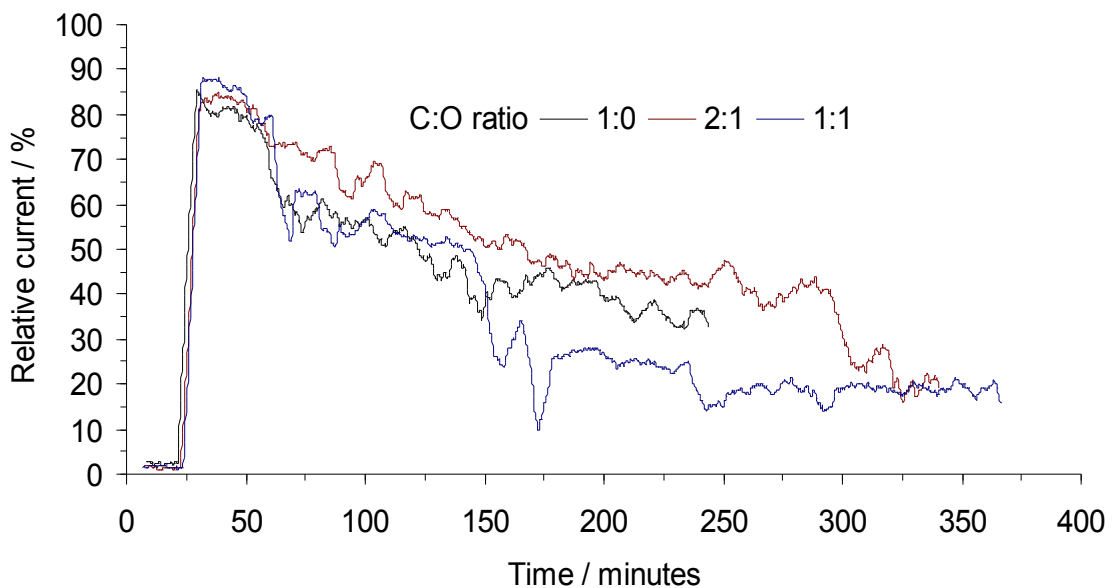


Figure 53: Trends of relative current against time for steam reformed methyl methanoate

At the 1:1 ratio, output levels were slightly lower than those for the other ratios as the fuel was more diluted, an effect that has been previously noted. The exhaust gas data showed good reforming with reasonable levels of H₂ and CO, and carbon deposition was low. Despite this, electrical output was generally poor - demonstrating that performance is governed by more than just gas composition and carbon levels.

5.5.3: Carbon deposition

Carbon levels at the 1:0 ratio were comparable to those of ethanol (Figure 38), which was unexpected given the lack of C-C bonds and dissimilar decomposition products. When even a substoichiometric amount of water was added, however, deposition rates dropped by a factor of ten (Figure 54).

As the principal difference between the 1:0 and other ratios was the presence of water (and hence the reforming reactions), the methyl methanoate decomposition products must have deposited carbon (though, at 0.2 %, not rapidly). Additional water has been shown to remove deposited carbon in some situations but not others, demonstrating that effects other than excess water oxidising deposited carbon exist. The most effective way of avoiding carbon build-up is therefore to match fuels and reforming reaction equilibria so that carbon formation is unfavourable.

As a SOFC has been shown to operate on carbon levels as high as 2 % (Figure 41), the levels for methyl methanoate are unlikely to be the sole cause of the decline in electrical output. The

decomposition products were similar to methanol, but are unlikely to damage the anode in the same way as that argument relied on on intact methanol vapours. It is possible that there was insufficient time to reach an equilibrium of steady operation, but more likely that the lack of water prevented effective reforming through inadequate humidity.

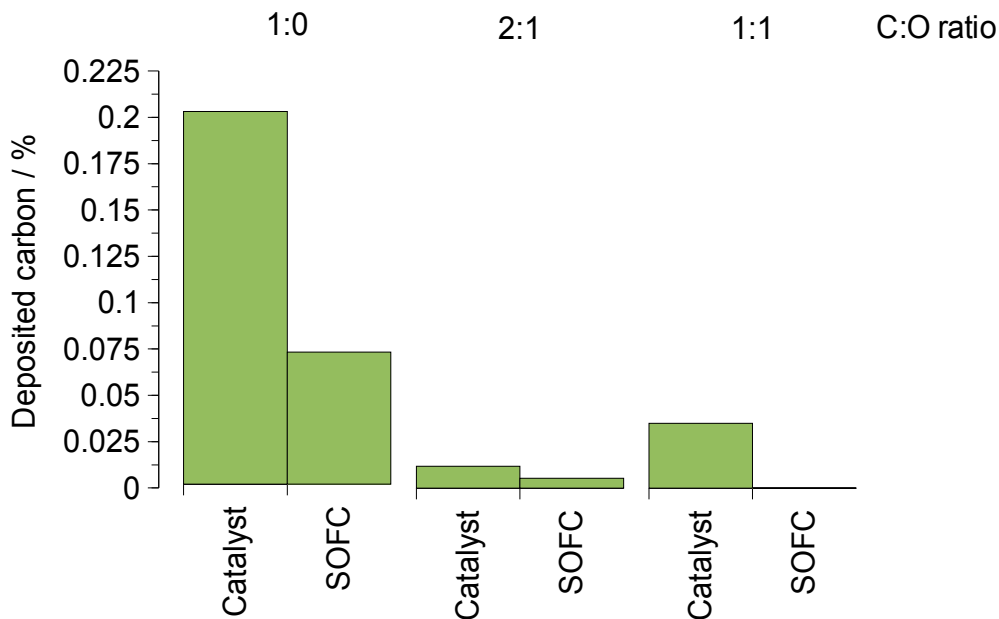


Figure 54: Carbon deposited as a percentage of carbon added for steam reformed methyl methanoate

5.6: N-methyl methanamide (N-methyl formamide)

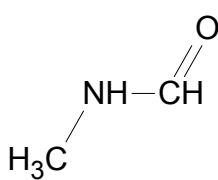


Figure 55: N-methyl methanamide

N-methyl methanamide is essentially identical to methyl methanoate, with a NH group linking the terminal carbons rather than an oxygen. If physical separation of the carbon atoms is the primary reason for a reduction in deposition rates, then the separating atom should have little

effect. If the reason is additional oxidant, then deposition rates should be higher. The -NH- link provides the same function of preventing a C-C bond with the advantage of extra potential fuel (through an additional hydrogen atom) and the disadvantage of slightly less reforming potential (through the lack of an additional oxygen atom). At SOFC operating temperatures, molecules are very likely to fragment and hence a NH-containing molecule will have additional fuel, whereas a O-containing molecule will have additional oxidant.

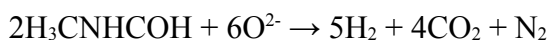
N-methyl methanamide can be produced from methanoic acid and methanamine, though the process is relatively energy intensive. Like methyl methanoate, no studies on the use of N-methyl methanamide in fuel cells or its reforming have been published. This may be due to the increased tendency of nitrogen-containing compounds to form NO_x in the exhaust, though ammonia has received much attention.^{[171]-[174]}

5.6.1: Steam reforming

N-methyl methanamide proved extremely stable when run uncatalysed, almost to the extent that it did not decompose at all (Figure 56). This was quite unexpected, as C-N bonds are known to be weaker than both C-O and C-C bonds, which have broken readily in past experiments, though thermal decomposition is not necessarily a function of bond strength.

At the 1:0 ratio, high levels of H₂ and CO but low levels of CO₂ were observed, with the “SOFC” experiment producing more CO than the “catalyst”. No NO_x products (NO, NO₂)

were seen in the exhaust stream, suggesting that SOFCs do not readily oxidise N to NO_x, and previous work^[172] suggests the formation of molecular nitrogen:



NO_x is only formed from atmospheric N₂ and O₂ at temperatures well over 1000 °C, so the same may be true for nitrogen embedded in a molecule. This is an advantage in terms of emissions (NO_x is a major cause of smog and acid rain), but other reaction products are also possible. Ammonia (NH₃) would give a trace at $m/z = 17$, which would be masked by -OH from H₂O; likewise N₂O ($m/z = 44$) would be masked by CO₂. However, no unusually high (apparent) H₂O or CO₂ levels were observed. Alternatively, the presence (though not the quantity) of ammonia could be detected with a pH meter or litmus paper due to its alkalinity. Other N-containing products such as HCN were not observed either. N₂, however, is stable under fuel cell operating conditions and gives a mass spectrometer peak at $m/z = 28$ (masked by CO). Apparently high levels of CO (i.e. $m/z = 28$) were observed, supporting this theory. N₂ also gives a peak at $m/z = 14$ (N), but this is weak and only distinguishable from noise at high N₂ levels.

At the 1:1 ratio the SOFC consumed significant amounts of H₂ and CO, which was reflected in the electrical performance. CO levels overall were lower than those in the 1:0 ratio - the lower deposition rates resulted in less oxidation of immobilised carbon (by O²⁻ or air).

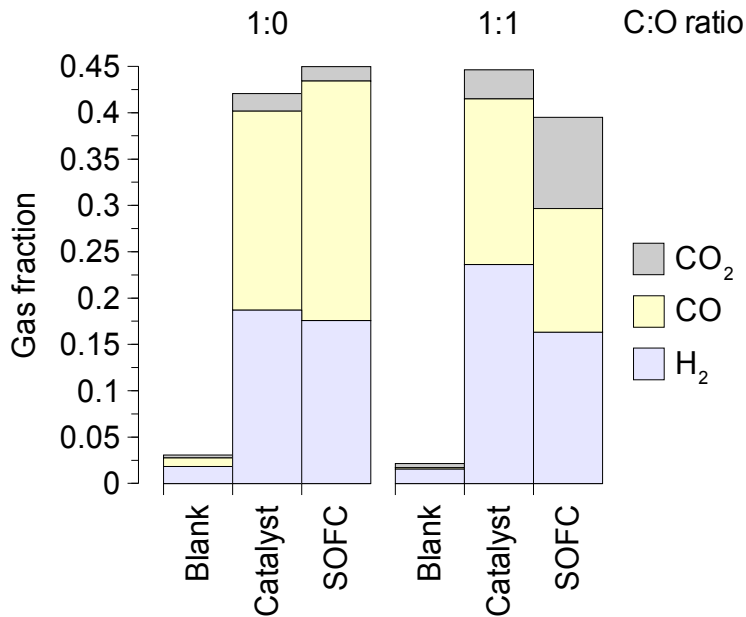


Figure 56: Exhaust gas compositions of steam reformed N-methyl methanamide

5.6.2: Electrical performance

The 1:0 ratio showed behaviour typical of high carbon deposition (Figure 19 type 5b and 5c), with an initial increase followed by a steep terminal decline. Although the end result was the same as that seen for methyl methanoate (Figure 53), the method of failure was substantially different.

The 1:1 ratio showed little initial decline in performance, with a slight downward trend over the course of the experiment (Figure 57). In contrast to methyl methanoate, the current output was 70 % - 80 % of peak value - this was partly a fuel concentration effect (higher H₂ and CO

levels) and partly the greater tendency of N-methyl methanamide to reform to useful products rather than decompose.

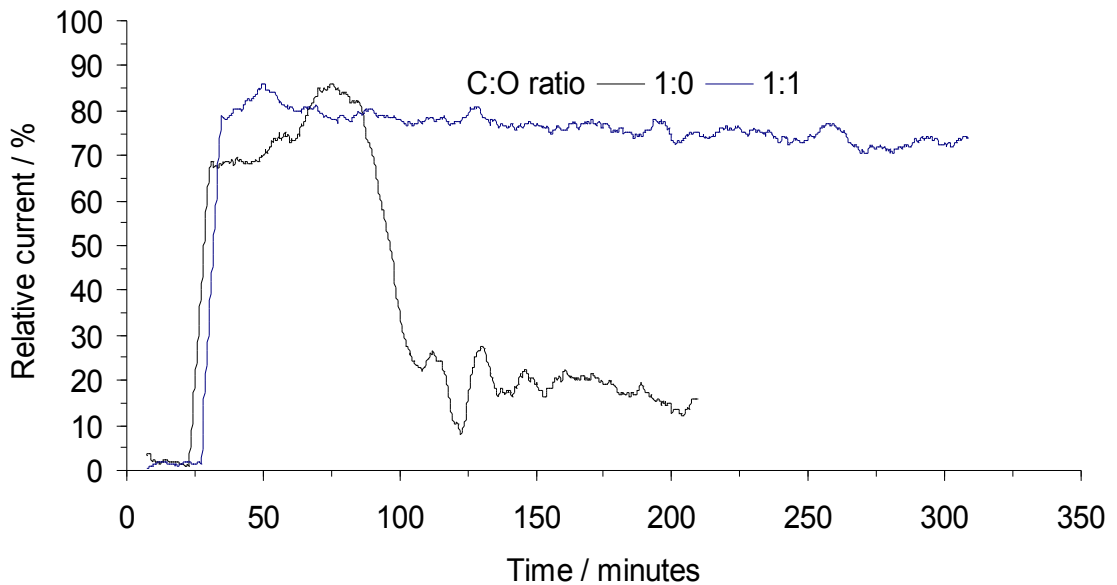


Figure 57: Trends of relative current against time for steam reformed N-methyl methanamide

5.6.3: Carbon deposition

Extremely high levels of carbon were seen for the 1:0 ratio “catalyst” experiment (Figure 58), confirming the exhaust gas composition data that N-methyl methanamide remains intact and breaks down on the Ni catalyst. The “SOFC” experiment showed a terminal decline in current output at a carbon deposition rate of around 0.5 %, but previous results have shown that the SOFC can tolerate a level as high as 2 % over the course of a typical experiment. Significant amounts of carbon were oxidised to CO, but this removal rate was not enough to prevent failure.

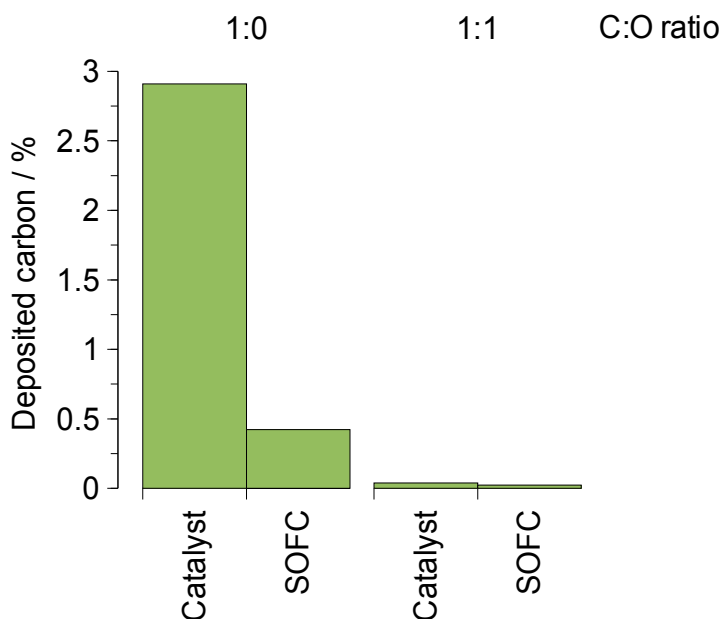


Figure 58: Carbon deposited as a percentage of carbon added for steam reformed N-methyl methanamide

The principal difference between this experiment and other high-deposition ones was the physical point of most deposition. With N-methyl methanamide, carbon deposition occurred almost as soon as the fuel came into contact with the anode. This caused a build-up of carbon at the entrance to the cell, blocking it and preventing any more fuel from passing, thus resulting in the loss of electrical output. Ethanoic acid was mixed with equimolar water, improving mobility and diluting the fuel slightly to allow more even deposition along the length of the anode. This carbon could then be removed by all the O^{2-} ions rather than only those nearest the fuel inlet. When equimolar water was added to the N-methyl methanamide, carbon levels were reduced to near-negligibility (<0.1 %). This was due to improved reforming and a more even deposition area, described above.

Replacing the carbon-separating oxygen atom with a NH group had a large impact on results. Although the molecule did not decompose as easily, causing problems if it was used without water, it was more readily reformed to useful gases. Optimal electrical output was significantly higher over the course of the experiments. Carbon levels were higher without added water, but similar with.

The higher levels of carbon deposition by the nitrogen-containing compound were, as outlined before, due to its reluctance to decompose at elevated temperatures. Even with water present to drive the thermodynamic equilibrium, the energy barrier was too high and the molecule entered the SOFC intact. The remarkably higher electrical output (at a 1:1 carbon-to-oxygen ratio) could only be due to a higher fuel concentration (i.e. the rate at which fuel molecules came into contact with the anode). As methyl methanoate contains two oxygenated carbon groups, it forms CO₂ readily; N-methyl methanamide contains only one, and additionally only decomposes on the anode. Thus the reforming reaction products were close to the three-phase boundary area when they were produced, rather than being in the main gas stream where there was a higher probability of passing through the cell. Finally, carbon levels (with added water) were similar, and lower than most other C-2 hydrocarbons. This partially supports the theory that carbon is deposited more easily if carbon atoms are adjacent - high levels of carbon were seen if no water was present, illustrating that there are more mechanisms than just the C-C bond transition state one. Even slight humidification was enough to almost eliminate deposition, though, so the carbon that would otherwise be formed during a reforming reaction was prevented from doing so by the molecular structure.

Chapter 6: C-3 and C-4 Hydrocarbons

6.1: Propane-1,2,3-triol (glycerol / glycerin)

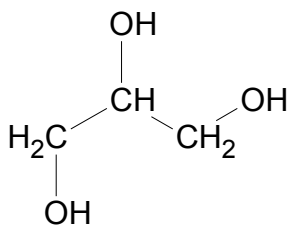


Figure 59: Propane-1,2,3-triol

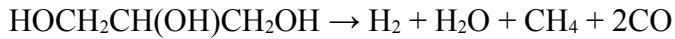
C-3 hydrocarbons are known to deposit carbon much more readily than C-2, and so a logical progression from the C-2 hydrocarbons would be propane-1,2,3-triol. This is essentially ethane-1,2-diol with an additional hydroxymethyl group, increasing the number of carbon atoms without increasing the overall pre-oxidation level.

Like ethane-1,2-diol, propane-1,2,3-triol is a viscous liquid that requires mixing with water before it is mobile enough to be injected into a fuel cell. It is a by-product of the biodiesel industry, formed when fatty acids are cleaved from a triglyceride - it can therefore be produced from virtually any fat or oil and so is easily derived from other biological sources.

Due to the high tendency to deposit carbon, propane-1,2,3-triol has not been extensively studied as a fuel cell fuel. Some work has been done on reforming^{[175], [176]} and on its potential as a feedstock in microbial fuel cells^[177], however.

6.1.1: Steam reforming

Without catalysis, propane 1,2,3-triol decomposed readily to give CO, and lower fractions of H₂ and CH₄, in a similar manner to ethane-1,2-diol (Figure 44):



At the 1:1 ratio, the presence of a catalyst increased the amounts of H_2 and CO_2 via steam reforming, and the “SOFC” experiment consumed CH_4 and produced CO_2 as would be predicted (Figure 60):

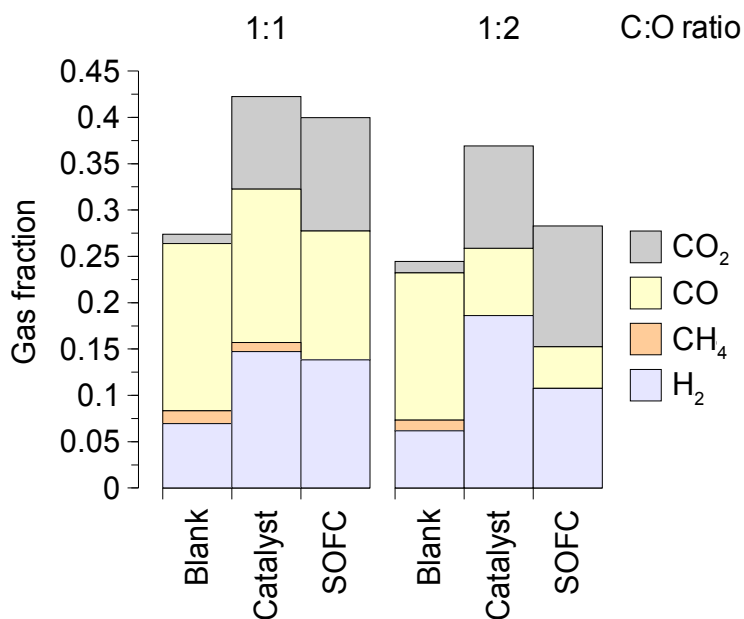


Figure 60: Exhaust gas compositions of steam reformed propane-1,2,3-triol

With an additional three moles of water (the 1:2 ratio), more H_2 and significantly less CO was produced. Some CO was oxidised to CO_2 , but the greater concentration of water allowed for

more complete steam reforming (and the reforming of decomposition products) and less carbon deposition. This was reflected in the lack of CH₄ in the 1:2 “catalyst” experiment.

6.1.2: Electrical performance

In contrast to ethane-1,2-diol, the electrical output of a propane-1,2,3-triol-fuelled SOFC showed a steady decline (Figure 61). Both 1:1 and 1:2 ratios dropped to $\approx 15\%$ of peak output over the course of the experiment, and the curved trend suggested that stable operation may have been possible after ≈ 250 minutes.

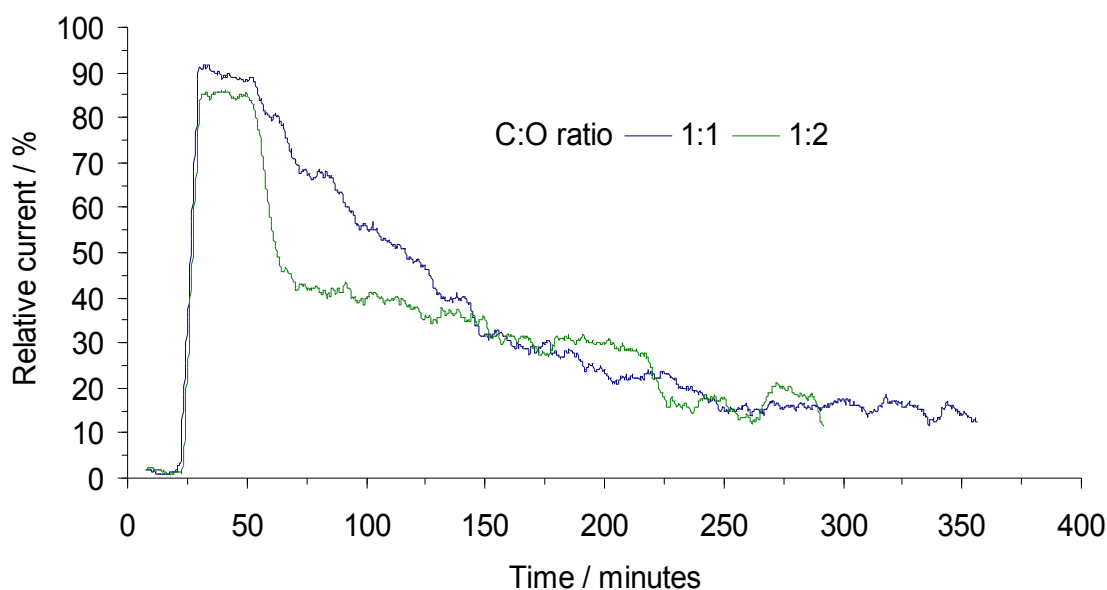


Figure 61: Trends of relative current against time for steam reformed propane-1,2,3-triol

The trends differed at the start of the experiment, with the 1:1 ratio declining steadily and the 1:2 showing a steep drop. This was due to the difference in fuel dilution - the additional water in the 1:2 ratio acted as a physical diluent and also reformed potential fuels such as CO and CH₄. As the final current output was similar for both ratios, the reforming products were offset by the decomposition products and offered similar fuel concentrations.

6.1.3: Carbon deposition

Relatively high rates of carbon deposition were seen for the “catalyst” experiments; higher by a factor of ten than those seen for ethane-1,2-diol (Figure 46). As the two molecules are essentially identical in structure type and pre-oxidation level, the presence of the additional -COH group (and hence C-C bond) had a large effect on the tendency to deposit carbon.

The “SOFC” experiments also gave higher rates of carbon deposition, but the difference was not as marked as the 1:2 ratio. Both types of experiment gave predicted trends of decreasing carbon deposition with increasing steam levels (Figure 62). For the “SOFC” experiments, this trend was the reverse of the one seen for ethane-1,2-diol and demonstrates a different equilibrium position for the various reforming reactions. As propane-1,2,3-triol deposits carbon readily when in contact with the Ni/YSZ anode, the increased steam levels (and hence increased reforming) prevented this from happening as much.

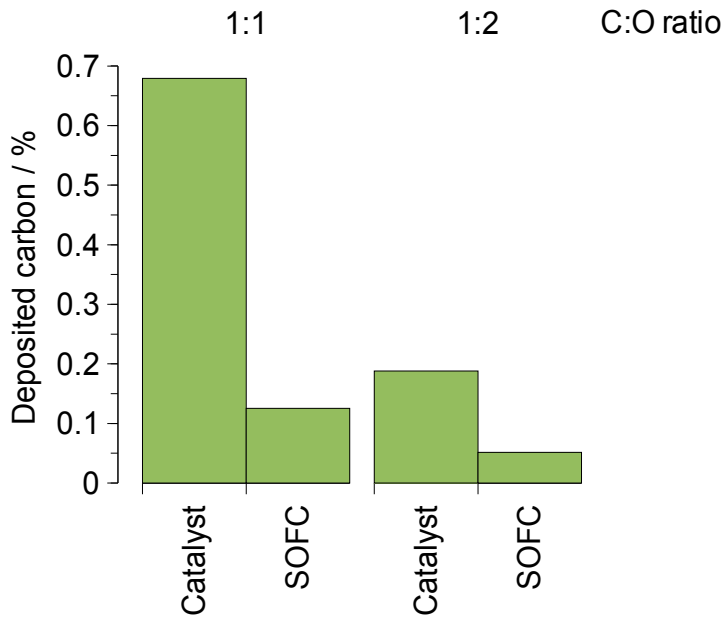


Figure 62: Carbon deposited as a percentage of carbon added for steam reformed propane-1,2,3-triol

6.2: 2-Methoxyethanol

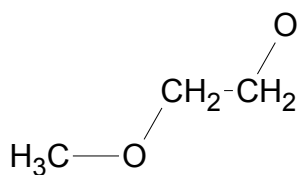


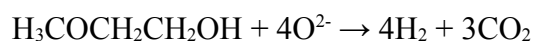
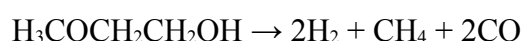
Figure 63: 2-Methoxyethanol

If the additional carbon atom added to ethane-1,2-diol is not added to the existing chain but attached to an oxygen as a methyl ether, 2-methoxyethanol is formed. This is also a primary progression from the C-2 hydrocarbons, but in a different direction to propane-1,2,3-triol - there is no unbroken carbon (alkane) chain. 2-Methoxyethanol can be derived from ethanol or ethane-1,2-diol, and hence sustainable sources, via chemical methods.

Perhaps due to the lack of a large global market for 2-methoxyethanol, there has been no published work undertaken on its suitability for reforming or as a SOFC fuel. It should behave in a similar manner to ethane-1,2-diol, with higher H₂ and CO_x levels due to the extra methyl group.

6.2.1: Steam reforming

Even without catalysis, no CH₃OH was observed in the exhaust stream, indicating that the molecule decomposed quickly and was able to form CO and CH₄. As the amount of added water increased, the fractions of CO and CH₄ decreased due to dilution, but the H₂ fraction remained constant due to increased steam reforming (Figure 64). Catalysing the decomposition reaction increased the H₂ fraction and decreased the CH₄ and CO fractions. The presence of the Ni/YSZ cermet allowed CH₄ reforming and carbon deposition, reducing the concentration of carbon-containing molecules. With SOFC operation, electrocatalytic oxidation was additionally possible:



At a carbon-to-oxygen ratio of 1, there was insufficient water to fully oxidise all carbon atoms to CO₂, leading to higher fractions of CO. At the 1:2 ratio, fractions were lower due to dilution but the relative proportion of CO₂ was higher. In the “SOFC” experiments, CO was produced overall at the 1:1 ratio and consumed overall at the 1:2. The incidence of electrocatalytic

oxidation was greater at the 1:1 ratio, as steam reforming was reduced due to insufficient steam levels:

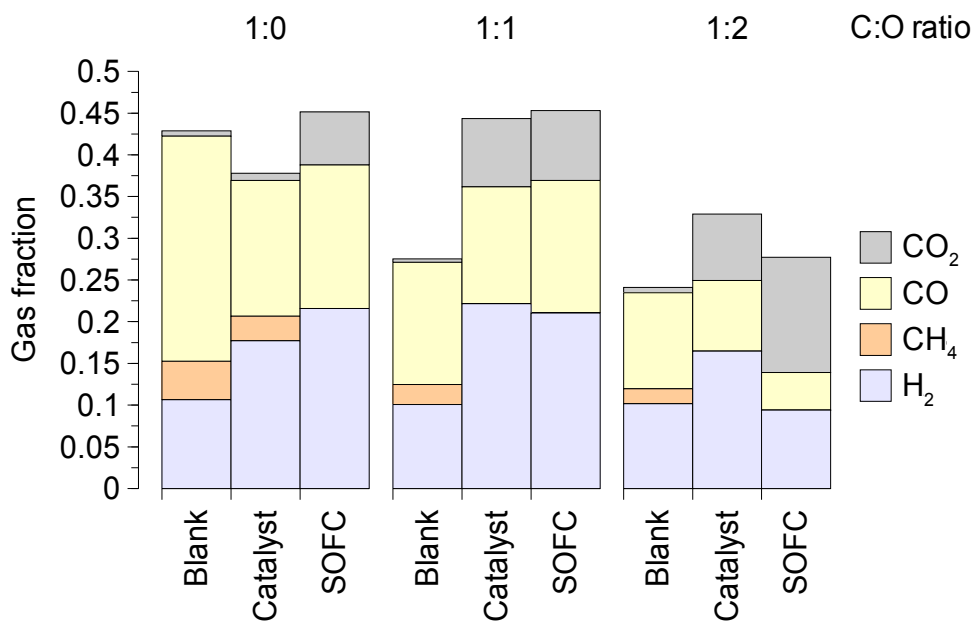
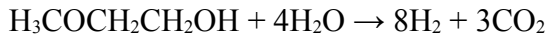


Figure 64: Exhaust gas compositions of steam reformed 2-methoxyethanol

6.2.2: Electrical performance

The “SOFC” experiments for three carbon-to-oxygen ratios show markedly different trends. At the 1:0 ratio, with no steam reforming taking place, there was a constant and terminal decline due to carbon deposition. A similar situation existed for the 1:1 ratio, though some current was obtained through oxidation of the deposited carbon. Only at the 1:2 ratio, with

sufficient steam levels to fully oxidise the fuel and reformat, was steady performance obtained (Figure 65).

The steep initial drop and stabilisation at $\approx 55\%$ of peak output was unlike ethane-1,2-diol in trend, but similar to the 1:1 ratio in performance (Figure 45). It was not unexpected, for the same output was obtained for a greater dilution level (as 2-methoxyethanol is a larger molecule and contains more potential fuel components).

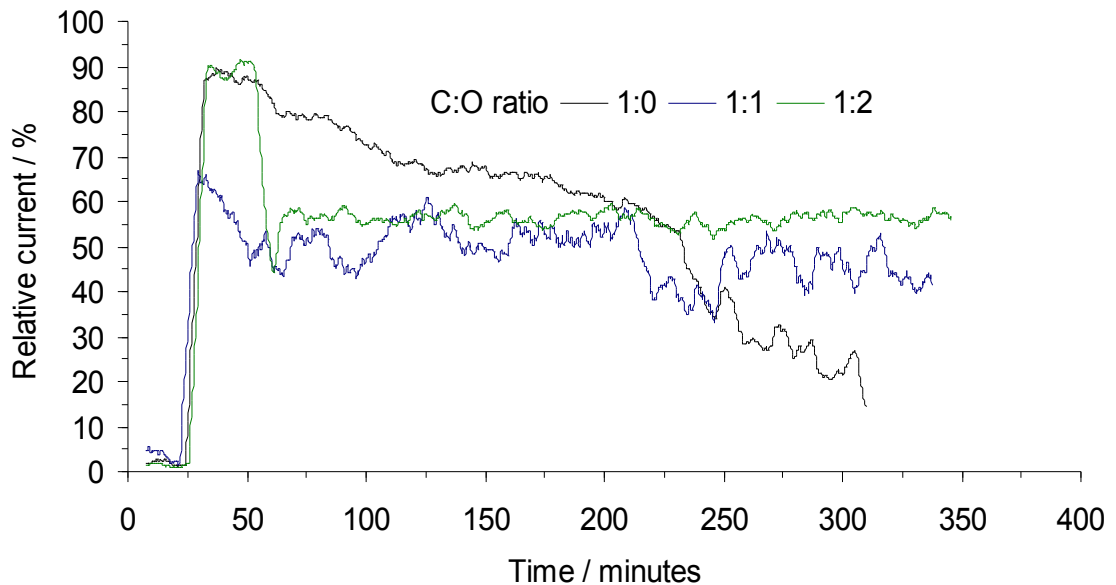


Figure 65: Trends of relative current against time for steam reformed 2-methoxyethanol

6.2.3: Carbon deposition

Relatively high rates of carbon deposition were seen for the 1:0 and 1:1 ratios, with the inverse trend (increasing deposition with increasing steam) seen for both experiment types

(Figure 66). The 1:2 ratio showed rates higher than those seen for ethane-1,2-diol, but far lower than those required to cause severe anode damage. In all cases, the “SOFC” experiments caused greater carbon deposition than the “catalyst” ones.

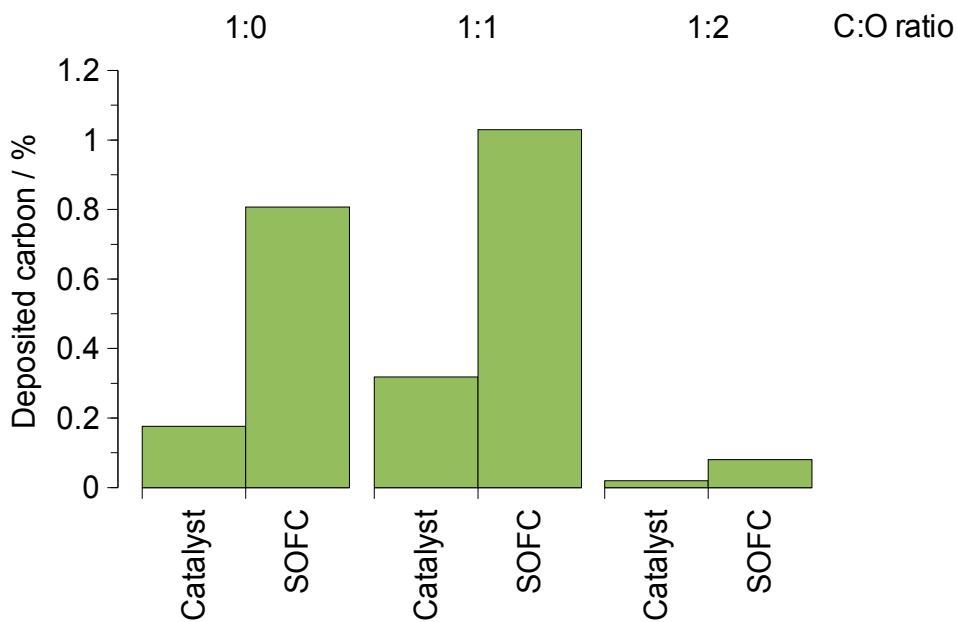


Figure 66: Carbon deposited as a percentage of carbon added for steam reformed 2-methoxyethanol

These effects are relatively easily explained by the presence of unreformed fuel. At the 1:0 and 1:1 ratios, there was insufficient steam to fully reform the 2-methoxyethanol and therefore it had a greater chance of coming into contact with the anode, causing carbon build-up. At the 1:2 ratio, full reforming could take place and the fuel was more diluted. More carbon was deposited in the “SOFC” experiments due to electrocatalytic oxidation, which required the fuel to contact the three-phase boundary area. This was not as marked in the “catalyst”

experiments as fuel could have rapidly decomposed instead of sticking to the catalyst for a greater length of time.

6.3: Dimethoxymethane (methylal / formaldehyde dimethyl acetal)

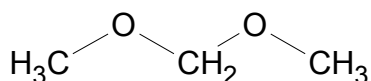


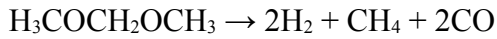
Figure 67: Dimethoxymethane

Dimethoxymethane is unlike any previous fuel studied. It is empirically identical to 2-methoxyethanol ($\text{C}_3\text{H}_8\text{O}_2$) and has structural elements of methoxymethane, but the high carbon content and lack of C-C bonds makes it unique. Another way of considering it, much like methyl formate, is as the result of adding $-\text{CH}_3$ groups to the oxygen atoms of methanoic acid. It can be derived from methanol, though the process is quite energy intensive.

The potential of dimethoxymethane as a hydrogen source for fuel cells has not gone unnoticed, but studies have only considered either precious metal reforming^{[178], [179]} or mid-temperature fuel cells.^[180]

6.3.1: Steam reforming

Like 2-methoxyethanol, dimethoxymethane decomposed into H_2 , CH_4 and CO , although much less readily. Decomposition products were similar for all carbon-to-oxygen ratios, indicating that any reforming was not affected by H_2O :



Catalysed reforming gave similar products at both the 1:0 and 1:1 ratios, in a similar manner to the methyl methanoate 1:0 and 2:1 ratios (Figure 52). The lack of sufficient water for full steam reforming increased the amount of CO produced, and also CH₄ through decomposition (Figure 68):

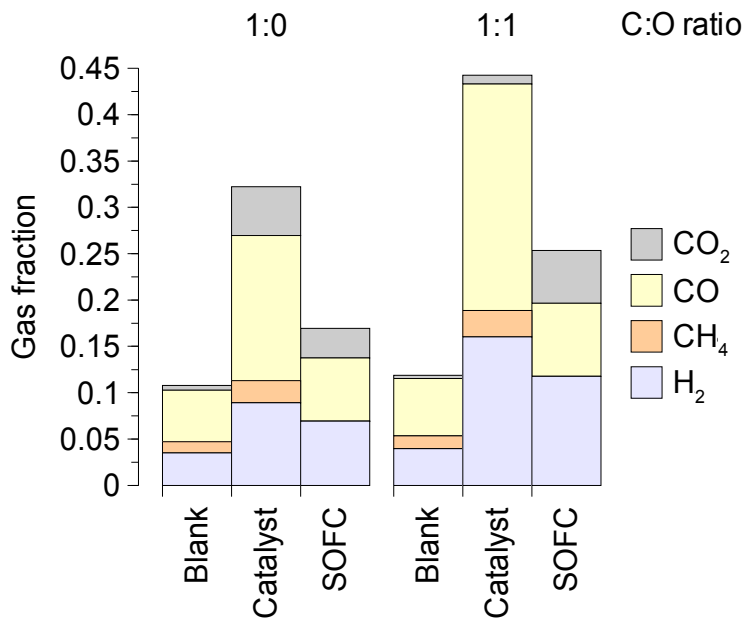
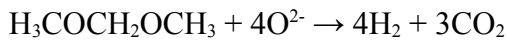


Figure 68: Exhaust gas compositions of steam reformed dimethoxymethane

The SOFC consumed H_2 , CH_4 and CO in addition to any electrocatalytic oxidation. Gas fractions were generally higher for the 1:1 ratio as, despite the dilution effect, more steam reforming products than decomposition products were exhausted.

6.3.2: Electrical performance

The trend in electrical performance was similar to that seen for methanoic acid (Figure 33), though the level of stabilisation was lower at $\approx 15\%$ (Figure 69). The very steep initial drop-off was characteristic of low fuel fractions, though the drop seen for the 1:1 ratio was less steep due to the presence of more reformat. Both carbon-to-oxygen ratios gave similar output levels - as described above, the additional reforming products compensated for the dilution effect.

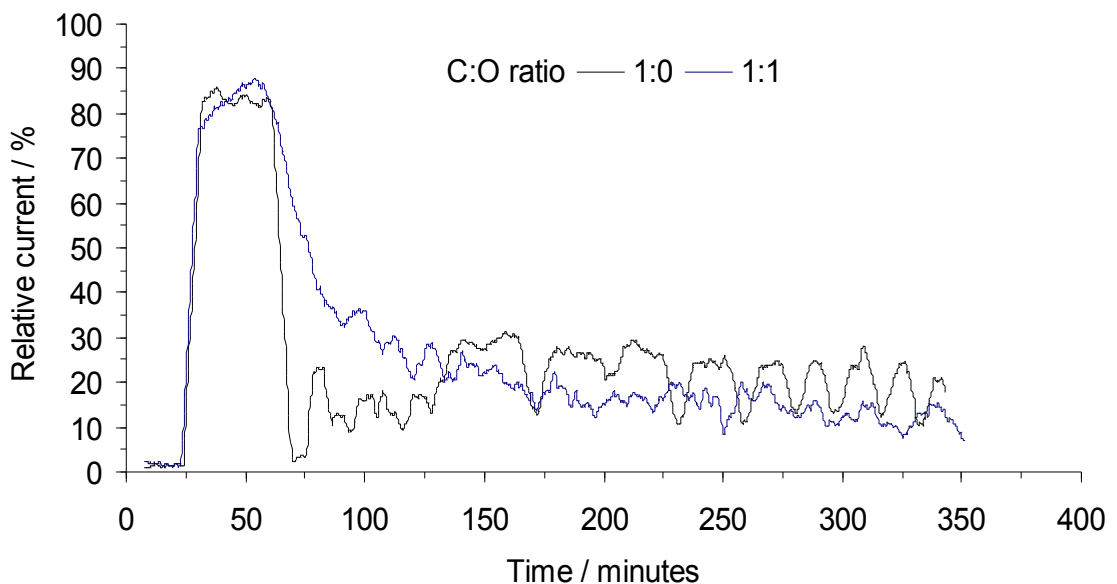


Figure 69: Trends of relative current against time for steam reformed dimethoxymethane

The 1:0 ratio showed more fluctuations in current output than usual, even taking into account the pulsed fuel delivery. Dimethoxymethane has a low boiling point (43 °C) and tends to evaporate inside the fuel lines, causing interruptions in the fuel supply. This effect was mitigated when water was added (even as a separate fuel stream), as the steam in the evaporation chamber provided a buffer between the fuel syringe and the cell.

6.3.3: Carbon deposition

Carbon deposition rates for a given experiment type were similar for both carbon-to-oxygen ratios (Figure 70). The “catalyst” experiments ($\approx 0.15\%$) showed far less carbon than the equivalent experiments for 2-methoxyethanol (Figure 66) - a strong indication (with the similar results for methyl methanoate) that separating the carbon atoms reduces carbon deposition for a given empirical formula.

The “SOFC” experiments showed a slight trend of decreasing carbon with increasing steam, although the difference ($\approx 0.05\%$ versus $\approx 0.04\%$) was within experimental error. This deposition rate was also lower than that seen for 2-methoxyethanol, and unexpectedly low for a C-3 hydrocarbon.

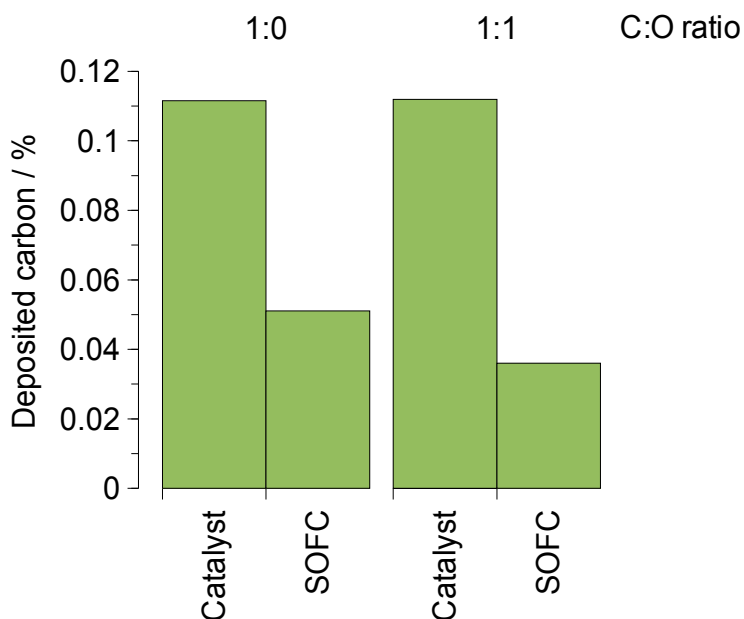


Figure 70: Carbon deposited as a percentage of carbon added for steam reformed dimethoxymethane

6.4: Ethoxyethane (diethyl ether)

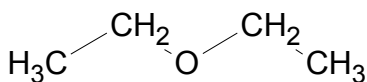


Figure 71: Ethoxyethane

When progressing to C-4 hydrocarbons, the choice of potential fuels is limited by structural requirements that the C-2 and C-3 hydrocarbons have demonstrated. Ethoxyethane is a progression from methoxymethane and, although the presence of carbon-carbon bonds will increase the likelihood of carbon deposition (when vaporised, it should behave much like ethane), it may perform better as it is a liquid.

Ethoxyethane was used historically as a general anaesthetic, and is currently manufactured widely for use as a solvent and in internal combustion engines. Its high volatility and tendency

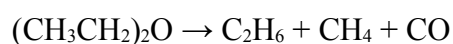
to form explosive gases and peroxides are significant disadvantages, though it can be made sustainably from ethanol.

6.4.1: Steam reforming

Ethoxyethane is immiscible with water, so a single-phase fuel could not be formulated.

Experiments using neat fuel were able to be run, but carbon often formed at the tip of the evaporator (leading into the cell), causing a blockage and pressure build-up. When separate syringes were used for fuel and water, the same issues were experienced with no apparent improvement in fuel reforming.

Fuel decomposition and electrocatalytic reforming products were similar for all experiment types (Figure 72). Although predicted from the fuel's structure, ethane was not observed in the exhaust stream, indicating further decomposition or reforming:



In the "SOFC" experiment, the expected higher fractions of CO_2 were seen. There is an upper limit to the amount of O^{2-} ions that may pass through the electrolyte, and the presence of CH_4 in the exhaust stream indicated that the ion flow is insufficient to oxidise all potential fuels - hence fuel utilisation was at a maximum.

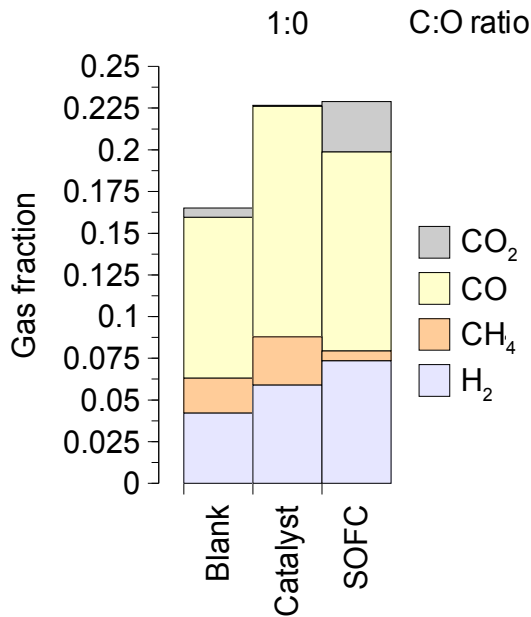


Figure 72: Exhaust gas compositions of ethoxyethane

6.4.2: Electrical performance

A large initial increase in current output followed by a decline and fluctuating steady operation (Figure 73) were typical of high levels of carbon deposition (Figure 19 type 5b and 5c). In the case of neat ethoxyethane, the absolute output of the SOFC was ≈ 100 mA and running principally on oxidised deposited carbon as the anode was completely covered. Similar results were obtained for ethoxyethane and water (added in separate fuel streams), indicating that either mixing in the evaporation chamber is poor or that ethoxyethane does not reform easily.

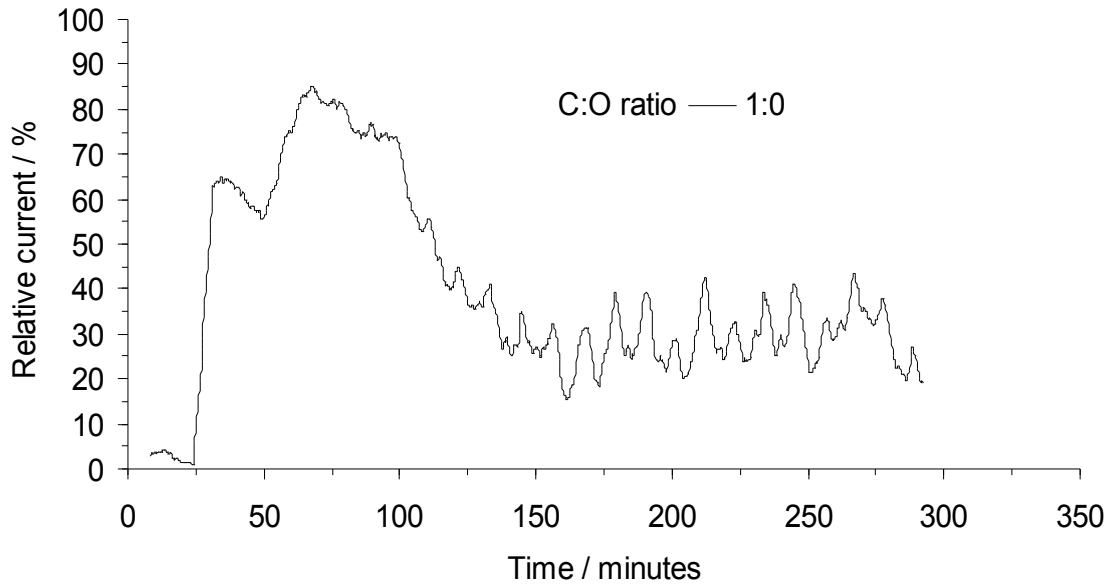


Figure 73: Trends of relative current against time for ethoxyethane

6.4.3: Carbon deposition

The rate of deposition for ethoxyethane was the highest encountered so far, with over 14 % of the fuel's carbon content left on the anode in the “catalyst” experiment (Figure 74). In the “SOFC” experiment, the rate was $\approx 2\%$, comparable to that of ethanoic acid (Figure 42) even though ethoxyethane has a much higher carbon content and a much lower pre-oxidation level. As the SOFC can oxidise deposited carbon to CO and CO₂, there may be an upper limit for deposition rates in a functioning cell - deposited carbon is oxidised preferentially as the O²⁻ ions will come into contact with it before any fuel. Should the rate of deposition exceed the potential rate of oxidation, the cell will fail.

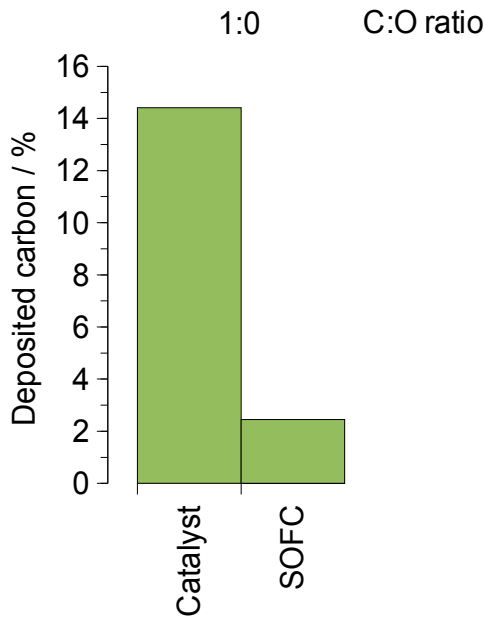


Figure 74: Carbon deposited as a percentage of carbon added for ethoxyethane

6.5: Trimethoxymethane (trimethyl orthoformate)

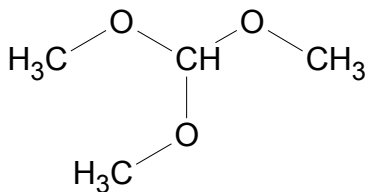


Figure 75: Trimethoxymethane

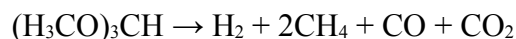
Trimethoxymethane is a progression from dimethoxymethane, with an additional methoxy group replacing a hydrogen on the central carbon atom. Although the molecule contains four carbon atoms, there are no C-C bonds. The chemical steps

required to manufacture this molecule are quite energy-intensive, reducing the potential sustainability.

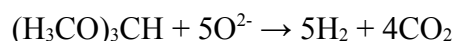
This molecule has been the subject of a PEMFC study^[181] and a reforming study^[179], but has received little other attention. It should behave in a similar manner to dimethoxymethane, with a greater tendency to decompose due to the molecule being less stable.

6.5.1: Steam reforming

In contrast to the relatively inert behaviour of dimethoxymethane (Figure 68), trimethoxymethane decomposed readily (without catalysis) due to the destabilising effect of the additional methoxy group. The CH₃OH in the exhaust stream was due to some trimethoxymethane remaining intact and fragmenting under electron impact rather than the presence of methanol:



Catalysis and electrocatalytic oxidation increased fuel levels to a level comparable to ethane-1,2-diol. The addition of steam increased H₂ and CO₂ levels and decreased CH₄ and CO levels (Figure 76), but a ratio of 1:1 was insufficient for full reforming. Both “SOFC” experiments produced more CO₂ than the “catalyst” experiments, and without steam reforming more H₂ was produced as well:



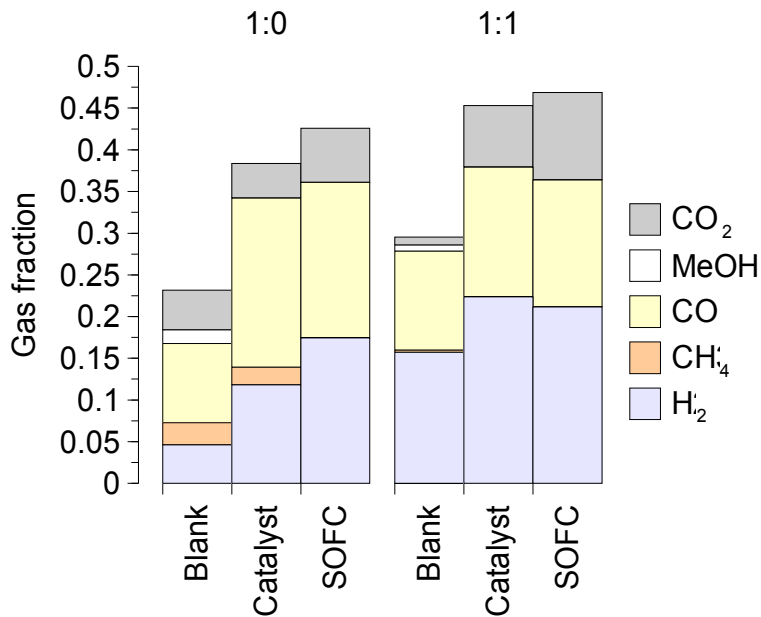


Figure 76: Exhaust gas compositions of steam reformed trimethoxymethane

6.5.2: Electrical performance

At the 1:0 ratio, the current output showed a steady decline over the course of the experiment (Figure 77). As carbon deposition was not excessive and fuel levels were typical of other experiments, this decline was most likely due to anode sintering and would eventually cease, giving steady performance.

The 1:1 ratio gave a decline and stabilisation at $\approx 35\%$ of peak output (as seen before), but was subject to several sharp drops in output. Analysis of the exhaust gas composition over time showed that these drops were caused by the loss of fuel supply to the SOFC. This in turn was caused by air bubbles in the fuel syringe, through fuel evaporation or pockets of air

trapped when the fuel was mixed. After each fuel interruption, the current output did not recover to the same level; rather there was a drop of $\approx 10\%$ - 15% . This was due to the anode sintering when there was no fuel present, as the drop was effectively a brief return to open circuit voltage.

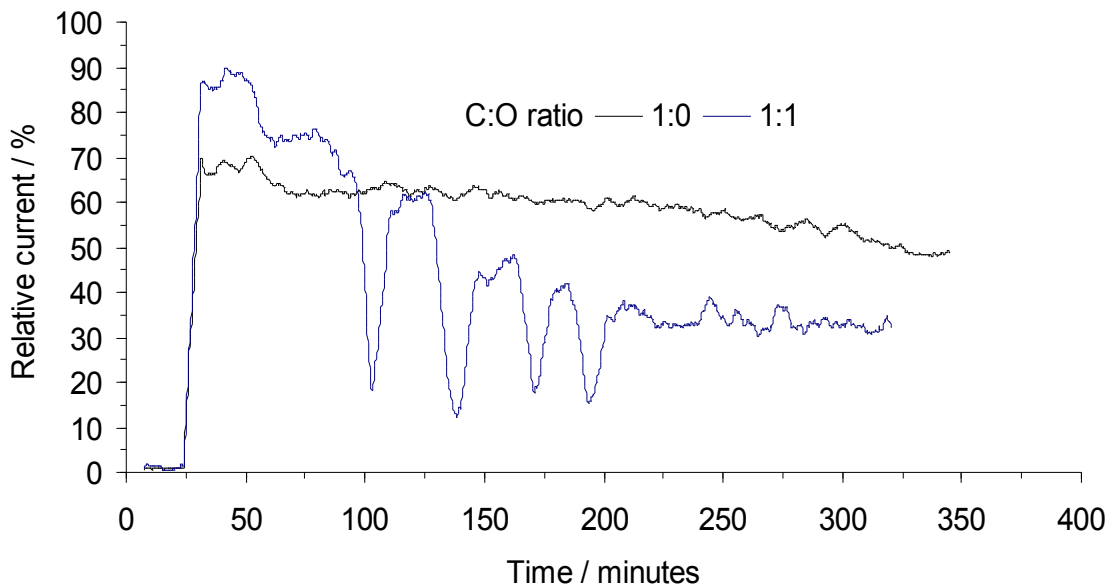


Figure 77: Trends of relative current against time for steam reformed trimethoxymethane

6.5.3: Carbon deposition

Both with and without water, trimethoxymethane deposited much less carbon than its carbon content would imply (Figure 78). At the 1:0 ratio, the level of $\approx 0.2\%$ was higher than that of dimethoxymethane, but lower than 2-methoxyethanol and several C-2 hydrocarbons. At the 1:1 ratio, levels were comparable to those of methanol ($\approx 0.01\%$; Figure 30) - even without

stoichiometric amounts of water. Given the high carbon content and reasonable electrical performance, trimethoxymethane appears to be an excellent possibility for a SOFC fuel.

As with 2-methoxyethanol (Figure 66), the “SOFC” experiment deposited more carbon than the “catalyst”. The reasons are the same - as there was insufficient water present for full fuel oxidation, unreformed fuel had a greater chance of contacting the anode.

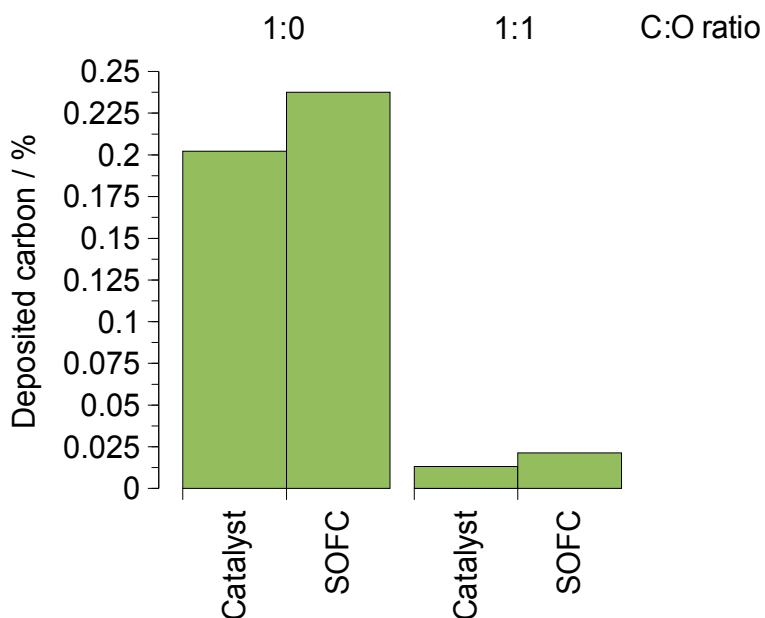


Figure 78: Carbon deposited as a percentage of carbon added for steam reformed trimethoxymethane

6.6: N,N-dimethyl methanamide (N,N-dimethyl formamide / DMF)

N,N-dimethyl methanamide a progression from N-methyl methanamide, with an extra methyl group replacing a hydrogen on the nitrogen atom - a similar case to that of 2-methoxyethanol

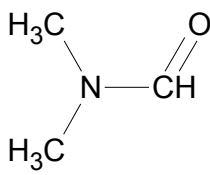


Figure 79: *N,N*-dimethylmethanamide

and ethanol. It is produced from formic acid and methylamine, both of which can be produced biologically.

Like *N*-methyl methanamide, no work on the potential of *N,N*-dimethyl methanamide as a fuel cell fuel or hydrogen source has been published. It

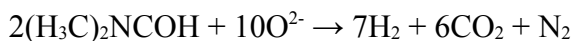
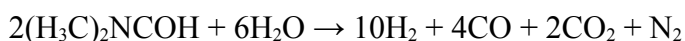
is expected to behave like *N*-methyl methanamide, with higher CR_x ($R = O, H$) levels due to the additional $-CH_3$ group.

6.6.1: Steam reforming

Unlike *N*-methyl methanamide, *N,N*-dimethyl methanamide decomposed readily into H_2 , CO and CH_4 (Figure 80); a result of the large destabilising effect of the additional $-CH_3$ group.

Again, no *N*-containing products appearing at a unique mass-to-charge ratio were observed in the exhaust stream, although HCN and H_2CNH could theoretically be formed as well as NO_x .

As predicted from theory, the addition of water increased H_2 and CO_2 levels, and decreased CO level through steam reforming and the water-gas shift reaction. A carbon-to-oxygen ratio of 1:1 was insufficient for full oxidation of the fuel, leading to higher CO levels and the SOFC consuming a greater proportion:



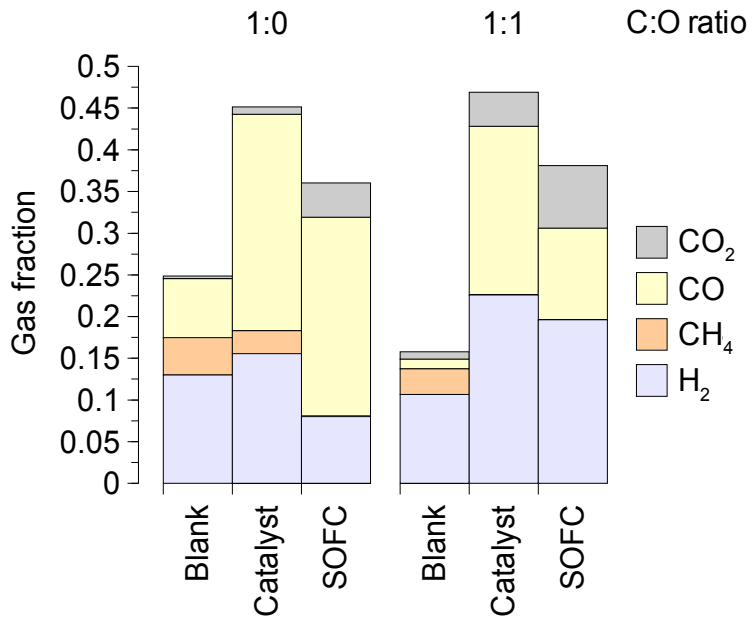


Figure 80: Exhaust gas compositions of steam reformed N,N-dimethyl methanamide

6.6.2: Electrical performance

The trends in electrical output were similar to those seen for N-methyl methanamide (Figure 57). The 1:0 ratio showed an initial gradual decline, becoming steeper and eventually terminal, which was typical of moderate carbon levels. The 1:1 ratio gave stable operation at $\approx 65\%$ of peak output, indicative of improved reforming (Figure 81).

Though the exhaust compositions were substantially different, the similarity in electrical performance trends between N-methyl and N,N-dimethyl methanamide suggested similar mechanisms of steam and electrocatalytic oxidation. Without firm data on the reforming of nitrogen, however, it is difficult to draw firm conclusions.

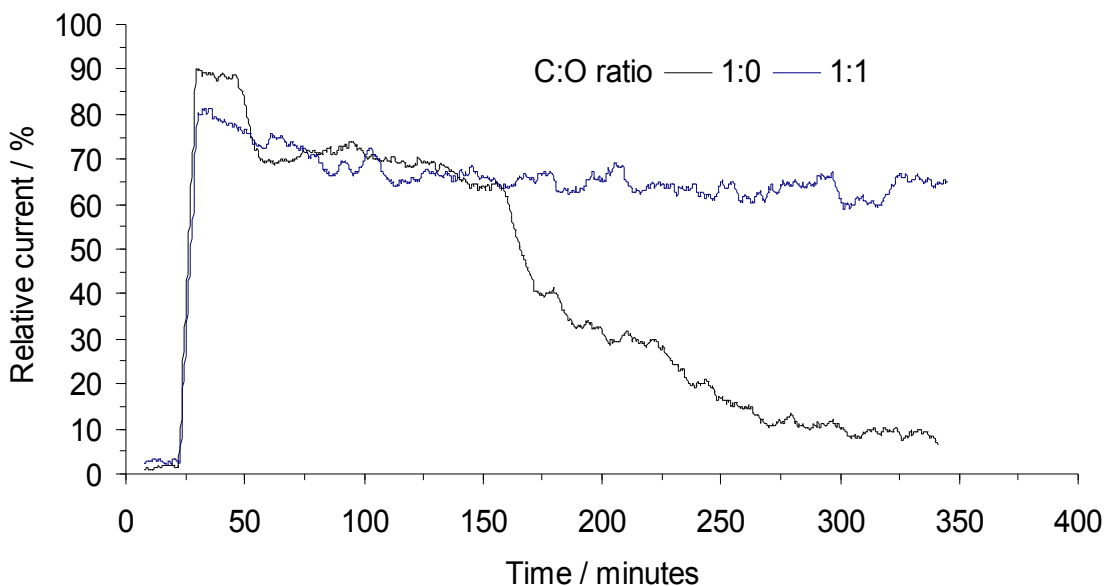


Figure 81: Trends of relative current against time for steam reformed *N,N*-dimethyl methanamide

6.6.3: Carbon deposition

The carbon deposition trends were also similar to those obtained for *N*-methyl methanamide (Figure 58); a further indication of similar reaction mechanisms. Without water addition, levels were high considering previous data and the lack of carbon-carbon bonds - though electrocatalytic oxidation reduced the deposition rate to $\approx 1\%$ (Figure 82). As this level was lower than the previously experienced degradation threshold, either equilibrium had not been reached or deposition was blocking the cell inlet and preventing fuel from entering.

The 1:1 ratio also showed slightly higher levels than may have been expected ($\approx 0.5\%$), but the substoichiometric amounts of water allow more intact fuel molecules to come into contact with the anode. However, unlike 2-methoxyethanol (Figure 66), the trend of the “SOFC”

experiments depositing more carbon than the “catalyst” experiments was not seen here - the deposition mechanism was different.

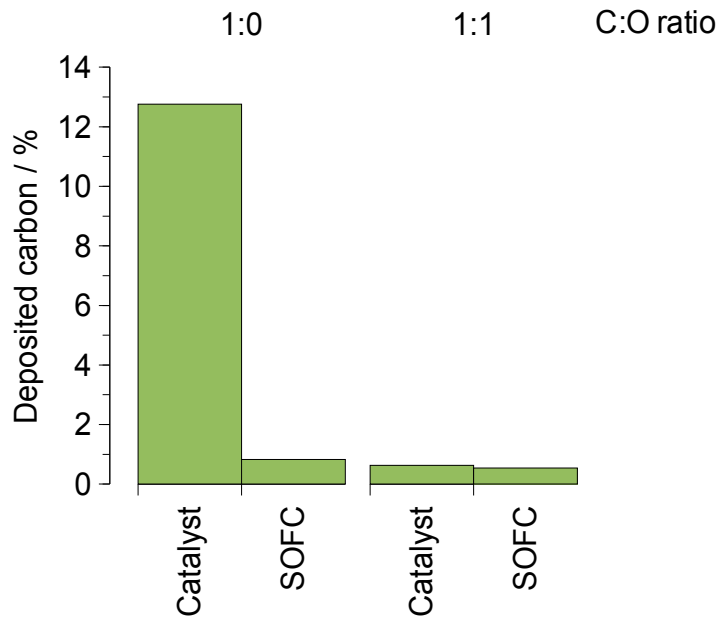


Figure 82: Carbon deposited as a percentage of carbon added for steam reformed *N,N*-dimethyl methanamide

Chapter 7: Blends with methanoic acid

7.1: Methanol / methanoic acid

So far, fuels have been oxidised using a combination of H₂O (added in varying proportions) and O²⁻ (during SOFC operation). As several experiments have shown, increasing the amount of water can improve reforming but decrease electrical output through dilution and catalyst deactivation. If a hydrocarbon fuel could be used as an oxidant, the energy density (and therefore current output) would increase as the non-fuel component would be smaller.

Methanoic acid, as demonstrated previously, has a carbon-to-oxygen ratio of 1:2 and can therefore be considered as an oxidising agent. Rather than acting as a “pure” oxidising agent like H₂O or O²⁻, it will effectively be a source of CO₂ that can be added to the fuel in liquid form. Replacing a mole of water with one of methanoic acid should mitigate the dilution effect and also allow previously immiscible fuel/water mixtures to form a single phase through reduced polarity.

7.1.1: Steam reforming

Equal parts of methanol and methanoic acid gave an approximate middle ground between the high H₂ and high CO₂ fractions characteristic of the individual fuels (Figure 83). No CH₃OH was observed in the “blank” experiments even with no added water, suggesting that the methanoic acid was able to perform some reforming. With equimolar water, fractions of all gases remained similar due to increased reforming offset by dilution as described before:

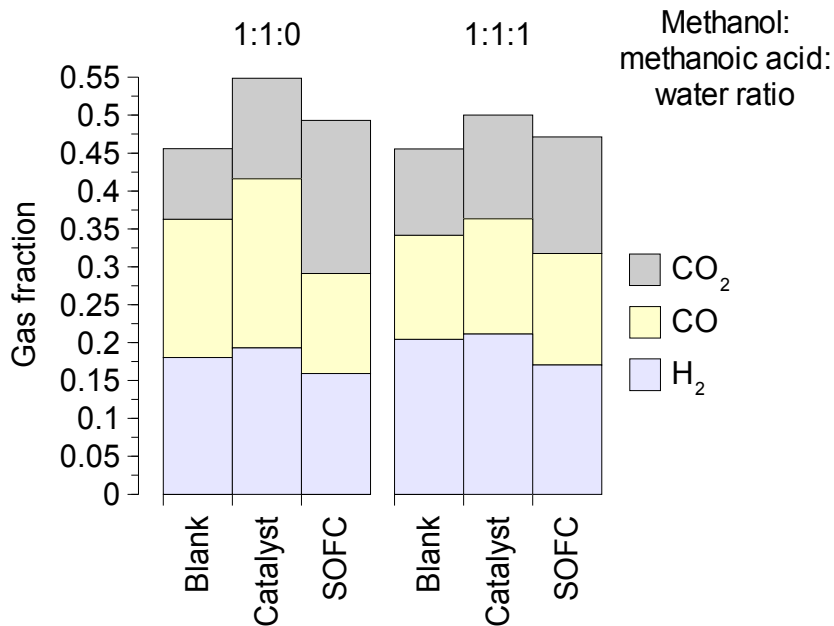
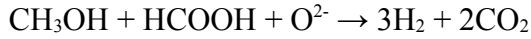
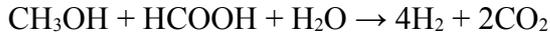
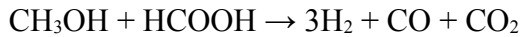


Figure 83: Exhaust gas compositions of steam reformed methanol / methanoic acid blends

7.1.2: Electrical performance

Both fuel compositions were characterised by large drops in electrical performance and subsequent recovery, brought on by breaks in the fuel supply in a similar manner to trimethoxymethane (Figure 77). Following a fuel interruption, the current output did not return to the same value due to anode sintering. Although both fuels are relatively volatile, this behaviour was not observed when they were run individually and was therefore a

consequence of the increased volatility of the blended fuel (neat fuels and water dilution allow better intermolecular interactions such as hydrogen bonding).

When not affected by fuel supply interruptions, both fuel blends gave steady performances or slight declines (Figure 84). This was an improvement on both individual fuels, and indicated that it may be possible to formulate a SOFC-optimised fuel blend in a similar manner to an internal combustion engine-optimised petroleum blend.

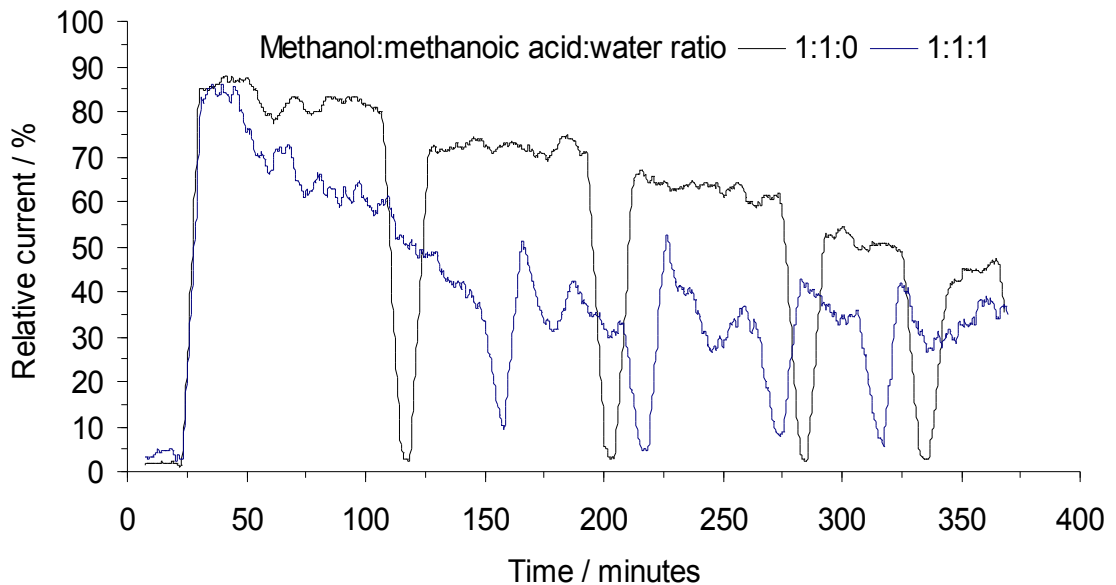


Figure 84: Trends of relative current against time for steam reformed methanol / methanoic acid blends

7.1.3: Carbon deposition

Rates of carbon deposition were similar for both blends, and comparable to those obtained for the individual fuels. The “catalyst” experiments had a typical trend of decreasing carbon with

increasing water, but the “SOFC” experiments had identical rates of deposition (Figure 85). This was a similar case to that of methanol (Figure 30), indicating that the rates of removal and deposition were the same.

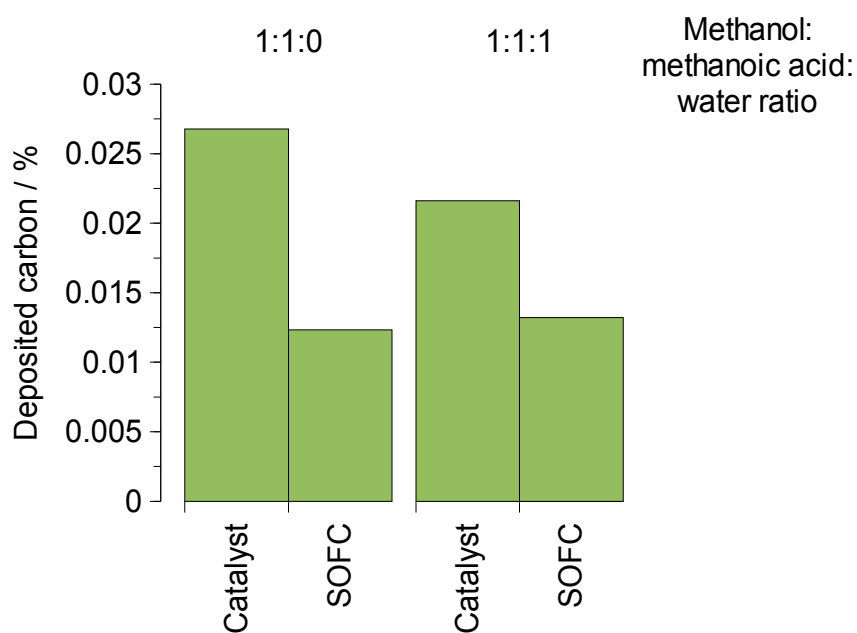


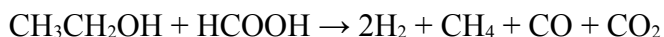
Figure 85: Carbon deposited as a percentage of carbon added for steam reformed methanol / methanoic acid blends

7.2: Ethanol / methanoic acid

7.2.1: Steam reforming

In a similar manner to the methanol / methanoic acid blend, the ethanol / methanoic blend acid gave a compositional middle ground between the two fuel components. This was most

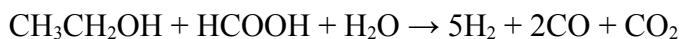
apparent in the “blank” experiments, where the two fuels decomposed to their constituent fragments (Figure 86):



This fragmentation was also visible in the 1:1:0 “catalyst” experiment, as no water was present to reform the CH_4 produced. In contrast to ethanol alone, dilution and (slight) reforming ability of methanoic acid prevented the cell from becoming blocked with carbon. The “SOFC” experiment produced high fractions of CO_2 , indicating that CO , CH_4 and the component fuels were being consumed:



With steam reforming, the single mole of water was insufficient to fully oxidise all the carbon present. CO levels were lower and CO_2 levels higher in the “catalyst” experiment, with the reverse being true in the “SOFC experiments”. This was due to the increased electrocatalytic oxidation at the 1:1:0 ratio as an alternative to steam reforming:



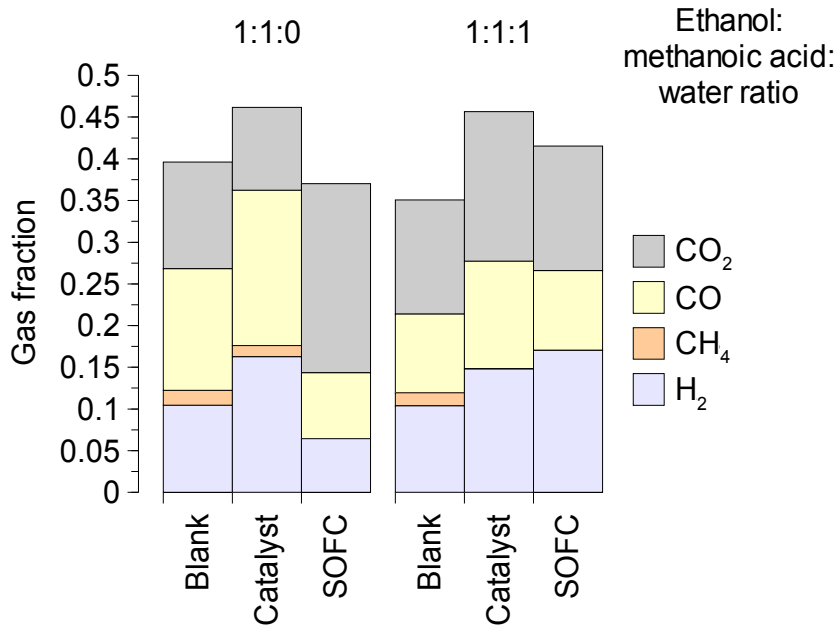


Figure 86: Exhaust gas compositions of steam reformed ethanol / methanoic acid blends

7.2.2: Electrical performance

An initial decline and stabilisation at $\approx 35\%$ of peak output was seen for both fuel blends (Figure 87). This was much more characteristic of methanoic acid than ethanol, and the blend performed slightly worse than the individual fuels. The decline, increase and subsequent stable operation for the 1:1:0 ratio indicated that some carbon deposition was taking place - this was to be expected given the presence of unreacted ethanol in the fuel mix.

The 1:1:1 ratio showed a less steep initial decline due to higher reformat fractions, but did not approach the output levels seen for ethanol (Figure 37) given the relatively low dilution level. This was because of the substoichiometric amount of water, which may have reacted preferentially with CH_4 or CO and allowed ethanol to reach the anode intact.

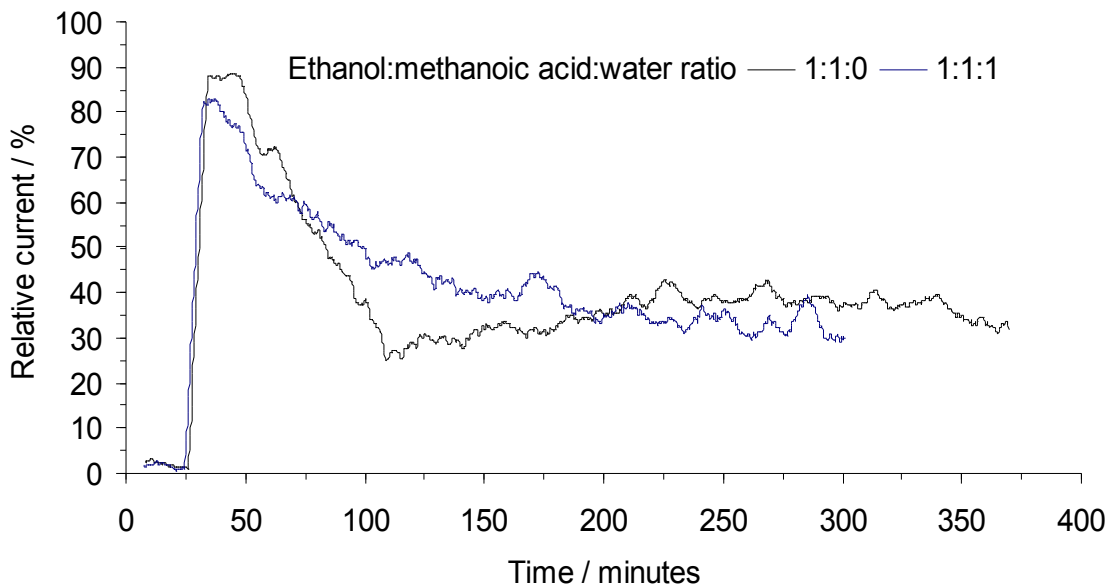


Figure 87: Trends of relative current against time for steam reformed ethanol / methanoic acid blends

7.2.3: Carbon deposition

The principal consequences of the substoichiometric amounts of water were apparent in the rates of carbon deposition. Both fuel ratios deposited more carbon than either ethanol or methanoic acid individually, which was to be expected given the presence of “free” ethanol. The rates of $\approx 0.4\%$ and $\approx 0.7\%$, while relatively high, were below the levels required to seriously damage the anode (Figure 88).

In a similar trend to ethane-1,2-diol (Figure 46) and the blend of methanol and methanoic acid, increasing steam levels decreased the rate of carbon deposition for the “catalyst” experiments but increased them for the “SOFC” experiments.

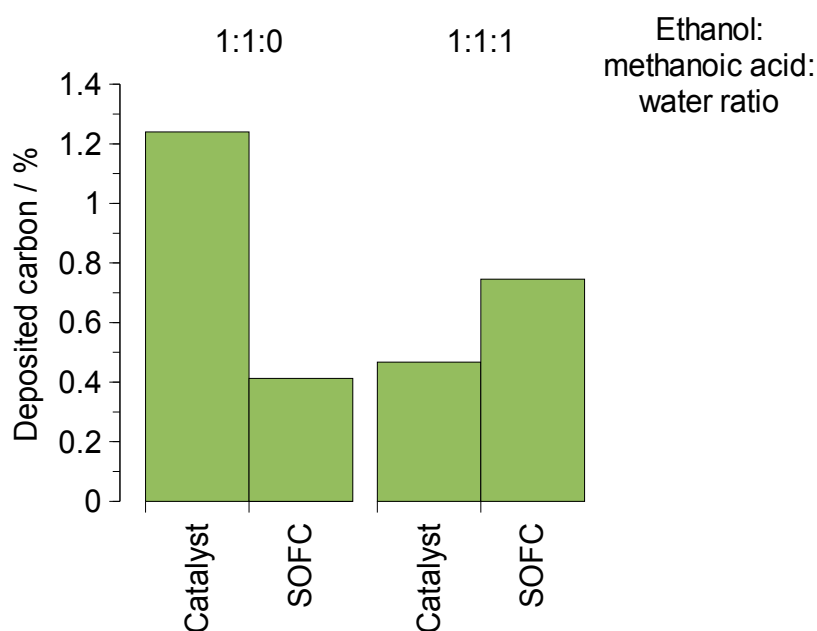


Figure 88: Carbon deposited as a percentage of carbon added for steam reformed ethanol / methanoic acid blends

7.3: Methyl methanoate / methanoic acid

7.3.1: Steam reforming

In contrast to the individual behaviour of methyl methanoate, the blend with methanoic acid decomposed readily to H₂, CO and CO₂ with no CH₄ or CH₃OH fragments (Figure 89), demonstrating again that methanoic acid had some reforming or equilibrium-changing ability:

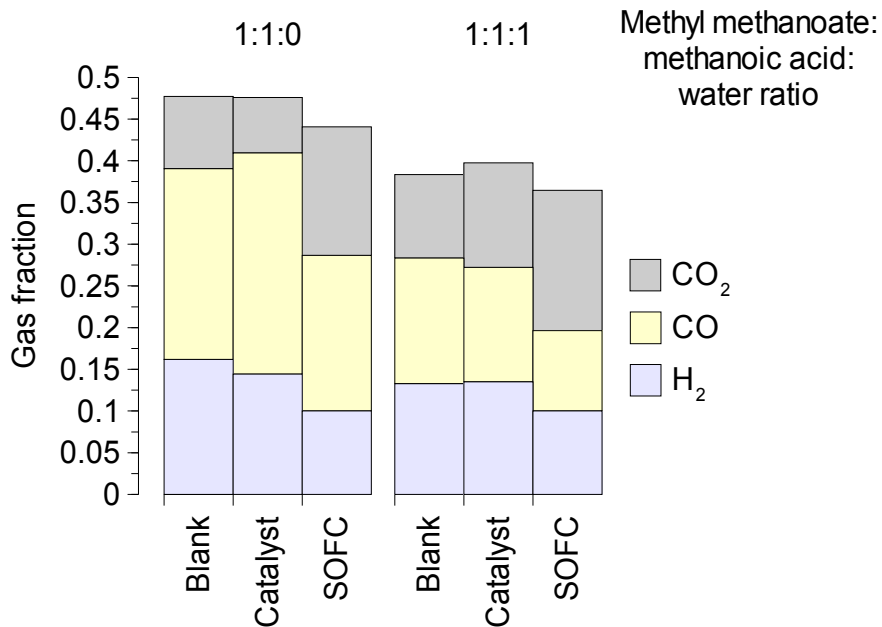
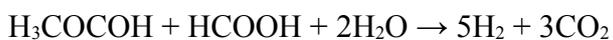
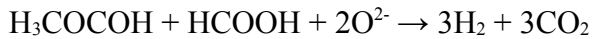


Figure 89: Exhaust gas compositions of steam reformed methyl methanoate / methanoic acid blends

For both blends, reformat levels were similar for the “blank” and “catalyst” experiments, with the “SOFC” experiments consuming H₂ and CO and producing CO₂ as expected. The decomposition rate of the blend components took place rapidly, so the catalyst had little effect beyond what had already taken place. Overall gas fractions were lower at the 1:1:1 ratio due to dilution. As with the blends previously investigated, substoichiometric amounts of water were added, increasing CO levels:





7.3.2: Electrical performance

In a similar manner to methyl methanoate (Figure 53), the blend with methanoic acid showed a downward trend over the course of the experiment (Figure 90). This behaviour was not predicted from the CO and H₂ levels of the exhaust, and could be explained in part by the breaks in fuel supply that have been seen for other blends. Once the anode was exposed to a non-fuel atmosphere, irreversible oxidation or sintering took place, causing a decrease in current output.

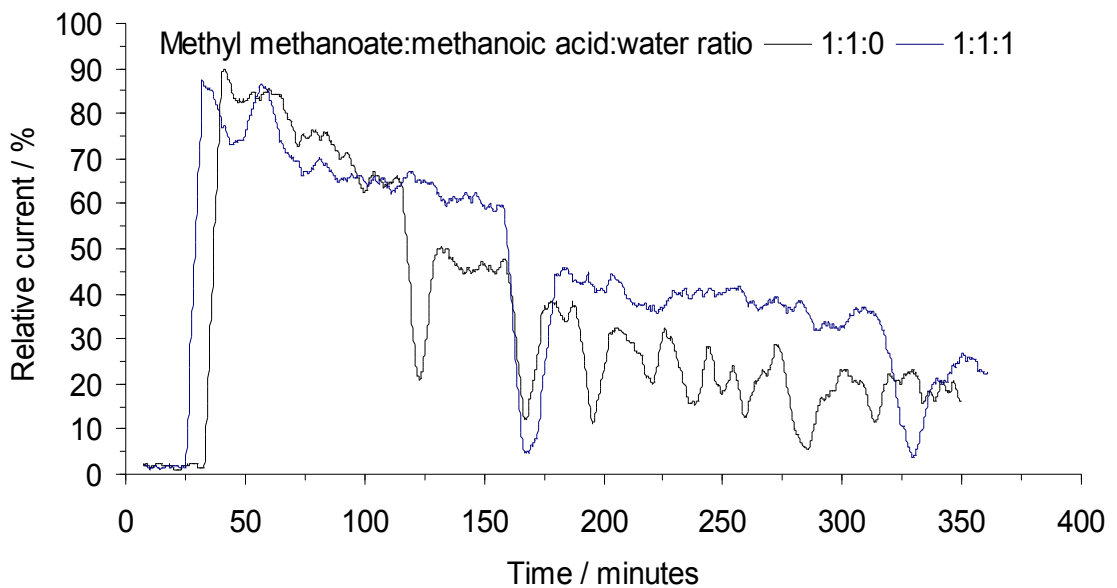


Figure 90: Trends of relative current against time for steam reformed methyl methanoate / methanoic acid blends

Methyl methanoate performed adequately with a 1:1 carbon-to-oxygen ratio, and so an extra

mole of water may have prevented the decline (at the expense of fuel density). A greater fuel flowrate may also have avoided breaks in supply, at the expense of increased carbon deposition. The performance of the 1:1:1 blend was better than that of the 1:1:0 despite lower fuel fractions, indicating that effective reforming can outweigh fuel quantity.

7.3.3: Carbon deposition

Overall carbon deposition rates were comparable to both methanoic acid and methyl methanoate, with both experiment types showing the trend of increasing carbon with increasing steam (Figure 91). At the 1:1:0 ratio, the “catalyst” and “SOFC” experiments deposited carbon at similar rates, but at the 1:1:1 the “SOFC” deposition rate was significantly higher. This was unlikely to be due entirely to electrocatalytic oxidation, as the exhaust gas showed high decomposition rates. The principal difference between the exhaust compositions of the two ratios was the CO/CO₂ ratio - high CO for the 1:1:0 and high CO₂ for the 1:1:1. This shows that CO was being oxidised (both catalytically and electrocatalytically), causing carbon build-up as it contacted the anode.

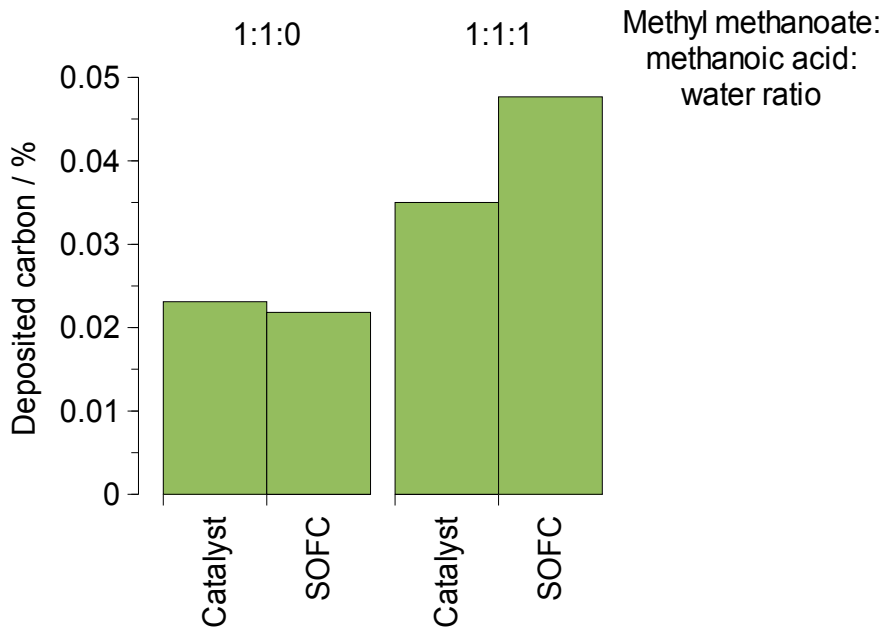


Figure 91: Carbon deposited as a percentage of carbon added for steam reformed methyl methanoate / methanoic acid blends

7.4: Dimethoxymethane / methanoic acid

7.4.1: Steam reforming

In marked contrast to pure dimethoxymethane (Figure 68), the blend with methanoic acid gave average levels of H₂, CO and CO₂ (Figure 92). The ability to formulate a single phase with water allowed good mixing of fuel and oxidant, improving the reforming reactions significantly. With and without water, decomposition was also promoted:



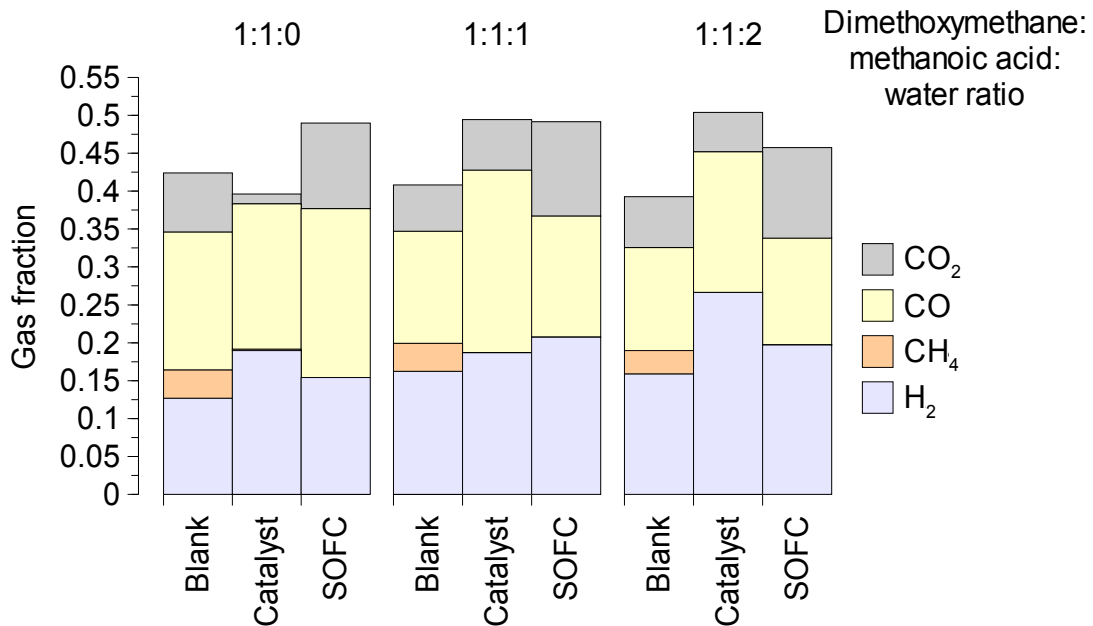
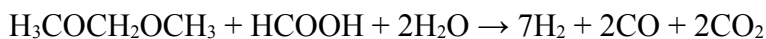


Figure 92: Exhaust gas compositions of steam reformed dimethoxymethane / methanoic acid blends

The amount of water added had little effect on the exhaust gas compositions. In both the 1:1:1 and 1:1:2 blends, the amount of water was less than that required for full oxidation and the principal difference was the oxidation of one CO molecule to CO₂. Had four moles of water been added, a more significant change would have been seen; for the one and two moles used here, the water-gas shift equilibrium resulted in similar levels. Although electrocatalytic oxidation was also possible, the exhaust composition suggested that the fuel components were reformed more quickly:





7.4.2: Electrical performance

All fuel blends showed a similar gradual decline to begin with, due to almost identical gas compositions entering the cell. The 1:1:0 and 1:1:1 ratios subsequently declined further, while the 1:1:2 ratio showed almost steady performance (Figure 93). Carbon deposition was not excessive, so the decline was most likely due to nickel agglomeration through low fuel concentration and would stabilise in time.

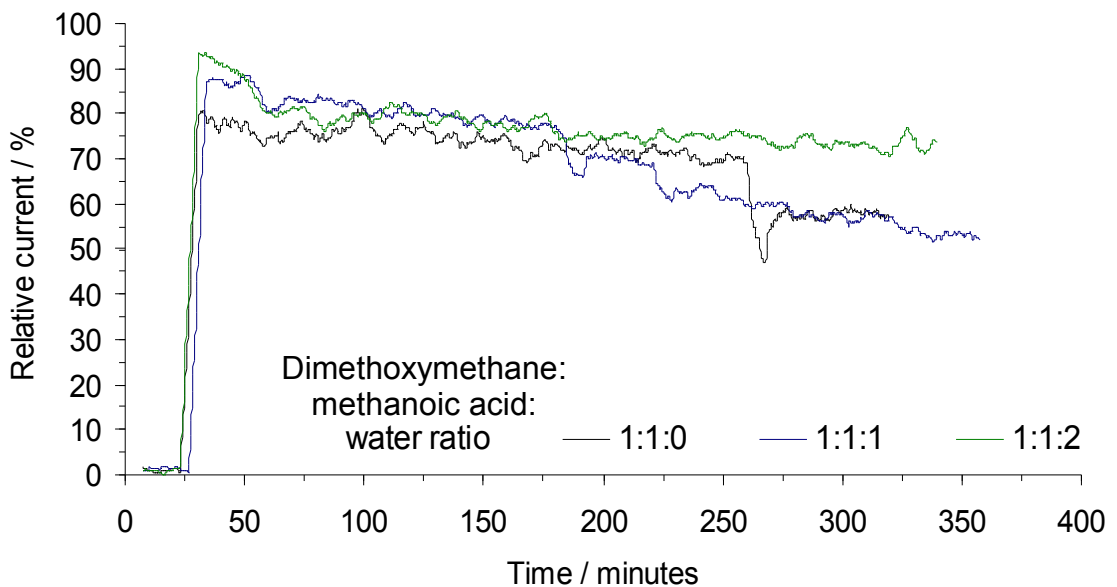


Figure 93: Trends of relative current against time for steam reformed dimethoxymethane / methanoic acid blends

7.4.3: Carbon deposition

In the absence of steam, the “SOFC” experiment deposited a relatively high amount of carbon due to electrocatalytic oxidation (replaced by steam reforming in other ratios). With even a single mole of water, the deposition rate was reduced to almost negligible levels ($\approx 0.005\%$). The “catalyst” experiments showed trends similar to those of methanoic acid (Figure 34), with the deposition rates increasing and then decreasing. As with methanoic acid, these could not be easily explained through existing theory - if anode composition was not the reason, then the first mole of water must have been used preferentially in a reforming reaction that did not prevent carbon formation and the second could then oxidise deposited carbon or prevent its formation.

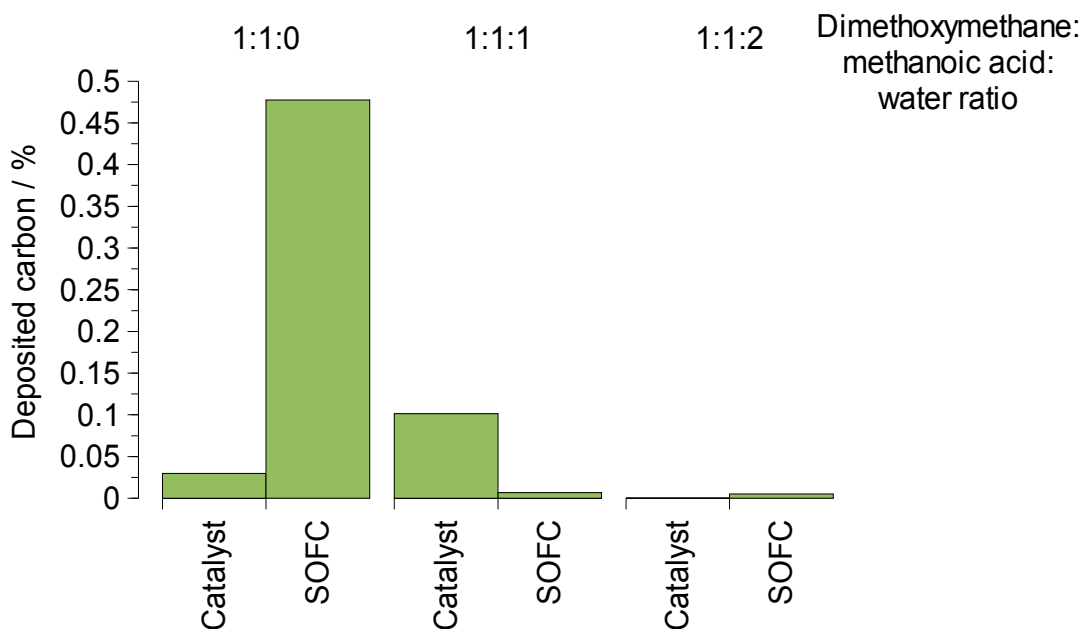


Figure 94: Carbon deposited as a percentage of carbon added for steam reformed dimethoxymethane / methanoic acid blends

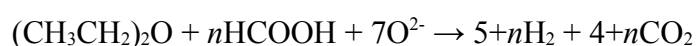
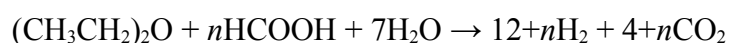
7.5: Ethoxyethane / methanoic acid

7.5.1: Steam reforming

With the addition of methanoic acid, water and ethoxyethane were miscible, though a greater proportion of methanoic acid was required to achieve a single phase. As with the blend of dimethoxymethane and methanoic acid, this allowed effective mixing of fuel and oxidant to facilitate steam reforming.

No ethyl (-CH₂CH₃) fragments were observed in the exhaust, and methane levels were lower than those seen for pure ethoxyethane. The presence of both water and methanoic acid allowed effective reforming of these components, and the overall exhaust compositions (Figure 95) were typical of other blended fuels.

Substoichiometric amounts of water were also used in the ethoxyethane blends, resulting in higher CO levels. The equivalent amount of methanoic acid required to for a single phase with an ethoxyethane:water ratio of 1:7 is unknown, but is likely to be at least 8:



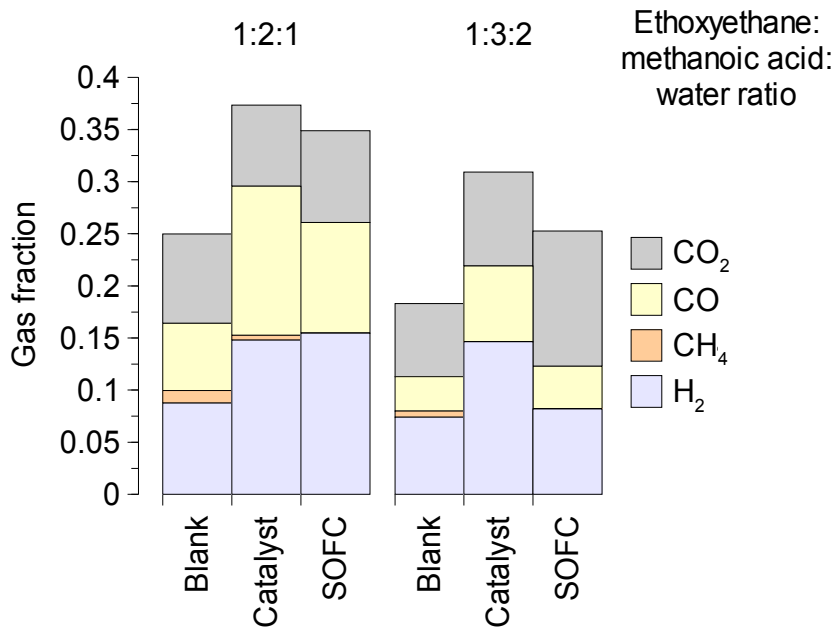


Figure 95: Exhaust gas compositions of steam reformed ethoxyethane / methanoic acid blends

7.5.2: Electrical performance

The electrical output trend of the 1:2:1 blend was a terminal decline, and the 1:3:2 blend progressed along a stabilisation curve before dropping due to a fuel supply interruption and stabilising again (Figure 96). As carbon deposition was much lower than that observed for pure ethoxyethane, the decline of the 1:2:1 ratio was due to anode degradation combined with a lack of suitable fuels to oxidise (lower levels of reformat due to lower levels of H₂O).

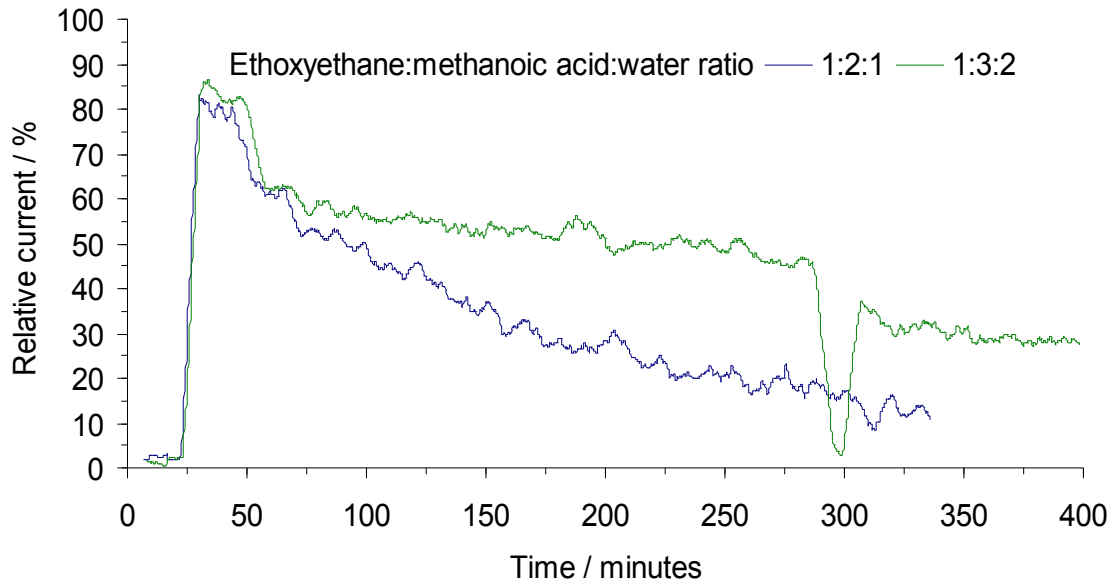


Figure 96: Trends of relative current against time for steam reformed ethoxyethane / methanoic acid blends

7.5.3: Carbon deposition

Considering the extremely high rates seen for pure ethoxyethane (Figure 74), the blended fuel showed a relatively low tendency to deposit carbon. This was a consequence of the physical dilution of the ethoxyethane, and the ability to add water in the same phase and hence increase both reforming and carbon removal.

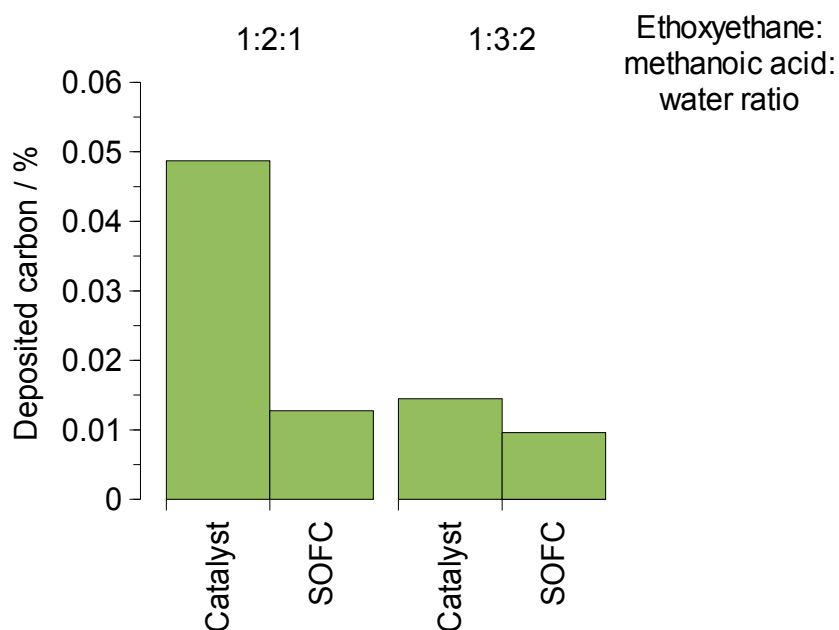


Figure 97: Carbon deposited as a percentage of carbon added for steam reformed ethoxyethane / methanoic acid blends

An expected trend of decreasing carbon with increasing water was obtained (Figure 97), with the “catalyst” experiments depositing more carbon than the “SOFC”. This suggested that little electrocatalytic oxidation of unreformed fuels was taking place, as the steam levels were too low to effectively oxidise large amounts of deposited carbon.

Chapter 8: Discussion of results

8.1: Overview of findings

For most fuels, the electrolyte tube was slightly catalytically active but the fixed Ni-YSZ cermet promoted efficient reforming to H₂, CO and CO₂. Steam reforming was most efficient when one molecule of water was added per fuel carbon atom. Most fuels were characterised by an initial drop in electrical output, followed by a plateau of stable operation - the best-performing fuels were from the C-2 group and did not contain an easily-formed CO₂ fragment. Carbon deposition was lowest in molecules that did not contain carbon-carbon bonds, and several fuels showed increasing deposition with increasing steam addition.

Absolute analysis of electrical data was hindered by degradation effects common to all fuels (including hydrogen), which were not distinguishable from any effects unique to the fuel being tested. However, useful information could be inferred from reforming and carbon deposition data.

This research can be applied to any type of SOFC, as the principal focus was on reducing carbon deposition through fuel structure. Although the underlying objective of this study was to investigate carbon-neutral generation, the fuels studied were chosen principally out of academic interest. All were readily available in the laboratory, but not all could be produced efficiently in a sustainable manner. Any real-world application would have to take this into account.

8.2: Performance of fuels and blends

As the cell is loaded after reduction under hydrogen, a certain current output is delivered. This is usually close to the maximum (100 %), as H₂ is an efficient fuel and the flowrate is relatively high. When the liquid fuel is injected, the current output rises if the new gas mixture has higher proportions of usable fuels, or remains the same if it does not (this can be seen in the 1:2 and 1:3 ratios for methanol, Figure 29). Theoretically, the output would drop if the new gas mixture contained lower proportions of usable fuels, but this is not usually observed experimentally due to the high H₂ fraction, which acts as a buffer. The optimum fuel flowrate varies depending on the structure of the fuel and the extent of reforming, but was kept constant (at around 0.01 ml min⁻¹) to enable better comparison between fuels. Lower flowrates tended to increase the number of breaks in fuel supply, while higher ones flooded the SOFC or mass spectrometer when high fractions of water were added.

When the reducing hydrogen is removed, the output will drop if the fuel reformat contains lower fractions of usable fuel. This behaviour is usually observed, as the effective flowrate of fuel from the injected liquid is lower than the 20 ml min⁻¹ H₂. If the usable fuel fractions are high or there is some carbon deposition (to provide links between Ni particles), the output remains steady. 20 ml min⁻¹ is more fuel than the SOFC is capable of oxidising, and so gives an indication of the cell output at maximum O²⁻ (and therefore electron) transport rates. It is possible to supply liquid fuel at such a rate that the predicted reforming products are approximately equivalent to 20 ml min⁻¹ H₂, however this inevitably leads to excessive carbon

deposition and saturation of the catalyst (if a significant amount of water is present). Lower fuel flowrates mean that more of the fuel is used, but supply interruptions can occur (for example, methyl methanoate / methanoic acid, Figure 90). A balance between fuel utilisation and cell performance needs to be found - a higher proportion of the fuel is used at the expense of the cell output being lower than its potential maximum. This allows long-term use of hydrocarbon fuels with less exhausting of potentially useful molecules.

Following the drop or steady performance after the loss of reducing hydrogen, the output may then rise, fall or remain steady. A rise indicates further carbon deposition, and is followed by a decline as the carbon damages the anode or forms a monolayer to inhibit catalytic activity (for example, ethoxyethane, Figure 73). A fall may be due to carbon deposition, an unsuitable fuel mix, lack of physical contact between anode and current collect or reduced anode activity through nickel agglomeration (sintering). The latter two effects are not fuel-dependent (they are observed for cells run on H₂) and are subject to some unpredictability due to the variability between cells. The decline will continue in the case of excessive carbon deposition or lack of usable fuel, but otherwise will stabilise as an equilibrium between the various mechanical and chemical effects is reached. The performance declines seen for cells run on H₂ hindered analysis for hydrocarbons, as the specific performance-related effects for each fuel could not be studied in isolation.

The highest relative outputs ($\approx 80\%$) were observed for ethanol at a carbon-to-oxygen ratio of 1:2 (Figure 37) and N-methyl methanamide at a carbon-to-oxygen ratio of 1:1 (Figure 57). Both of these fuel mixes, despite different structures, had similar exhaust gas compositions

and rates of carbon deposition. A typical adequately-performing fuel showed a short drop or decline followed by steady performance at $\approx 35\%$ - 65% of peak output (Table 4, Table 5; \downarrow indicates a declining trend).

Fuel	C:O ratio	Average relative output / %
Ethanol	1:2	80
N-methyl methanamide	1:1	80
Methoxymethane	6:1 (saturated gas)	65
N,N-dimethyl methanamide	1:1	65
Methanol	1:3	60 (\downarrow)
2-methoxyethanol	1:2	55
Ethane-1,2-diol	1:1	50
Ethanoic acid	1:2	45
Methanoic acid	1:0	45
Trimethoxymethane	1:1	35
Ethoxyethane	1:0	25 (\downarrow)
Dimethoxymethane	1:1	20
Methyl methanoate	1:1	20
Propane-1,2,3-triol	1:1	15

Table 4: Highest electrical performances of pure fuels

Additional fuel	Fuel:methanoic acid:water ratio	Average relative output / %
Dimethoxymethane	1:1:2	75
Methanol	1:1:0	45 (\downarrow)
Ethanol	1:1:0	40
Ethoxyethane	1:1:2	35 (\downarrow)
Methyl methanoate	1:1:1	25 (\downarrow)

Table 5: Highest electrical performances of blended fuels

In terms of the trend in and relative level of electrical output, four of the five best-performing fuels (including the blended mixtures) were hydrocarbons with O- or N-separated carbon atoms. Further, fuel-specific, refinement of the SOFC design and fuel composition will improve absolute performance.

Fuels containing nitrogen (N-methyl methanamide and N,N-dimethyl methanamide) showed no unique N-containing compounds in the exhaust, as discussed in the accompanying text. The presence of N_2 , suggested by similar existing work, was indistinguishable from that of CO, as both gave a mass spectrometer trace at $m/z = 28$ (although it may be inferred from N at $m/z = 14$). One way to determine the fate of the fuel N atoms would be to perform an isotopic labelling experiment using ^{15}N , as unique products would appear at $m/z = 29$ ($^{15}N\equiv^{14}N$) and $m/z = 30$ ($^{15}N_2$). A deliberately leaky system and the presence of $^{14}N_2$ in the air would significantly increase the errors in other methods.

Blended fuels tended to show a compositional middle ground between the two pure fuels, with lower rates of carbon deposition and either higher or lower electrical performance. A principal effect was the formation of a single phase with certain (previously immiscible) fuels and water, allowing better steam reforming. The addition of methanoic acid does have a slight reforming effect (through CO_2), although not as pronounced as that of water. This is to be expected, as CO_2 is a desired reforming product and methanoic acid has effectively already formed it. The effect on carbon deposition is partly due to dilution (the fuel is being mixed with another fuel that does not deposit large amounts of carbon) and partly due to the increased reforming. Carbon deposition via the disproportionation of CO should increase (due

to increased CO₂ levels and the CO/CO₂ equilibrium), but this is offset by the dilution effect and the presence of water. The effect on electrical performance is similar - the fuel is being diluted by another fuel that gives moderate ($\approx 45\%$) electrical output, so if the pure fuel had a higher output then the blended output will be lower, and vice versa. The largest increases in electrical performance were seen for fuels that were previously immiscible with water, due to improved reforming (for example, dimethoxymethane, Figure 69, versus dimethoxymethane / methanoic acid, Figure 93). Existing work^[156] on iso-octane blends gave similar results, and suggested that blending changes the way in which fuels adsorb onto and react on the catalyst.

8.3: Mechanism(s) of carbon deposition

In general, the removal of C-C bonds from a fuel reduces the amount of carbon deposition. For example, ethoxyethane (Figure 74) and trimethoxymethane (Figure 78), both C-4 hydrocarbons, differ in the amount of carbon deposited by a factor of ten. Butane, the alkane equivalent of these fuels, is known to cause cell failure through carbon build-up even more quickly. The theoretical argument supporting this is fairly simple - carbon deposition on a nickel surface proceeds via dissociative adsorption to monoatomic carbon, and this process is faster for higher hydrocarbons.^[182] In liquid-phase/solid reactions, Ni-C bonding can occur through a three- or four-membered transition state with two C atoms and one or two Ni atoms, and a similar mechanism may apply in gas-phase/solid reactions. By increasing the C atom separation distance, this mechanism is disrupted and other, less efficient, mechanisms must be used instead. This method of avoiding carbon build-up affects the energy density of the fuel,

as two hydrogen atoms are effectively replaced by an oxygen, but reduces the need for additional steam.

The separating atom does have some effect - N-methyl methanamide and methyl methanoate are effectively the same molecule with the $-CH_3$ and $-C=O$ separated by $-NH-$ and $-O-$ respectively. Without any steam addition, N-methyl methanamide (Figure 58) deposits almost ten times as much carbon as methyl methanoate (Figure 54); however the levels are similar once steam reforming is employed. Although the C-N bond is weaker than the C-O, the exhaust gas composition indicates that O-separated molecules decompose more readily - at least on YSZ surfaces. This may mean that a N-separated molecule has a greater chance of approaching the anode intact (rather than disproportionating to smaller fragments with only one carbon atom) and causing carbon deposition by reacting on the Ni surface. Steric effects are unlikely to be a significant factor, as O and NH (or even N) are similar in size.

The lowest rates of carbon deposition in “SOFC” experiments were observed for methyl methanoate (below the detection limit) and the blend of dimethoxymethane, methanoic acid and water (0.005 %). A typical deposition rate was $\approx 0.01\%$ - 0.04% . All fuels with O- or N-separated carbon atoms deposited less than 0.1 % of their fuel's carbon content.

Several molecules (for example, the 1:0 ratio of N-methyl methanamide, Figure 57) showed terminal declines in electrical output with levels of carbon deposition that were relatively high ($\approx 0.5\%$), but significantly lower than those seen for different molecules showing steady output (up to $\approx 2\%$). A key issue to note here is the rapidity, and therefore the location, of the

carbon deposition. If carbon deposition occurs rapidly, then carbon builds up near the fuel inlet and prevents fuel from entering the SOFC, reducing electrical output even though only a small amount of carbon is present. If carbon deposition occurs more slowly, then it can be spread over the whole length of the anode and therefore more carbon can be laid down without hindering fuel flow. The extent of this effect can be inferred from the electrical performance and carbon deposition rates, but not absolutely separated from other performance-related effects such as nickel agglomeration.

Fuel	C:O ratio	Deposited carbon / %
Methyl methanoate	1:1	0
Ethane-1,2-diol	1:2	0.012
Methanoic acid	1:0	0.016
Methanol	1:2	0.018
Ethanol	1:3	0.020
Trimethoxymethane	1:1	0.021
N-methyl methanamide	1:1	0.023
Dimethoxymethane	1:1	0.036
Propane-1,2-3-triol	1:2	0.051
N,N-dimethyl methanamide	1:1	0.055
2-methoxyethanol	1:2	0.080
Methoxymethane	6:1 (saturated gas)	0.565
Ethanoic acid	1:1	1.791
Ethoxyethane	1:0	2.451

Table 6: Lowest carbon deposition rates for "SOFC" experiments of pure fuels

Additional fuel	Fuel:methanoic acid:water ratio	Deposited carbon / %
Dimethoxymethane	1:1:2	0.005
Ethoxyethane	1:3:2	0.008
Methanol	1:1:0	0.012
Methyl methanoate	1:1:0	0.022
Ethanol	1:1:0	0.412

Table 7: Lowest carbon deposition rates for "SOFC" experiments of blended fuels

With hydrocarbon fuels, declines in electrical performance are often ascribed entirely to carbon deposition. This is often true, especially during long-term operation with no other degradation effects, but these experiment demonstrate that there are other factors. For example, methyl methanoate (section 5.5) has extremely low levels of carbon deposition (0-0.005 %) and yet poor (20 %) electrical output. There was only a correlation between performance decline and carbon levels at high deposition rates (for example, ethoxyethane).

Chapter 9: Conclusions

The effects of pre-oxidation, fuel molecular structure and oxidant addition upon reforming products, electrical performance and carbon deposition for microtubular solid oxide fuel cells were studied for a series of hydrocarbon-based fuels. The carbon content of the fuel varied from one to four atoms per molecule, and the extent of carbon-carbon bonding was varied. Aspects of this work have been published.^{[1] - [3]}

Increasing the pre-oxidation level of a fuel to an alcohol or aldehyde improves reforming and electrical output and decreases carbon deposition through a favourable route to CO and the presence of more oxygen. Increasing the pre-oxidation level to a carboxylic acid decreases electrical output through a favourable route to CO₂, and can increase carbon deposition if decomposition to CO₂ also creates a saturated carbon-containing fragment.

Removing carbon-carbon bonds from a molecule gives similar carbon deposition rates to pre-oxidised fuels, and reduces them relative to saturated fuels through favourable alteration of the C:O ratio. As with pre-oxidation, a carbon-to-oxygen ration of a least one is required to promote CO formation. If the separating atom is not oxygen, carbon deposition can be increased due to a lower pre-oxidation level.

When adding water and/or hydrocarbons as oxidants, electrical output can increase through improved reforming or decrease through dilution. Carbon deposition can increase through the reverse water-gas shift reaction or decrease through improved reforming and oxidation of solid carbon. Equimolar water at the least is required for efficient reforming, but the fact that

all of the above effects are seen experimentally demonstrates the difficulty in predicting how fuels will perform.

Based on the conclusions drawn, an ideal liquid fuel would be miscible with water, contain no carbon-carbon bonds and have an oxygen atom bonded to each carbon in such a way that CO fragments could easily be formed. The most promising fuels studied (for example, the mixture of dimethoxymethane and methanoic acid) will require further investigation to refine the optimal carbon-to-water ratio and operating conditions. Carbon-neutral methods of production must also be developed, for the reasons outlined in the introduction.

Further refinement of the microtubular SOFC design is required. The largest issue is that of irreproducibility between cells - manual extrusion, electrode application and current collection wiring lead to inconsistencies which make comparisons difficult. For complete reproducibility, the liquid fuel injection apparatus design must also be refined to eliminate leaks and thus allow absolute analysis of exhaust gases.

Further investigation on the long-term and cycling behaviour of fuels and microtubular SOFCs would be of benefit, as any real-world application is likely to include both these situations. At present, SOFC performance declines over time due to anode sintering and thermal cycling causes the anode current collect mesh to loosen. Electrical cycling is only problematic when fuels are likely to deposit carbon. This leads to the need for anode compositional refinement, optimised for a particular fuel blend, and anode-supported cells with greater catalytic activity and reduced ionic resistance.

List of References

- [1] G. Saunders, J. Preece, K. Kendall, Formulating liquid hydrocarbon fuels for SOFCs, *Journal of Power Sources* 131 (1-2), 23-26, 2004
- [2] J. Preece, G. Saunders, K. Kendall, *Proceedings of the 6th European SOFC Forum*, 1552-1559, 2004
- [3] J. Preece, K. Kendall, *Ninth Grove Fuel Cell Symposium*, 2005
- [4] C. Song, Fuel processing for low-temperature and high-temperature fuel cells - challenges and opportunities for sustainable development in the 21st century, *Catalysis Today* 77 (1-2), 17-49, 2002
- [5] H. Linden, Rising expectations of ultimate oil, gas recovery to have critical impact on energy, environmental policy - part 1, *Oil & Gas Journal* 102 (3), 18, 2004
- [6] H. Linden, Rising expectations of ultimate oil, gas recovery to have critical impact on energy, environmental policy - part 2, *Oil & Gas Journal* 102 (4), 18, 2004
- [7] H. Tu, U. Stimming, Advances, aging mechanisms and lifetime in solid-oxide fuel cells, *Journal of Power Sources* 127 (1-2), 284-293, 2004
- [8] S. Singhal, K. Kendall, *High Temperature Solid Oxide Fuel Cells*, 2003
- [9] N. Minh, T. Takahashi, *Science and Technology of Ceramic Fuel Cells*, 1995
- [10] J. Larminie, A. Dicks, *Fuel Cell Systems Explained*, 2002
- [11] I. Kilbride, Preparation and properties of small diameter tubular solid oxide fuel cells for rapid start-up, *Journal of Power Sources* 61 (1-2), 167-171, 1996
- [12] N. Bessete, *Siemens Power* 1 (10), 2001
- [13] T. Hibino, H. Iwahara, Simplification of solid oxide fuel cell system using partial oxidation of methane, *Chemistry Letters* (7), 1131-1134, 1993
- [14] K. Sundmacher, L. Rihko-Struckmann, V. Galvita, Solid electrolyte membrane reactors: Status and trends, *Catalysis Today* 104, 185-199, 2005
- [15] S. Jiang, S. Chan, A review of anode materials development in solid oxide fuel cells, *Journal of Materials Science* 39, 4405-4439, 2004
- [16] C. McPheeters, T. Claar, *1986 Fuel Cell Seminar Abstracts*, 64-67, 1986
- [17] R. Huiberts, J. Huijsmans, *Solid Oxide Fuel Cells VII*, 155-158, 2001
- [18] N. Minh et al., *1988 Fuel Cell Seminar Abstracts*, 105-108, 1988
- [19] S. Singhal, Science and technology of solid-oxide fuel cells, *MRS Bulletin*, 16-21, 2000
- [20] K. Kendall, *International Forum on Fine Ceramics*, 143-148, 1992
- [21] Y. Du, N. Sammes, G. Tompsett, Optimisation parameters for the extrusion of thin YSZ tubes for SOFC electrolytes, *Journal of the European Ceramic Society* 20 (7), 959-965, 2000
- [22] W. Schafer et al., Materials, interfaces and production techniques for planar solid oxide fuel cells, *Solid State Ionics* 86 (8), 1235-1239, 1996

- [23] N. Nakagawa, C. Kuroda, M. Ishida, Preparation of thin-film zirconia electrolyte fuel-cell by RF-sputtering, *Denki Kagaku* 57 (3), 215-218, 1989
- [24] L. Wang, S. Barnett, Deposition, structure and properties of cermet thin-films composed of Ag and Y-stabilized zirconia, *Journal of the Electrochemical Society* 139 (4), 1134-1140, 1992
- [25] S. deSouza, S. Visco, L. DeLonghe, Thin-film solid oxide fuel cell with high performance at low-temperature, *Solid State Ionics* 98 (1-2), 57-61, 1997
- [26] C. Chen, M. Nasrallah, H. Anderson, 1992 *Fuel Cell Seminar Abstracts*, 515, 1992
- [27] K. Moe, T. Tagawa, S. Goto, Preparation of electrode catalyst for SOFC reactor by ultrasonic mist pyrolysis of aqueous solution, *Journal of the Ceramic Society of Japan* 106 (3), 242-247, 1998
- [28] L. Lunot, Y. Denos, *Proceedings of the 1998 International Gas Research Conference*, 834, 1998
- [29] T. Ishira et al., Preparation of yttria-stabilized zirconia films for solid oxide fuel-cells by electrophoretic deposition method, *Chemistry Letters* (6), 943-946, 1992
- [30] H. Takebe, N. Yoshihara, K. Morinaga, The processing of YSZ films for solid oxide fuel-cell by the slip casting, *Journal of the Ceramic Society of Japan* 98 (2), 136-143, 1990
- [31] A. Isenberg, *Symposium on Electrode Materials and Processes for Energy Conversion and Storage*, 572-583, 1977
- [32] S. Singhal, U. Pal, Electrochemical vapor-deposition of yttria-stabilized zirconia films, *Journal of the Electrochemical Society* 137 (9), 2937-2941, 1990
- [33] H. Sato, High temperature solid electrolyte fuel cell, *Energy Development in Japan* 4, 111-128, 1981
- [34] P. Gellings, H. Bouwmeester, Ion and mixed conducting oxides as catalysts, *Catalysis Today* 12, 1-105, 1992
- [35] A. Appleby, Fuel cell technology: status and future prospects, *Energy* 21 (7-8), 521-653, 1996
- [36] L. Gauckler et al., Solid oxide fuel cells: systems and materials, *Chimia* 58, 837-850, 2004
- [37] N. Minh, Ceramic fuel cells, *Journal of the American Ceramic Society* 76 (3), 563-588, 1993
- [38] T. Etsell, S. Flengas, Electrical properties of solid oxide electrolytes, *Chemical Reviews* 70 (3), 339-376, 1970
- [39] E. Subbarao, H. Maiti, Solid electrolytes with oxygen ion conduction, *Solid State Ionics* 11 (4), 317-338, 1984
- [40] S. Badwal, Zirconia-based solid electrolytes - microstructures, stability and ionic-conductivity, *Solid State Ionics* 52 (1-3), 23-32, 1992
- [41] I. Kosacki et al., Electrical conductivity of nanocrystalline ceria and zirconia thin films, *Solid State Ionics* 136, 1225-1233, 2000

- [42] H. Tuller, Solid state electrochemical systems - Opportunities for nanofabricated or nanostructured materials, *Journal of Electroceramics* 1 (3), 211-218, 1997
- [43] J. Ying, T. Sun, Research needs assessment on nanostructured catalysts, *Journal of Electroceramics* 1 (3), 219-238, 1997
- [44] S. Badwal, F. Ciacchi, D. Milosevic, Scandia-zirconia electrolytes for intermediate temperature solid oxide fuel cell operation, *Solid State Ionics* 136, 91-99, 2000
- [45] O. Yamamoto et al., Electrical-conductivity of stabilized zirconia with ytterbia and scandia, *Solid State Ionics* 79, 137-142, 1995
- [46] R. Blumenthal, F. Brugner, J. Garnier, Electrical conductivity of CaO-doped nonstoichiometric cerium dioxide from 700 degrees to 1500 degrees C, *Journal of the Electrochemical Society* 120 (9), 1230-1237, 1973
- [47] H. Inaba, H. Tagawa, Ceria-based solid electrolytes - Review, *Solid State Ionics* 83 (1-2), 1-16, 1996
- [48] R. Doshi et al., Development of solid-oxide fuel cells that operate at 500 degrees C, *Journal of the Electrochemical Society* 146 (4), 1273-1278, 1999
- [49] M. Mogensen, N. Sammes, G. Tompsett, Physical, chemical and electrochemical properties of pure and doped ceria, *Solid State Ionics* 129 (1-4), 63-94, 2000
- [50] P. Shuk et al., Oxide ion conducting solid electrolytes based on Bi₂O₃, *Solid State Ionics* 89 (3-4), 179-196, 1996
- [51] N. Sammes et al., Bismuth based oxide electrolytes - Structure and ionic conductivity, *Journal of the European Ceramic Society* 19 (10), 1801-1826, 1999
- [52] F. Abraham et al., The BIMEVOX series - a new family of high performance oxide ion conductors, *Solid State Ionics* 40-41 (2), 934-937, 1990
- [53] T. Takahashi, H. Iwahara, Ionic conduction in perovskite-type solid oxide solution and its application to solid electrolyte fuel cell, *Energy Conversion* 11 (3), 105, 1971
- [54] R. Cook, R. MacDuff, A. Sammells, Perovskite solid electrolytes for intermediate temperature solid oxide fuel-cells, *Journal of the Electrochemical Society* 137 (10), 3309-3310, 1990
- [55] T. Ishihara, H. Matsuda, Y. Takita, Doped LaGaO₃ perovskite-type oxide as a new oxide ionic conductor, *Journal of the American Chemical Society* 116 (9), 3801-3803, 1994
- [56] T. Ishihara et al., Improved oxide ion conductivity in La_{0.8}Sr_{0.2}Ga_{0.8}Mg_{0.2}O₃ by doping Co, *Chemistry of Materials* 11 (8), 2081-2088, 1999
- [57] S. Kim et al., Oxygen-ion conductivity of BaO- and MgO-doped LaGaO₃ electrolytes, *Journal of Power Sources* 93 (1-2), 279-284, 2001
- [58] J. Mizusaki et al., Electrical-conductivity, defect equilibrium and oxygen vacancy diffusion-coefficient of La_{1-x}CaxAlO_{3-δ} single-crystals, *Journal of the Electrochemical Society* 140 (2), 467-471, 1993
- [59] K. Nomura, S. Tanase, Electrical conduction behavior in (La_{0.9}Sr_{0.1})M_{III}O_{3-δ} (M-III=Al, Ga, Sc, In, and Lu) perovskites, *Solid State Ionics* 98 (3-4), 229-236, 1997

- [60] J. Goodenough, J. Ruizdiaz, Y. Zhen, Oxide-ion conduction in Ba₂In₂O₅ and Ba₃In₂CeO₈, Ba₃In₂HfO₈, or Ba₃In₂ZrO₈, *Solid State Ionics* 44 (1-2), 21-31, 1990
- [61] K. Kendall et al., Recent developments in perovskite-based oxide ion conductors, *Solid State Ionics* 82 (3-4), 215-223, 1995
- [62] S. Nakayama, M. Sakamoto, Electrical properties of new type high oxide ionic conductor RE₁₀Si₆O₂₇ (RE = La, Pr, Nd, Sm, Gd, Dy), *Journal of the European Ceramic Society* 18 (10), 1413-1418, 1998
- [63] H. Iwahara et al., Proton conduction in sintered oxides based on BaCeO₃, *Journal of the Electrochemical Society* 135 (2), 529-533, 1988
- [64] H. Iwahara, T. Shimura, H. Matsumoto, Protonic conduction in oxides at elevated temperatures and their possible applications, *Electrochemistry* 68 (3), 154-161, 2000
- [65] K. Kreuer et al., Proton conducting alkaline earth zirconates and titanates for high drain electrochemical applications, *Solid State Ionics* 145 (1-4), 295-306, 2001
- [66] W. Coors, Protonic ceramic fuel cells for high-efficiency operation with methane, *Journal of Power Sources* 118 (1-2), 150-156, 2003
- [67] H. Mobius, On the history of solid electrolyte fuel cells, *Journal of Solid State Electrochemistry* 1 (1), 2-16, 1997
- [68] T. Setoguchi et al., Effects of anode material and fuel on anodic reaction of solid oxide fuel-cells, *Journal of the Electrochemical Society* 139 (10), 2875-2880, 1992
- [69] A. Atkinson et al., Advanced anodes for high-temperature fuel cells, *Nature Materials* 3 (1), 17-27, 2004
- [70] M. Mori et al., Thermal expansion of nickel-zirconia anodes in solid oxide fuel cells during fabrication and operation, *Journal of the Electrochemical Society* 145 (4), 1374-1381, 1998
- [71] B. de Boer et al., The effect of the presence of fine YSZ particles on the performance of porous nickel electrodes, *Solid State Ionics* 127 (3-4), 269-276, 2000
- [72] M. Mogensen, S. Skaarup, Kinetic and geometric aspects of solid oxide fuel cell electrodes, *Solid State Ionics* 86 (8), 1151-1160, 1996
- [73] D. Dees et al., Conductivity of porous Ni/ZrO₂-Y₂O₃ cermets, *Journal of the Electrochemical Society* 134 (9), 2141-2146, 1987
- [74] Y. Matsuzaki, I. Yasuda, The poisoning effect of sulfur-containing impurity gas on a SOFC anode: Part I. Dependence on temperature, time, and impurity concentration, *Solid State Ionics* 132 (3-4), 261-269, 2000
- [75] C. Chun, J. Mumford, T. Ramanarayanan, Carbon-induced corrosion of nickel anode, *Journal of the Electrochemical Society* 147 (10), 3680-3686, 2000
- [76] T. Markin et al., *Conference on Superionic Conductors*, 15-35, 1976
- [77] H. Sasaki et al., High power density solid oxide electrolyte fuel cells, *Journal of the Electrochemical Society* 139 (1), L12-L13, 1992
- [78] M. Joerger, B. Gauckler, *Solid Oxide Fuel Cells VII*, 662, 2001

- [79] T. Inagaki et al., *Solid Oxide Fuel Cells VII*, 963, 2001
- [80] M. Mori et al., Evaluation of Ni and Ti-doped Y₂O₃ stabilized ZrO₂ cermet as an anode in high-temperature solid oxide fuel cells, *Solid State Ionics* 160 (1-2), 1-14, 2003
- [81] S. Park et al., Direct oxidation of hydrocarbons in a solid oxide fuel cell I. Methane oxidation, *Journal of the Electrochemical Society* 146 (10), 3603-3605, 1999
- [82] S. Park, J. Vohs, R. Gorte, Direct oxidation of hydrocarbons in a solid-oxide fuel cell, *Nature* 404 (6775), 265-267, 2000
- [83] R. Gorte et al., Anodes for direct oxidation of dry hydrocarbons in a solid-oxide fuel cell, *Advanced Materials* 12 (19), 1465-1469, 2000
- [84] B. Steele, Appraisal of Ce_{1-y}Gd_yO_{2-y/2} electrolytes for IT-SOFC operation at 500 degrees C, *Solid State Ionics* 129 (1-4), 95-110, 2000
- [85] W. Worrell, Electrical properties of mixed-conducting oxides having high oxygen-ion conductivity, *Solid State Ionics* 52 (1-3), 147-151, 1992
- [86] S. Tao, J. Irvine, Optimization of mixed conducting properties of Y₂O₃-ZrO₂-TiO₂ and Sc₂O₃-Y₂O₃-ZrO₂-TiO₂ solid solutions as potential SOFC anode materials, *Journal of Solid State Chemistry* 165 (1), 12-18, 2002
- [87] P. Slater, D. Fagg, J. Irvine, Synthesis and electrical characterisation of doped perovskite titanates as potential anode materials for solid oxide fuel cells, *Journal of Materials Chemistry* 7 (12), 2495-2498, 1997
- [88] S. Hui, A. Petric, Evaluation of yttrium-doped SrTiO₃ as an anode for solid oxide fuel cells, *Journal of the European Ceramic Society* 22 (9-10), 1673-1681, 2002
- [89] S. Primdahl et al., Sr-doped LaCrO₃ anode for solid oxide fuel cells, *Journal of the Electrochemical Society* 148 (1), A74-A81, 2001
- [90] J. Sfeir, LaCrO₃-based anodes: stability considerations, *Journal of Power Sources* 118 (1-2), 276-285
- [91] E. Sverdrup, D. Archer, A. Glasser, *Fuel Cell Systems II*, 301-314, 1969
- [92] S. Carter et al., Oxygen-transport in selected nonstoichiometric perovskite-structure oxides, *Solid State Ionics* 53 (6), 597-605, 1992
- [93] A. Hammouche, E. Siebert, A. Hammou, Crystallographic, thermal and electrochemical properties of the system La_{1-x}Sr_xMnO₃ for high-temperature solid electrolyte fuel-cells, *Materials Research Bulletin* 24 (3), 367-380, 1989
- [94] O. Yamamoto et al., Perovskite-type oxides as oxygen electrodes for high-temperature oxide fuel-cells, *Solid State Ionics* 22 (2-3), 241-246, 1987
- [95] H. Uchida, S. Arisaka, M. Watanabe, High performance electrodes for medium-temperature solid oxide fuel cells: Activation of La(Sr)CoO₃ cathode with highly dispersed Pt metal electrocatalysts, *Solid State Ionics* 135 (1-4), 347-351, 2000
- [96] A. Petric, P. Huang, F. Tietz, Evaluation of La-Sr-Co-Fe-O perovskites for solid oxide fuel cells and gas separation membranes, *Solid State Ionics* 135 (1-4), 719-725, 2000

- [97] A. Mackor et al., *Proceedings of the 25th Intersociety Energy Conversion Engineering Conference*, 251-255, 1990
- [98] M. Mori et al., A new cathode material $(\text{La,Sr})_{1-z}(\text{Mn}_{1-y}\text{Cr}_y)\text{O}_3$ ($0 \leq y \leq 0.2$) for SOFC, *Denki Kagaku* 58 (6), 528-532, 1990
- [99] H. Fukunaga et al., Reaction model of dense $\text{Sm}_{0.5}\text{Sr}_{0.5}\text{CoO}_3$ as SOFC cathode, *Solid State Ionics* 132 (3-4), 279-285, 2000
- [100] J. Bae, B. Steele, Properties of pyrochlore ruthenate cathodes for intermediate temperature solid oxide fuel cells, *Journal of Electroceramics* 3 (1), 37-46, 1999
- [101] H. Yu, K. Fung, $\text{La}_{1-x}\text{Sr}_x\text{CuO}_{2.5-\delta}$ as new cathode materials for intermediate temperature solid oxide fuel cells, *Materials Research Bulletin* 38 (2), 231-239, 2003
- [102] D. Karim, A. Aldred, Localized level hopping transport in $\text{La}(\text{Sr})\text{CrO}_3$, *Physical Review B* 20 (6), 2255-2263, 1979
- [103] R. Koc, H. Anderson, Electrical conductivity and Seebeck coefficient of $(\text{La}, \text{Ca})(\text{Cr}, \text{Co})\text{O}_3$, *Journal of Materials Science* 27 (20), 5477-5482, 1992
- [104] G. Carini et al., Electrical conductivity, Seebeck coefficient and defect chemistry of Ca-doped YCrO_3 , *Solid State Ionics* 49, 233-243, 1991
- [105] L. Group and H. Anderson, Densification of $\text{La}_{1-x}\text{Sr}_x\text{CrO}_3$, *Journal of the American Ceramic Society* 59 (9-10), 449-450, 1976
- [106] W. Quadackers et al., Metallic interconnectors for solid oxide fuel cells - a review, *Materials at High Temperatures* 20 (2), 115-127, 2003
- [107] W. Kock et al., *Solid Oxide Fuel Cells IV*, 841, 1995
- [108] S. Taniguchi et al., Development of a ferritic alloy separator for a planar SOFC, *Denki Kagaku* 65 (7), 574-579, 1997
- [109] S. Linderoth et al., Investigations of metallic alloys for use as interconnects in solid oxide fuel cell stacks, *Journal of Materials Science* 31 (19), 5077-5082, 1996
- [110] D. England, A. Virkar, Oxidation kinetics of some nickel-based superalloy foils in humidified hydrogen and electronic resistance of the oxide scale formed part II, *Journal of the Electrochemical Society* 148 (4), A330-A338, 2001
- [111] W. Meulenberg et al., Improved contacting by the use of silver in solid oxide fuel cells up to an operating temperature of 800 degrees C, *Journal of Materials Science* 36 (13), 3189-3195, 2001
- [112] C. Gindorf, L. Singheiser, K. Hilpert, Chromium vaporisation from Fe,Cr base alloys used as interconnect in fuel cells, *Steel Research* 72 (11-12), 528-533, 2001
- [113] W. Zhu, S. Deevi, Opportunity of metallic interconnects for solid oxide fuel cells: a status on contact resistance, *Materials Research Bulletin* 38 (6), 957-972, 2003
- [114] H. Schmidt, B. Bruckner, K. Fischer, *Solid Oxide Fuel Cells IV*, 869, 1995
- [115] H. Buchkremer et al., *Solid Oxide Fuel Cells V*, 160, 1997
- [116] T. Alston et al., A 1000-cell SOFC reactor for domestic cogeneration, *Journal of Power Sources* 71 (1-2), 271-274, 1998

- [117] F. Gardner et al., SOFC technology development at Rolls-Royce, *Journal of Power Sources* 86, 122-129, 2000
- [118] A. Demin et al., Thermodynamic analysis of methane fuelled solid oxide fuel-cell system, *International Journal of Hydrogen Energy* 17 (6), 451-458, 1992
- [119] E. Achenbach, E. Riensche, Methane steam reforming kinetics for solid oxide fuel-cells, *Journal of Power Sources* 52 (2), 283-288, 1994
- [120] A. Dicks, K. Pointon, A. Siddle, Intrinsic reaction kinetics of methane steam reforming on a nickel/zirconia anode, *Journal of Power Sources* 86 (1-2), 523-530, 2000
- [121] J. Amphlett et al., Hydrogen production by the catalytic steam reforming of methanol. 1. The thermodynamics, *Canadian Journal of Chemical Engineering* 59 (6), 720-727, 1981
- [122] S. Asprey, B. Wojciechowski, B. Peppley, Kinetic studies using temperature-scanning: the steam-reforming of methanol, *Applied Catalysis A - General* 179 (1-2), 51-70, 1999
- [123] Y. Lwin et al., Hydrogen production from steam-methanol reforming: thermodynamic analysis, *International Journal of Hydrogen Energy* 25 (1), 47-53, 2000
- [124] S. Assabumrungrat et al., Thermodynamic analysis of carbon formation in a solid oxide fuel cell with a direct internal reformer fuelled by methanol, *Journal of Power Sources* 139 (1-2), 55-60, 2005
- [125] S. Cavallaro, S. Freni, Ethanol steam reforming in a molten carbonate fuel cell. A preliminary kinetic investigation, *International Journal of Hydrogen Energy* 21 (6), 465-469,
- [126] S. Freni, G. Maggio, S. Cavallaro, Ethanol steam reforming in a molten carbonate fuel cell: A thermodynamic approach, *Journal of Power Sources* 62 (1), 67-73, 1996
- [127] E. Garcia, M. Laborde, Hydrogen production by the steam reforming of ethanol - thermodynamic analysis, *International Journal of Hydrogen Energy* 16 (5), 307-312, 1991
- [128] K. Vasudeva et al., Steam reforming of ethanol for hydrogen production: Thermodynamic analysis, *International Journal of Hydrogen Energy* 21 (1), 13-18, 1996
- [129] P. Tsiakaras, A. Demin, Thermodynamic analysis, of a solid oxide fuel cell system fuelled by ethanol, *Journal of Power Sources* 102 (1-2), 210-217, 2001
- [130] F. Aupretre et al., Le vaporeformage catalytique: Application a la production embarquee d'hydrogene a partir d'hydrocarbures ou d'alcools, *Annales de Chimie - Science des Materiaux* 26 (4), 93-106, 2001
- [131] B. Hagh, Stoichiometric analysis of autothermal fuel processing, *Journal of Power Sources* 130 (1-2), 85-94, 2004
- [132] T. Semelsberger et al., Equilibrium products from autothermal processes for generating hydrogen-rich fuel-cell feeds, *International Journal of Hydrogen Energy* 29 (10), 1047-1064, 2004
- [133] F. Coutelieres, S. Douvartzides, P. Tsiakaras, The importance of the fuel choice on the efficiency of a solid oxide fuel cell system, *Journal of Power Sources* 123 (2), 200-205, 2003

- [134] A. Dicks, Hydrogen generation from natural gas for the fuel cell systems of tomorrow, *Journal of Power Sources* 61 (1-2), 113-124, 1996
- [135] A. Dicks, Advances in catalysts for internal reforming in high temperature fuel cells, *Journal of Power Sources* 71 (1-2), 111-122, 1998
- [136] P. Aguiar, D. Chadwick, L. Kershenbaum, Modelling of an indirect internal reforming solid oxide fuel cell, *Chemical Engineering Science* 57 (10), 1665-1677, 2002
- [137] J. Rostrup-Nielsen, Production of synthesis gas, *Catalysis Today* 18 (4), 305-324, 1993
- [138] S. Bharadwaj, L. Schmidt, Catalytic partial oxidation of natural-gas to syngas, *Fuel Processing Technology* 42 (2-3), 109-127, 1995
- [139] A. Naidja et al., Cool flame partial oxidation and its role in combustion and reforming of fuels for fuel cell systems, *Progress in Energy and Combustion Science* 29 (2), 155-191, 2003
- [140] P. Vernon et al., Partial oxidation of methane to synthesis gas, and carbon-dioxide as an oxidizing-agent for methane conversion, *Catalysis Today* 13 (2-3), 417-426, 1992
- [141] H. Swaan et al., Deactivation of supported nickel-catalysts during the reforming of methane by carbon dioxide, *Catalysis Today* 21 (2-3), 571-578, 1994
- [142] M. Pena, J. Gomez, J. Fierro, New catalytic routes for syngas and hydrogen production, *Applied Catalysis A - General* 144 (1-2), 7-57, 1996
- [143] S. McIntosh, R. Gorte, Direct hydrocarbon solid oxide fuel cells, *Chemical Reviews* 104 (10), 4845-4865, 2004
- [144] C. Bartholomew, Carbon deposition in steam reforming and methanation, *Catalysis Reviews - Science and Engineering* 24 (1), 67-112, 1982
- [145] C. Finnerty et al., Carbon formation on and deactivation of nickel-based/zirconia anodes in solid oxide fuel cells running on methane, *Catalysis Today* 46 (2-3), 137-145, 1998
- [146] T. Kim et al., A study of carbon formation and prevention in hydrocarbon-fueled SOFC, *Journal of Power Sources* (In press), 2005
- [147] S. Clarke et al., Catalytic aspects of the steam reforming of hydrocarbons in internal reforming fuel cells, *Catalysis Today* 38 (4), 411-423, 1997
- [148] N. Triantafyllopoulos, S. Neophytides, The nature and binding strength of carbon adspecies formed during the equilibrium dissociative adsorption of CH₄ on Ni-YSZ cermet catalysts, *Journal of Catalysis* 216 (2), 324-333, 2003
- [149] C. Mallon, K. Kendall, Sensitivity of nickel cermet anodes to reduction conditions, *Journal of Power Sources* 145 (2), 154-160, 2005
- [150] R. Ormerod, Internal reforming in solid oxide fuel cells, *Studies in Surface Science and Catalysis* 122, 35-46, 1999
- [151] I. Proctor, A. Hopkin, R. Ormerod, Development of anodes for direct electrocatalytic oxidation of methane in solid oxide fuel cells, *Ionics* 9 (3-4), 242-247, 2003

- [152] W. Sangtongkitcharoen et al., Comparison of carbon formation boundary in different modes of solid oxide fuel cells fueled by methane, *Journal of Power Sources* 142 (1-2), 75-80,
- [153] A. Muller, D. Herbristrit, E. Ivers-Tiffée, Development of a multilayer anode for solid oxide fuel cells, *Solid State Ionics* 152 (SI), 537-542, 2002
- [154] H. Kishimoto et al., Attempt of utilizing liquid fuels with Ni-SeSZ anode in SOFCs, *Solid State Ionics* 175 (1-4), 107-111, 2004
- [155] M. Cassidy, G. Lindsay, K. Kendall, The reduction of nickel-zirconia cermet anodes and the effects on supported thin electrolytes, *Journal of Power Sources* 61 (1-2), 189-192, 1996
- [156] G. Saunders, *Reactions of hydrocarbons in zirconia fuel cells*, University of Birmingham, 2003
- [157] S. Assabumrungrat et al., Thermodynamic analysis for a solid oxide fuel cell with direct internal reforming fueled by ethanol, *Chemical Engineering Science* 59 (24), 6015-6020, 2004
- [158] G. Maggio, S. Freni and S. Cavallaro, Light alcohols/methane fuelled molten carbonate fuel cells: a comparative study, *Journal of Power Sources* 74 (1), 17-23, 1998
- [159] K. Vasudeva et al., Steam reforming of ethanol for hydrogen production: Thermodynamic analysis, *International Journal of Hydrogen Energy* 21 (1), 13-18, 1996
- [160] I. Fishtik et al., A thermodynamic analysis of hydrogen production by steam reforming of ethanol via response reactions, *International Journal of Hydrogen Energy* 25 (1), 31-45, 2000
- [161] M. Ihara et al., Solid state fuel storage and utilization through reversible carbon deposition on an SOFC anode, *Solid State Ionics* 175 (1-4), 51-54, 2004
- [162] D. Wang, D. Montane and E. Chornet, Catalytic steam reforming of biomass-derived oxygenates: Acetic acid and hydroxyacetaldehyde, *Applied Catalysis A - General* 143 (2), 245-270, 1996
- [163] M. Markevich et al., Hydrogen from biomass: Steam reforming of model compounds of fast-pyrolysis oil, *Energy & Fuels* 13 (6), 1160-1166, 1999
- [164] K. Takanabe et al., Sustainable hydrogen from bio-oil - Steam reforming of acetic acid as a model oxygenate, *Journal of Catalysis* 227 (1), 101-108, 2004
- [165] R. Davda et al., A review of catalytic issues and process conditions for renewable hydrogen and alkanes by aqueous-phase reforming of oxygenated hydrocarbons over supported metal catalysts, *Applied Catalysis B - Environmental* 56 (1-2), 171-186, 2005
- [166] R. Davda et al., Aqueous-phase reforming of ethylene glycol on silica-supported metal catalysts, *Applied Catalysis B - Environmental* 43 (1), 13-26, 2003
- [167] E. Murray, S. Harris, H. Jen, Solid oxide fuel cells utilizing dimethyl ether fuel, *Journal of the Electrochemical Society* 149 (9), A1127-A1131, 2002
- [168] S. Wang, T. Ishihara, Electrocatalytic oxidation of dimethyl ether, *Chinese Journal of Catalysis* 24 (9), 695-700, 2003

- [169] E. Murray et al., Direct solid oxide fuel cell operation using a dimethyl ether/air fuel mixture, *Electrochemical and Solid State Letters* 8 (10), A531-A533, 2005
- [170] A. Rozovskii, G. Lin, Fundamentals of methanol synthesis and decomposition, *Topics in Catalysis* 22 (3-4), 137-150, 2003
- [171] N. Gamanovich, V. Gorbunova, G. Novikov, Oxidation of alcohol-ammonia mixtures in high-temperature fuel cell with various electrodes, *Russian Journal of Applied Chemistry* 74 (5), 746-749, 2001
- [172] A. Wojcik et al., Ammonia as a fuel in solid oxide fuel cells, *Journal of Power Sources* 118 (1-2), 342-348, 2003
- [173] S-F. Yin et al., Investigation on the catalysis of CO_x-free hydrogen generation from ammonia, *Journal of Catalysis* 224 (2), 384-396, 2004
- [174] J. Staniforth, R. Ormerod, Clean destruction of waste ammonia with consummate production of electrical power within a solid oxide fuel cell system, *Green Chemistry* 5 (5), 606-609, 2003
- [175] J. Shabaker, G. Huber, J. Dumesic, Aqueous-phase reforming of oxygenated hydrocarbons over Sn-modified Ni catalysts, *Journal of Catalysis* 222 (1), 180-191, 2004
- [176] T. Hirai et al., Production of hydrogen by steam reforming of glycerin on ruthenium catalyst, *Energy & Fuels* 19 (4), 1761-1762, 2005
- [177] C. Pham et al., A novel electrochemically active and Fe(III)-reducing bacterium phylogenetically related to *Aeromonas hydrophila*, isolated from a microbial fuel cell, *FEMS Microbiology Letters* 233 (1), 129-134, 2003
- [178] N. Wakabayashi et al., Characterization of methoxy fuels for direct oxidation-type fuel cell, *Journal of the Electrochemical Society* 151 (10), A1636-A1640, 2004
- [179] S. Narayanan et al., Direct electro-oxidation of dimethoxymethane, trimethoxymethane, and trioxane and their application in fuel cells, *Journal of the Electrochemical Society* 144 (12), 4195-4201, 1997
- [180] K. Otsuka, T. Ina, I. Yamanaka, The partial oxidation of methanol using a fuel cell reactor, *Applied Catalysis A - General* 247 (2), 219-229, 2003
- [181] J. Wang et al., Trimethoxymethane as an alternative fuel for a direct oxidation PBI polymer electrolyte fuel cell, *Electrochimica Acta* 43 (24), 3821-3828, 1998
- [182] D. Trimm, Catalysts for the control of coking during steam reforming, *Catalysis Today* 49 (1-3), 3-10, 1999